From Customized Cellular Adhesion to Synthetic Ecology: Characterizing the Cyanobacterium *Synechocystis* PCC 6803 for Biofuel Production

by

Rebecca Allen

A Dissertation Presented in Partial Fulfillment
of the Requirements for the Degree
Doctor of Philosophy

Approved November 2016 by the
Graduate Supervisory Committee:

Roy Curtiss III, Co-Chair
Rosa Krajmalnik-Brown, Co-Chair
Bruce Rittmann
Willem Vermaas

ARIZONA STATE UNIVERSITY

December 2016

ABSTRACT

Sustainable global energy production is one of the grand challenges of the 21st century. Next-generation renewable energy sources include using photosynthetic microbes such as cyanobacteria for efficient production of sustainable fuels from sunlight. The cyanobacterium *Synechocystis* PCC 6803 (*Synechocystis*) is a genetically tractable model organism for plant-like photosynthesis that is used to develop microbial biofuel technologies. However, outside of photosynthetic processes, relatively little is known about the biology of microbial phototrophs such as *Synechocystis*, which impairs their development into market-ready technologies. My research objective was to characterize strategic aspects of *Synechocystis* biology related to its use in biofuel production; specifically, how the cell surface modulates the interactions between *Synechocystis* cells and the environment. First, I documented extensive biofouling, or unwanted biofilm formation, in a 4,000-liter roof-top photobioreactor (PBR) used to cultivate *Synechocystis,* and correlated this cell-binding phenotype with changes in nutrient status by developing a bench-scale assay for axenic phototrophic biofilm formation. Second, I created a library of mutants that lack cell surface structures, and used this biofilm assay to show that mutants lacking the structures pili or S-layer have a non-biofouling phenotype. Third, I analyzed the transcriptomes of cultures showing aggregation, another cell-binding phenotype, and demonstrated that the cells were undergoing stringent response, a type of conserved stress response. Finally, I used contaminant Consortia and statistical modeling to test whether *Synechocystis* mutants lacking cell surface structures could reduce contaminant growth in mixed cultures. In summary, I have identified genetic and environmental means of manipulating

Synechocystis strains for customized adhesion phenotypes, for more economical biomass harvesting and non-biofouling methods. Additionally, I developed a modified biofilm assay and demonstrated its utility in closing a key gap in the field of microbiology related to axenic phototrophic biofilm formation assays. Also, I demonstrated that statistical modeling of contaminant Consortia predicts contaminant growth across diverse species. Collectively, these findings serve as the basis for immediately lowering the cost barrier of *Synechocystis* biofuels via a more economical biomass-dewatering step, and provide new research tools for improving *Synechocystis* strains and culture ecology management for improved biofuel production.

DEDICATION

I dedicate this dissertation to my grandmother, Shirley Dudas, with all my love.

ACKNOWLEDGMENTS

First I would like to thank my two thesis co-advisors, Dr. Roy Curtiss III and Dr. Rosa Krajmalnik-Brown, for taking a chance on an unknown student, an untested topic, and an unfamiliar collaboration as co-advisors together. It's really a testament to you that you took on this endeavor with me, especially considering this work was not tied directly to your existing research grant portfolios. It was truly an honor for me to be accepted as your PhD student, and given a science home with your research groups. I also want to thank my committee members, Dr. Bruce E. Rittmann and Dr. Willem Vermaas, for sharing their excellence in their respective fields to help move this project forward. All four of you were part of creating a world-class research environment for industrial-scale microbial biofuel production that was a dream come true for me. Having the chance to make connections by doing rotations in all of your labs, and being a part of this research program at ASU was such an incredible opportunity for a graduate student. I am sure that I will continue to reap the rewards of that experience for the rest of my scientific career.

I want to thank my fellow lab members, especially my co-authors including Dr. Michael Fisher and Dr. Alex Zevin for collaborating with me, and the very kind and generous people that took time to help me even though we weren't working on the same project, like Michelle Young, Dr. Michal Ziv-El, Dr. Wei Kong, Toby Gates, Dr. Hyun-Woo Kim, Josh McIlwain, and others. My fellow students and teachers in the Biological Design Graduate Program, who are a constant source of inspiration for their consistently high standards as scientists and individuals. My very dear and tremendously talented friends: Myonnie Bada-Albrecht, Katie Baker, Eric Templeton, and most especially, René Daer, my fellow grad school soldier-at-arms, for their advice and encouragement,

and believing in me as a person and a scientist, and making me laugh. I literally could not have done this without them. I also want to thank the brilliant online community of feminists at Autostraddle.com, for helping me maintain good mental and social health while navigating the patriarchy during grad school. They were essential, too.

I would like to acknowledge some very important teachers that made it possible for me to join a PhD program. The Brun Lab at Indiana University, Bloomington was an incredibly valuable training ground. Their excellence made it possible for me to be a truly independent researcher at ASU. My chemistry teacher, Dr. William Lamb, for taking a chance on allowing me into his independent research program in high school, and being such a phenomenal educator. The Oregon Museum of Science and Industry, especially the Demonstrator team led by Lynn Vanderkamp. My family, for encouraging me to get an education. Although it's unusual to do so, I am sincere in also thanking tax payers for making it possible for people like me from a working-class background to earn a PhD, become a member of a community of scholars, and try to make a better life.

Finally, I want to give the Arthur Ashe Leadership Award to Carole Flores and Maria Hanlin. Arthur Ashe said that true leadership* isn't the urge to surpass others at whatever cost, but the urge to help lift others up. A lot of times, people don't receive appreciation until after they have already succeeded, when it's the people who haven't succeeded yet that benefit the most from encouragement. Carole and Maria are my role models for their skill in this area of leadership, and I will do my best to emulate their example in the future. I went many years at ASU before I started to have some success, and their kindness and encouragement during those long years made a huge difference to me, as I'm sure it did to many others. (*He said heroism, but leadership works too).

TABLE OF CONTENTS

Page

CHAPTER Page

APPENDIX Page

LIST OF TABLES

LIST OF FIGURES

LIST OF ABBREVIATIONS

AHL	Acyl homoserine lactone
ANOVA	Analysis of variance
BLAST	Basic localized alignment search tool
BCA	Bicinchoninic acid assay
c-di-GMP	cyclic diguanylate monophosphate
DC1; DC2	Defined Consortium 1; Defined Consortium 2
DCMU	3-(3,4-dichlorophenyl)-1,1-dimethylurea
ECM	Extracellular matrix
EPS	Exopolysaccharide
FPKM	Fragments per kilobase of transcript per million reads
FWLSD	Fresh water lake sequence database
GC	Gas chromatography
Kan	Kanamycin sulfate
KEGG	Kyoto encyclopedia of genes and genomes
LB	Lysogeny broth
LPS	Lipopolysaccharide
NC1; NC2	Negative Control 1; Negative Control 2
OM	Outer membrane
ORF	Open reading frame
OTU	Operational taxonomic unit
PBR	photobioreactor

PICRUSt	Phylogenetic investigation of communities by reconstruction of unobserved states
(p)ppGpp	guanosine polyphosphate
QIIME	Quantitative insights into microbial ecology
RIN	RNA integrity number
RPS	Released polysaccharide
RSH	RelA/SpoT homolog
SDS-PAGE	Sodium dodecyl sulfate polyacrylamide gel electrophoresis
SMP	Soluble microbial products
STRING	Search tool for retrieval of interacting genes/proteins
SR	Stringent response
TCW	Tempe Canal water
TR1;TR2	Treatment 1; Treament 2
UC1; UC2	Undefined Consortium 1; Undefined Consortium 2
WT	wild-type

CHAPTER 1

INTRODUCTION

1.1 Motivation and historical socio-technological perspective

Across the entire course of prehistory, and throughout subsequent civilization, humans have been influenced by the activities of microbes along two major trajectories: enduring the negative effects of infectious diseases, and enjoying the benefits of microbial processes for sustainable food, health, and environment. In the present day, these influences continue, and frequently overlap, in the formal study of microbiology. That these opposing influences share common ground can be partly attributed to the fundamental nature of microbes such as bacteria, which is to combine an enormous diversity of metabolic processes and capabilities across species, while reusing the structural design of a single membrane-bound cell. Such physical and organizational constraint drives extreme efficiency, including reusing subcellular structures that are shared across microbial species and passed down along generations. Thus the ability and mechanisms of bacteria to colonize a surface, for example, is equally relevant to pathogenesis of an unfortunate human host, or increasing yields of farmer's crops by colonizing and fertilizing plant rood nodules.

Inspiration is an important driver of scientific progress; nature-inspired design has as much relevance today as it did when Leonardo Da Vinci built flying machines in the shape of a bird's wings. Nature's first engineers were microbes: the twentieth century marked the beginning of the first golden age of molecular biology, and enabled researchers for the first time to directly use molecular tools evolved by microbes billions of years ago in order to address technological challenges facing society. A relatively

recent example includes the isolation of extremophiles such as *Thermus aquaticus* by Thomas Brock and his undergraduate student, Hudson Freeze, of Indiana University, Bloomington. They isolated this thermophile from hot springs at Yellowstone National Park, and it was used to produce the source of heat-stable DNA Taq polymerase, which was key to the advancement of the polymerase chain reaction (PCR), the single most widely used procedure in molecular biology. This single innovation enabled PCR to become an automated high-throughput process, which was a crucial lynchpin in the development of genomics, bringing with it the second golden age of molecular biology in the 21st century (10) (9).

Since the discovery of *Thermus aquaticus*, many more microbes been isolated that have remarkable capabilities to grow in extreme environments, such as in conditions nearly 20 times as salty as the ocean, in radioactive waste that is 3000 times the strength of the lethal human dose, and in acid so strong it measures pH 0 (11). Bacteria and other microbes have been solving difficult chemical engineering challenges for billions of years in order to survive harsh environments during the course of evolution. They are also uniquely suited to solve one of the grand challenges of the 21st century: that of a sustainable global energy supply (12). According to the U.S. Energy Information Administration's International Energy Outlook for 2016, the global population will increase to 9 billion by 2050, driving energy use up by 40% (13). In order to meet this new energy demand, 26 trillion dollars of investment in new energy infrastructure must be developed, and will result in a atmospheric carbon dioxide concentration of 1000 ppm, over twice the level recommended by the International Panel on Climate Change. In addition, new oil fields will be smaller and fewer, and therefore new petroleum will be

derived from oil shale, or by converting coal and natural gas into liquid fuels, further driving up prices of fuel as well as basic necessities like food and clean water.

In the modern era, renewable energy has become essential to a sustainable food supply, adding energy to the services that microbes provide to society as part of our basic sustenance. Abiotic processes have recently been developed that enable direct conversion of CO_2 to ethanol at 63% yield using only a small amount of electricity-driven catalyst (14), but it is unclear whether this nanotechnology will be scalable to industrial levels. However, evidence in the fossil record shows that microbial phototrophs have a proven ability to consume carbon dioxide and produce liquid fuel on a global scale: most crude oil and other fossil fuels are derived from ancient algae and other photosynthetic microbes that formed massive blooms in bodies of water hundreds of millions of years ago. Furthermore, the first living organisms to cause global climate change were these same photosynthetic microbes, driving the oxygenation of the earth's atmosphere, and greatly increasing the mineral diversity of the Earth's crust (15).

Researchers in labs around the world are therefore investigating the use of photosynthetic microbes such as cyanobacteria to make renewable, carbon-neutral biofuels (16). However, historically, research of phototrophic organisms lags behind that of microbial pathogens. For example, the cyanobacterium *Prochlorococcus marinus*, on a per-organism basis, is estimated to be the most abundant species on Earth, and produces about 20% of the world's oxygen, in addition to being a major contributor to the global carbon cycle. Yet despite its importance and its ubiquity, *Prochlorococcus* was not discovered until 1991 (17). These relative priorities are maintained today, as can be seen in the percentage of genome and meta-genome sequencing projects related to medicine

(47.5%) compared to environmental microbiology (7.9%) on the Genomes Online Database (18), a storehouse of sequence information for 250,000 different organisms (including a minority of non-microbial species).

1.2 Dissertation objectives and outline

Knowledge gaps in our understanding of the basic microbiology of phototrophs are one of the bottlenecks that need to be addressed in order to bring microbial biofuel production to market. My research objectives in this dissertation aim to address strategic questions about the basic microbiology of the cyanobacterium *Synechocystis*, as detailed below and in the following outline of each chapter. A common theme throughout these chapters is the importance of the defining feature of all cells, namely, the cell wall. This feature separates the cell's inner contents from its outside boundary, regulates its interaction with other cells and the environment, and can serve as a reservoir of nutrients such as fixed carbon, among other functions, all of which are relevant to biofuel production in phototrophic microbes like *Synechocystis* (19).

Starting at the cell surface, my objective was to characterize the genetics and physiology of biofilm formation by *Synechocystis,* to determine how cells of a single phototrophic species interact with each other, and with abiotic surfaces such as glass and plastic, which are frequently used materials to culture microbial biofuel feedstocks. I chose to focus on biofilms due to their relevance to basic science and to biofuel applications, as described in more detail in the Background section. Next, I investigated differential regulation of the transcriptome in aggregated and unaggregated *Synechocystis* cultures in order to correlate regulatory networks on the inside of the cell with adhesion phenotypes on the outside of the cell. Finally, I investigated whether altered

Synechocystis cell surface phenotypes may improve biofuel yield at the scale of microbial populations by studying mixed-species cultures. I specifically tested whether *Synechocystis* mutants correlated with increased biofuel yield by reducing the ability of heterotrophic bacterial contaminants to grow in *Synechocystis* cultures.

A summary of each of these research aims is described for each Chapter in more detail below. In Chapter 3, I report that biofuel-producing cultures of *Synechocystis* underwent extensive biofouling of a large, outdoor photobioreactor under conditions correlated with nutrient limitation. I hypothesized that phototrophic bacteria such as *Synechocystis* are able to form axenic biofilms, and use cell surface structures such as pili, S-layer, and exopolysaccharides (EPS) to attach and adhere to surfaces, similar to other biofilm-forming heterotrophic bacteria. I developed a modified crystal violet assay and found that axenic wild-type (WT) *Synechocystis* forms biofilms of cells and extra-cellular material when shifted to altered nutrient conditions. Axenic WT *Synechocystis* does not form biofilms in nutrient-replete medium (BG11). Also, unlike WT *Synechocystis*, mutants lacking genes required for synthesis of cell surface structures such as type IV pili and the S-layer do not form biofilms under altered nutrient status. I conclude that pili and the S-layer are necessary but not sufficient for biofilm formation by *Synechocystis*: an additional adhesion-mediating factor must be induced, such as through dilution of growth medium, in order for pili and S-layer to facilitate biofilm formation.

To further elucidate the molecular mechanisms of cell-cell binding by *Synechocystis*, I developed an aggregation assay and found that both pili and the S-Layer were required for consistent aggregation, but mutants lacking *wza*, a gene required for exopolysaccharide production in *Synechocystis*, has a super-binding phenotype. I

compared outer membrane (OM) fractions of WT and mutant cultures under treatment and control conditions for aggregation. Coomassie stain of SDS-PAGE of these OM proteins showed no difference in protein profiles, and preliminary data suggest aggregated cells were not dispersed by treatment with cellulase. Overall, these data support that the molecular mechanism for aggregation by WT *Synechocystis* is synthesis and/or modification of cell surface structures by non-protein adhesive molecules in response to environmental stimuli inducing aggregation, such as change in growth medium status. In summary, I report that *Synechocystis* is a good candidate for a model organism for axenic phototrophic biofilm formation, and describe two new rapid, ecologically-relevant assays for further development of this area of study. I demonstrate the utility of these assays in identifying non-biofouling mutant strains of *Synechocystis*, and identifying environmental signals for rapid aggregation of wild-type *Synechocystis* biomass; both useful phenotypes for biofuel applications.

In Chapter 4, I investigated the relationship between aggregation and stress response in *Synechocystis*. The paradigm for bacterial aggregation is that it is an adaptive response to environmental stress. Both cellulose-dependent aggregation and stringent response (SR), a type of stress response, are widely conserved bacterial phenotypes that can be induced by nutrient limitation and other environmental signals; however, they use distinct regulatory pathways coordinated by different secondary messengers (c-di-GMP and (p)ppGpp, respectively). It may therefore be possible for bacteria to coordinate these two phenotypes separately, for example undergoing SR without aggregation, or vice versa. Previous studies of photosynthetic bacteria such as the cyanobacterium *Synechococcus elongatus* and the alpha-proteobacterium *Rhodobacter sphaeroides*

demonstrate that SR occurs upon shift to dark conditions. Additionally, several cyanobacterial species, including *Synechocystis*, have been shown to use c-di-GMP-dependent aggregation. I sought to better understand the possible role of SR in *Synechocystis* aggregation. Here I report preliminary data from RNA sequencing supporting the conclusion that aggregated cultures of *Synechocystis* have undergone SR. Additionally, aggregation has been shown to be a light-dependent process in *Synechocystis*; my data support that aggregated cells have not undergone SR from dark conditions such as self-shading during aggregation. This represents the first known evidence of SR correlated with aggregation in cyanobacteria, and the first report using an environmental signal other than darkness to induce SR in cyanobacteria. I summarized my findings by highlighting implications of the relationship between aggregation and SR on cyanobacterial lifestyle and application, such as sedimentation and biofuel production.

In Chapter 5, I assessed the microbial ecology of the photobioreactor (PBR). *Synechocystis* was previously engineered to secrete elevated levels of long-chain fatty acids such as laurate, a jet fuel precursor (20). An outdoor 4,000-liter PBR of *Synechocystis* culture that became contaminated by heterotrophic bacteria had reduced yield of fatty acids. Current practice for maintaining very large outdoor monocultures include use of chemical additives (salinity, alkalinity, and antibiotics) to create selective growth conditions for crop protection, including microalgae. I hypothesized that using additives well-tolerated by *Synechocystis*, such as salt, alkalinity and/or antibiotic, would inhibit growth of heterotrophic bacteria (heterotrophs) while allowing *Synechocystis* to flourish, improving biofuel yields. In the current study, I used regression analysis to make quantitative predictions of heterotroph growth in response to levels of added salinity,

alkalinity, and the antibiotic kanamycin in LB liquid media and also in *Synechocystis* supernatants. Defined Consortia of heterotrophs that included laurate-consuming species isolated from PBRs and also freshwater sources were used to reproducibly simulate the PBR contaminome under controlled laboratory conditions.

In LB liquid media, heterotroph growth responses were accurately predicted by levels of these three additives (NaCl, pH, and kanamycin) across diverse Defined and Undefined Consortia. In *Synechocystis* supernatants, presence of additives was able to protect laurate for over 72 hours by suppressing heterotroph growth. High-throughput 16S rRNA gene sequencing and PICRUSt metagenomic analysis (Phylogenetic Investigation of Communities by Reconstruction of Unobserved States) of Defined and Undefined Consortia growth were consistent with predictions that abundant contaminant taxa grown in presence of additives belong to an unrelated guild of phylotypes carrying a common 'minimum core' of 7 different adaptive trait marker genes conferring tolerance or adaptation to these three additives; abundant taxa in negative control samples had fewer and/or absent resistance trait genes. I concluded that this pilot study supports use of this modular platform of statistical modeling, sequence analysis, and artificial Consortia to quantitatively model bacterial contamination and biofuel productivity of PBRs under controlled conditions.

In Chapter 6, I summarized my findings and outline the implications of this work. I identify several high-priority studies to advance the most significant of these findings.

CHAPTER 2

BACKGROUND: TOWARDS A MODEL ORGANISM FOR AXENIC PHOTOTROPHIC BIOFILM FORMATION

2.1. Phototrophic biofilms are relevant to ecology and biotechnology

There are many more bacteria on Earth than there are stars in the known universe (21); most of them exist in multi-cellular communities called biofilms (22). Mixed-species phototrophic biofilms (containing heterotrophs and phototrophs) contribute to global nutrient cycling in terrestrial and aqueous environments (23-28). Phototrophs occur in all three domains of life, including diverse phyla distributed across the bacterial domain: *Proteobacteria* (purple sulfur and non-sulfur bacteria), *Chloroflexi* and *Chlorobi* (green sulfur and non-sulfur bacteria), *Cyanobacteria* (oxygenic phototrophs)*, Firmicutes (Heliobacteria)*, and *Acidobacteria*; each of these bacterial phyla have been identified in mixed biofilm communities (29-34). Among phototrophs, members of phylum *Cyanobacteria* are noteworthy both as primary producers capable of carbon and nitrogen fixation, and for their prevalence in biofilms across time and space. Contemporary stromatolites in Shark Bay, Australia and a few other locations (35-37) are cyanobacteria-containing microbial mats that mineralize carbonate as part of their metabolic activities (lithification). They are of particular importance to understanding how biogeochemical cycles were established on early Earth, as they occur prominently in the fossil record at least 3.4 billion years ago (15, 38-40) (although recent genomic evidence indicates these were likely ancestors of cyanobacteria that predate the evolution of oxygenic photosynthesis (41)). Additionally, the incidence of cyanobacteria in surface-associated consortia from extreme environments including hot springs (28), hyper-saline lakes (42),

desert crusts (43-45), and outside the International Space Station and simulated Mars surface conditions (46-48) support their relevance to astrobiological studies.

The ability of phototrophic biofilms to cycle carbon and other nutrients has obvious applications for bioremediation and bioenergy applications. Compared to traditional photobioreactors (PBRs), where cells remain suspended in culture, biofilm PBRs were over three times more efficient at removing sulfate from waste water effluent (49). Likewise, hydrogen production by biofilm PBRs was 25 times more efficient than traditional PBRs (50). However, in traditional PBRs or open ponds, unwanted biofilm formation (termed biofouling) can interfere with flow of growth medium, immersed sensor function, and light penetration. Studies of marine environments have shown that biofouling in the photic zone is dominated by phototrophs (51). Biofouling countermeasures in open ponds include plastic polyvinylchloride liners and raceway flushing, with limited success (52). Current practice to mitigate industrial-scale biofouling use biocides such as copper-containing paints for the hulls of ships; the environmental toxicity of heavy metals is driving research into alternatives including less toxic chemical paint additives (53-56). Knowledge of genetic and molecular mechanisms of biofilm formation by phototrophs would enable rational engineering of strains with customized adhesive properties, such as non-biofouling strains for traditional cultivation systems, or enhanced performance of biofilm PBRs.

The literature describing *in situ* mixed-species phototrophic biofilms is extensive, but there are few studies (reviewed below) describing biofilm formation by a single (axenic) species of WT phototrophic microbe; thus the role of phototrophs in colonizing environments in order to establish these essential biogeochemical cycles and

biotechnology processes is poorly understood. An as-yet untested paradigm of mixed-species biofilms is that these microbial communities are initiated by species other than phototrophs, which may lack the ability to initiate biofilm formation and are only able to join pre-existing biofilms. For example, one study found that surfaces pre-colonized by heterotrophs had more rapid subsequent growth by phototrophs (57).

Since there are no extant examples of growing axenic phototrophic biofilms, methods to utilize phototrophs in simulated biofilms for biotechnology applications tend to use physical or chemical means to artificially create multi-cellular communities; examples include immobilization of phototrophs such as *R. palustris* and *Synechocystis* on various thin-film substrates or alginate beads for use as a biocatalyst (58-61). Benthic sedimentary axenic biofilms have been developed using artificial sand as a biofilm substrate for *Prosthecochloris aestuarii* strain CE 2404, a green sulfur photolithotroph, and *Thiocapsa roseopersicina* strain 5811, a purple sulfur anoxygenic photoautotroph (62).

Colony formation on agar plates has been described as a type of biofilm; for example, studies with model heterotrophic bacteria *Bacillus subtilis* and *Salmonella enterica* use colonies on agar plates as a standard biofilm assay (63, 64); these species form colonies with pronounced macroscopic and symmetrical reproducible three-dimensional structures. Many species of phototrophic microbes can also form colonies on agar plates, and some have had three-dimensional aspect of the colonies characterized biochemically (65); this type of growth mode assay would be especially relevant to epilithic ecology, such as biodegradation of stone Mayan artifacts (66). However, a study of *Pseudomonas aeruginosa* suggests that colony formation, biofilm formation and

planktonic growth (liquid cultures) are distinct modes of growth and that colony protein profiles are more similar to that of planktonic cells (67).

Some mutant strains of *Synechocystis* (68, 69) and *Synechococcus elongatus* PCC 7942 (70, 71) (described in more detail in Chapter 3) with altered exopolysaccharide and/or other cell surface structures have been found to be aggregative and/or form biofilms in liquid cultures as detected by small flocks or adherence to glass test tube or flask surfaces. These mutants have revealed important insights into the molecular mechanisms of adhesion by phototrophs, but are perhaps less ecologically relevant models for biofilm formation than WT strains. WT *Synechocystis* can form biofilms on the bottoms of standing flasks of culture after several weeks' incubation in blue light, but the growth rate is linear rather than exponential in this condition, limiting the ability to compare these results to standard biofilm assays of exponentially-growing heterotrophic bacteria. Similarly, WT *Thermosynechococcus vulcanus* RKN is shown to aggregate when shifted from standard growth conditions to blue light in the cold (72). In summary, my review of the literature did not identify any extant studies establishing that an axenic WT phototrophic species from any domain of life is able to initiate biofilm formation in conditions analogous to characteristic biofilm studies conducted with heterotrophic bacteria, as described below, which limits our ability to perform comparative analysis.

2.2 Features of heterotrophic bacterial biofilm formation are conserved

In contrast to the dearth of literature describing mechanisms of biofilm formation by phototrophs, a vast and expanding literature describes the molecular mechanisms, genetic regulation, and physiological characteristics of biofilm formation by heterotrophic bacteria (73, 74), most notably that of human pathogens such as

Escherichia coli (75), *Salmonella* species (76), and *Pseudomonas aeruginosa* (77). Biofilm formation has also been well-characterized in a few other heterotrophic bacteria such as *Agrobacterium tumifaciens*, a pathogen of many agriculturally important plants (78), and *Caulobacter crescentus*, a model organism for cell cycle control and polar development (79). Although there is not a consensus definition of biofilm formation (partly because the qualities and mechanisms of forming biofilms varies greatly between species and also across different conditions by the same species), certain characteristic features of a biofilm have emerged, which were largely conducted using axenic exponentially-growing liquid-phase biofilm assays over the course of a few hours to days, using a submerged abiotic biofilm substratum such as a microscope slide coverslip. Specifically, biofilm formation requires cell energy input and is characterized by distinct stages of development from initiation of cell-surface contact to biofilm maturation, and results in a population of cells that are surface-bound and enclosed in an extracellular matrix (80). These characteristics likely do not apply to all bacteria, but are commonly encountered among bacterial biofilms studied to date.

2.3 Environmental and molecular signals induce biofilm formation

Initial attachment is frequently the focus of experiments to determine the environmental signals causing a transition from suspended to attached growth modes comprising the first stage of biofilm formation. These signals include but are not limited to change in nutrient status, quorum-sensing, or detection of specific surface molecules on host cells during infection by pathogens (reviewed in (73)). The effect of nutrient status (limited or replete) on biofilm formation varies greatly, depending on bacterial species and also environmental factors. For example, nutrient limitation enhances biofilm

formation by *Salmonella enterica* serovar Typhimurium (81), suggesting biofilm formation is a type of stress response. On the other hand, abundant sugars enhance biofilm formation by *Vibrio cholerae*, which could be interpreted as colonizing nutrient-rich environments as part of a chemotactic response (82). Similarly, change in osmotic pressure (salts, sugars, or other osmolytes) can either induce or inhibit biofilm formation depending on strain physiology of diverse heterotrophs (83-85).

Some strains generate their own biofilm signaling molecules. Quorum-sensing in bacteria such as *Vibrio fischeri* require a minimum concentration of specific metabolites such as acyl homoserine lactone (AHL) before attaching to surfaces (86). While AHL has been detected in environmental (multi-species) biofilms containing the cyanobacterium *Gloeothece* PCC 6906 (66), it is still unknown whether these biofilms are induced by quorum sensing from *Gloeothece*. I and others found no other studies that identified quorum sensing by a phototroph whether in a biofilm or other growth phase (87), although quorum-quenching signals were detected in *Anabaena* PCC 7120 liquid cultures (88). Removal of biofilm suppression is another initiation mechanism: a study of *Synechococcus elongatus* PCC 7942 found that WT secretes an as-yet unidentified small molecule into the growth medium that inhibits biofilm formation; thus certain mutant strains form biofilms as they are deficient at one or more steps in the inhibitor secretion pathway (71). In any case, once a signal is detected allowing a bacterial cell to transition from planktonic to sessile states, molecular cascades occur to coordinate wide-ranging physiological changes in the cell, including the down-regulation of genes required for swimming and up-regulation of extracellular matrix synthesis genes for adhesion; c-di-

GMP appears to be a conserved metabolite signal molecule coordinating this transition across bacterial species (89, 90), discussed further in Chapter 3.

2.4 Mechanisms of attachment require cell surface structures

The initial stages of biofilm formation (transient attachment and more permanent adhesion of single cells to a substratum) are mediated by cell surface structures such as filaments of protein and glycoprotein (pili, flagella) and adhesive exopolysaccharides (74, 91, 92). Flagella and pili are hypothesized to contribute to attachment by changing the charge distribution of a cell, thereby reducing the amount of electrostatic and hydrophilic repulsion between cell and substratum in aqueous solutions (93). The filamentous shapes of these appendages have reduced surface area compared with the cell body, thereby reducing the electrostatic and hydrophilic repulsion to be overcome in order to initiate contact with the substratum. These protein filaments are frequently tipped with adhesins such as glycoproteins, promoting surface adhesion. Pili and flagella also contribute motility to cells, which is thought to facilitate overcoming repulsion between cell and substratum as well. In addition, once pili have initiated contact with the surface, the pilin motors are activated and retract the pili into the cell, thereby drawing the cell body closer to the substratum in an energy-dependent process, until the pili are completely retracted and the cell body is in contact with the substratum (91). Mutants lacking pili and/or flagella are unable to attach to surfaces, and have reduced biofilm formation; those studies will be described in more detail in Chapter 3.

2.5 Towards a model organism for axenic phototrophic biofilm formation

Growth of axenic phototrophic biofilms under controlled laboratory conditions would enable controlled study of their molecular mechanisms, genetic regulation, and

physiology, but there is currently a lack of rapid, ecologically relevant assays for phototrophs that are analogous to those used in the existing canon of axenic heterotrophic bacterial biofilm formation. Furthermore, identification of genes and structures essential for a phototroph to form biofilms would inform rational engineering of strains with customized adhesive properties for different biotechnology applications. Despite the importance of phototrophic biofilms to ecology and biotechnology, there is currently a lack of genetically tractable phototrophic model organism(s) to use in an analogous manner as has been established with laboratory studies of heterotrophic bacteria biofilms. The cyanobacterium *Synechocystis* is a model organism for the study of oxygenic photosynthesis, is genetically modifiable with a fully annotated genome sequence, and as such increasingly used as a microbial biofuel feedstock strain (20, 94, 95). I hypothesized that phototrophs, specifically *Synechocystis,* are able to form axenic biofilms, and use cell surface structures such as pili, S-layer and EPS to attach and adhere to surfaces, similar to other biofilm-forming heterotrophic bacteria. To test this hypothesis, I screened the literature to identify genes required for cell surface structures important for biofilm formation in heterotrophic bacteria that had putative homologs in *Synechocystis*; these were targeted for deletion and their biofilm formation and aggregation were studied using modified assays.

Customizing the cell surface may confer added benefits to feedstock strains with regard to improved nutrient fluxes, increased permeability of exported biofuels, reduced sensitivity to pathogens or predators, or suppressing the growth of contaminants by reducing concentrations of soluble microbial products (SMPs) (19). Some of these aspects are described in Chapter 5.

CHAPTER 3

SYNECHOCYSTIS PCC 6803 FORMS AXENIC BIOFILMS AND AGGREGATES, WHICH REQUIRE CELL SURFACE STRUCTURES AND ARE INDUCED BY CHANGE IN NUTRIENT STATUS

3.1 Introduction

3.1.1 Overview and hypotheses

Synechocystis is model organism for photosynthesis, and has been genetically modified for biofuel production (20). Knowledge of the environmental signals and molecular mechanisms of biofilm formation by phototrophic bacteria would inform rational engineering of customized cellular adhesion for biofuel applications, as well as ecological insights into the physiology of mixed-species biofilms containing heterotrophs and phototrophs (23, 96, 97). A review of the literature did not identify any studies reporting a biofilm assay for WT phototrophic bacteria using exponentially-growing cultures, as is typically used for biofilm studies of heterotrophic bacteria. Thus, although a few recent studies of cyanobacterial biofilms have been reported with mutant strains, and also WT under slow-growing conditions, has given important initial progress in this area (described below), progress has been limited by the lack of a model organism and assays for axenic phototrophic biofilm formation enabling comparative biology studies with the canon of related work in heterotrophic bacteria. This area of research remains understudied relative to its importance in basic and applied microbiology.

I hypothesize that phototrophs, specifically WT *Synechocystis,* are able to form axenic biofilms in log phase, and use cell surface structures such as pili to attach and adhere to surfaces, similar to other biofilm-forming heterotrophic bacteria. To test this

hypothesis, I screened the literature to identify genes required for cell surface structures important for biofilm formation in heterotrophic bacteria that had putative homologs in *Synechocystis*; these were targeted for deletion. *Synechocystis* cell structures of interest to putative biofilm formation include the S-layer (surface layer protein), EPS (exopolysaccharide), and pili.

3.1.2 Role of S-layer in biofilm formation

Synechocystis S-layer protein (Sll1951) is visible in TEM as a honeycomb-like surface texture on wild-type cells (R. Roberson, unpublished) (98, 99). It is a glycosylated protein, which may contribute to adhesive or electrostatic properties of the *Synechocystis* cell surface. Deletion of S-layers enhances biofilm formation in *Bacillus cereus* (100) and *C. crescentus* (Yves Brun, personal communication).

3.1.3 Role of pili in biofilm formation and motility

Synechocystis has thousands of Type IV pili arranged peritrichously on its surface (101). These pili are glycosylated along their entire length; mutations causing altered glycosylation of PilA, the pilin subunit, cause motility defects (102). PilC has been shown to be a chaperone protein for assembly of PilA monomers into pili structures in heterotrophic bacteria (103). In *Synechocystis, pilC* mutants (*slr0162-0163*) are apiliate (bald) (104), consistent with this predicted role. Pili are required for biofilms in *E. coli* and *C. crescentus* (91, 105). Interestingly, knockout of a putative *pilC* homolog, *pcc7942_2069* confers a biofilm-forming phenotype to *S. elongatus* (71), which is believed to be related to the role of PilC in secreting an unidentified biofilm-inhibiting small molecule by WT strains of *S. elongatus*.

Motility is a feature of initiating biofilm formation in many bacterial species (74). Pili confer twitching motility to *Synechocystis* (106), which allows it to move over hydrated surfaces but not swim through liquid. Pili, EPS and S-layer have all been implicated in motility for cyanobacteria, including *Synechocystis*. Specifically, EPS is hypothesized to play a role in gliding motility in *Synechocystis*, independent of the glycosylated pili (106). S-layer (oscillin protein) (107) and EPS (108) are both required for motility in filamentous gliding cyanobacteria (43); their role in coccoid *Synechocystis* twitching motility has not yet been reported to my knowledge.

3.1.4 Role of EPS in biofilm formation: Wzy-dependent Group 1 capsular EPS.

Many cyanobacteria synthesize EPS (109, 110); here I review relevance of cellulose, Wza/Wzc dependent EPS, and released polysaccharides (RPS) such as colanic acid to *Synechocystis* EPS. *Synechocystis* EPS has been biochemically characterized using acid hydrolysis and chromatography of resulting monomers (111). The negative charge conferred on the cell surface by uronic acids and sulfate groups is a common feature of cyanobacterial EPS structure (reviewed in (110)). Bacterial EPS export systems are best characterized in *E. coli*, which includes Group 1 capsule export (112). Group 1 capsule is one of four major groups of capsular EPS characterized in *E. coli* based on features of biochemistry and genetic regulation. Group 1 capsule shares Wzy-dependent polymerization and Wza-dependent export with Group 4 capsule, but has different immunological properties (previously categorized under K-antigen groups), and unlike Group 4 capsule, is conserved in *Klebsellia* and *Erwinia* species.

A bioinformatic search of the *Synechocystis* predicted proteome revealed two putative homologs to proteins required for Group 1 capsular export in *E coli*.

Specifically, a BLASTP (113) search for Wza, Wzc, Wzx, and Wzy homologs in the *Synechocystis* predicted proteome identified putative homologs to Wzc and Wza, which act as a gating mechanism / polymerase and outer membrane porin of Group 1 capsule synthesis and export in *E. coli*, respectively (114).

Sll1581 is a putative homolog to Wza (28% identity, 42% similarity using default BLASTP search parameters) (this study and (115)). The predicted role for Sll1581 is consistent with its localization to the outer membrane of *Synechocystis* as determined previously by mass spectroscopy (116). Deletion of *wza* homologs in various heterotrophic bacteria results in loss of capsule (117) and also impaired biofilm formation (118-120). *sll1581* was deleted in *Synechocystis* and the resulting mutants had EPS levels about 25% of that for wild-type, but no change in released polysaccharide (RPS) level. This mutant showed spontaneous auto-sedimentation as measured by a 3-week standing flask assay of liquid cultures compared to wild-type cells; the biofilm phenotype of this mutant was not tested (121). A second putative homolog Sll0923 has 21% identity and 39% similarity to *E. coli* Wzc. I determined that the Walker A and B boxes and the C-terminal tyrosine-rich domain required for Wzc activity are conserved in this homolog (not shown). In a previous study, this mutant did not sediment, having the same sedimentation phenotype as wild-type (121). Interestingly, the *wzc* mutant had a less severe EPS defect, maintaining about 50% of wild-type EPS levels, whereas it showed a 50% reduction in RPS, compared to the *wza* mutant that had WT levels of RPS. It is unknown whether these mutants had altered EPS composition, in addition to EPS quantity.

Despite these two homologs, *Synechocystis* lacks putative homologs to Wzx or Wzy, which characterize Group 1 (and Group 4) capsule export, a Wzy-dependent process in *E. coli* (112). It may be that the functions of Wzx and Wzy in *Synechocystis* are provided by ABC transporters or other enzymes, similar to Group 2 and Group 3 capsule export in *E. coli*. This hypothesis was previously raised in the literature using bioinformatic comparison across many phototrophic phyla including diverse cyanobacteria (115), in addition to *Synechocystis*. Additional support for this hypothesis found that deleting genes originally identified in the *Synechocystis* genome as putative homologs in LPS O-antigen (lipopolysaccharide, comprising the outer leaflet of the outer membrane) transport had WT LPS but altered EPS quantity and quality, with different monomer ratios compared to WT EPS (69). The mutated genes *slr0977* and *slr0982* had homology to *wzm* and *wzt* in *E. coli*, whose products function together as an ABC-transferases in O-antigen LPS export across the inner membrane. Since Wzm and Wzt are exclusive to LPS O-antigen export in *E. coli*, whereas homologous ABC transporters KpsT and KpsM function in EPS export (122) it is possible that these *Synechocystis* putative ABC transporters are more accurately described as homologs to KpsM and KpsT, rather than Wzm and Wzt.

Thus my current model for Wza/Wzc dependent EPS synthesis and export in *Synechocystis* includes a hybrid of two canonical EPS export systems in *E. coli*: Group 2 (or 3) capsule biosynthesis by ABC-transporter activity of KpsMT homologs including Slr0977 and Slr0982, and Group 1 (or 4) EPS export by outer membrane porin and gating/polymerase enzyme homologs of Wza and Wzc, namely Sll1581 and Sll0923. Colanic acid is synthesized and exported in a similar way as Group 1 capsule in *E. coli*,

but it is under different genetic regulation and, because it lacks the Wzi anchor protein, is released into the supernatant rather than remaining attached to the cell (112, 123). I did not find a homolog to Wzi in *Synechocystis*, using BLASTP search default parameters (124). Thus I cannot eliminate the possibility that *Synechocystis* produces RPS analogous to colanic acid of *E. coli*, though if not, it may be that *Synechocystis* uses an alternate anchoring mechanism than Wzi.

3.1.5 Role of EPS in biofilm formation: cellulose

Cellulose is a component of cell-surface associated EPS in some bacteria. In heterotrophic bacteria, genes for cellulose biosynthesis have been best characterized in *E. coli* and *S. typhimurium* (*bcs* genes) where they contribute to biofilm formation (125); some homologs to *bcs* genes were found in cyanobacteria, but not others (115). However, cellulose has been detected in the EPS of several cyanobacterial species (72, 126) with homologs to CesA, the cellulose synthase conserved in eukaryotic plants (127). In two other studies, cyanobacteria closely related to *Synechocystis,* namely *Synechococcus* strain PCC 7002 (126) and *Thermosynechococcus vulcanus* RKN (72, 128) were shown to have cellulose-dependent aggregation.

Cellulose synthase genes are not found in all cyanobacterial species (127). *Synechocystis* contains one cellulose synthase motif DDD35QXXRW, in Sll1377, which has homology to CesA of *Thermosynechococcus vulcanus* RKN (query coverage showing regions of homology to 48% of the full Sll1377 protein length). However, in another study of 12 diverse cyanobacterial species, cellulose was not detected in *Synechocystis* or *Synechococcus elongatus* PCC 7942; these studies were presumably conducted under nutrient replete growth conditions. This survey included both

filamentous nitrogen-fixing species and coccoid-shaped non-nitrogen-fixing species (such as *Synechocystis* and *Synechococcus* species) screened for the presence of cellulose (in non-aggregated cultures) using four different methods, including nano-gold labeling, and x-ray crystallography. This study confirms presence of cellulose in 6 species, and is inconclusive for the remaining species.

A second line of evidence in the literature ties cellulose-dependent aggregation to environmental signals via the highly conserved secondary messenger, c-di-GMP (cyclic diguanosine monophosphate). This metabolite was first identified as required for bacterial cellulose production by the cellulose synthase BcsA in *Gluconacetobacter xylinus* (129). *S. enterica, E. coli* and *Pseudomonas fluorescens* have all shown aggregation via c-di-GMP dependent cellulose production. (129, 130). A series of studies shows that the cyanobacterium *T. vulcanus* aggregates at low temperatures in response to blue light (72, 128). In their three-step model, supported with mutational analysis, *in vitro* diguanylate cyclase activity and other data, SesA (Tlr0924) was shown to have diguanylate cyclase activity (formation of c-di-GMP) in response to blue light. Subsequently, the c-di-GMP is predicted to bind to cellulose synthase CesA (Tvtll0007), as has been shown with cellulose synthases in other bacteria. Finally, CesA activity results in synthesis of cellulose, which causes *T. vulcanus* cells to aggregate.

Not all cyanobacteria have protein sequence predicted for diguanylate cyclases necessary for synthesis of c-di-GMP (131). Therefore, it is likely that this c-di-GMP mechanism of cellulose-mediated aggregation is not universal across all cyanobacterial species. c-di-GMP levels have been correlated with aggregation in *Synechocystis*, which has 27 putative diguanylate cyclases. Specifically, constitutive expression of transgenic

diguanylate cyclase from *E. coli* that is known to be active in other species of bacteria was sufficient to cause aggregation and biofilm formation by *Synechocystis* in white light (132). In WT *Synechocystis*, levels of c-di-GMP from endogenous diguanylate cyclase activity are naturally low under white light and high in blue light; increase in biofilm and aggregation correlated with increase in c-di-GMP under blue light conditions, though this study did not report cellulose status.

Interestingly, the authors concluded that additional factors besides c-di-GMP levels may be governing these cell-binding phenotypes based on the observation that in green light, c-di-GMP levels were higher but biofilm and aggregation levels were still low. The same pattern was true for aggregation and c-di-GMP levels in green vs blue light for *T. vulcanus*. It may be that c-di-GMP levels must reach a certain unknown threshold before cell binding occurs, and mid-level c-di-GMP levels in green light are below this threshold. It is worth noting that growth rate correlates with c-di-GMP levels as reported in this study: fastest growth and lowest c-di-GMP in white light; intermediate growth and c-di-GMP in green light, and slowest growth/highest c-di-GMP in blue light. This raises the possibility that light wavelengths are indirectly influencing c-di-GMP levels via growth rate. This is consistent with a previous report suggesting that arithmetic (linear, rather than exponential) growth rate in blue light is attributed to reduced photosynthesis (133). If so, then growth in blue light corresponds to low cellular energy level for *Synechocystis*. Nutrient limitation such as carbohydrate starvation is frequently correlated with increased c-di-GMP levels in heterotrophs (134), but since heterotrophs get both nutrients and energy from their carbon sources, these data do not preclude that c-di-GMP is responding to energy limitation. This would be consistent with phototrophs

upregulating c-di-GMP levels during energy limitation as well, such as during growth in blue light, corresponding with reduced photosynthetic activity.

3.1.6 Summary of findings

In this Chapter, I report incidence of extensive mixed-species phototrophic biofilm formation in a large outdoor photobioreactor used to grow WT *Synechocystis*. Next, I adapted the crystal violet assay commonly used for biofilm study of heterotrophic bacteria and identified growth conditions which induce axenic WT *Synechocystis* cultures to form biofilms. I also developed a rapid aggregation assay to compare results of the biofilm assay for environmental conditions inducing rapid cell-cell binding behavior. I engineered targeted genetic mutations of genes *sll1581 (wza)*, *slr0923 (wzc), sll1951 (S-layer)* and *slr0162-0163 (pilC)* required for cell surface structures and screened these mutants for biofilm formation and aggregation phenotypes. Finally, I present preliminary experiments describing the cell surface biochemistry and motility of these mutants to correlate biofilm, aggregation, and motility data with cellulase sensitivity of aggregated cells, and protein measurements of outer membrane proteins. I summarize my findings of cell-cell binding in *Synechocystis* for testing in future studies, and discuss the implications of my model to biofuel production.

3.2 Materials and Methods

3.2.1 Culture growth conditions

Unless indicated otherwise, *Synechocystis* cultures were grown as follows: 100 mL starter cultures were grown in 500 mL Erlenmeyer flasks in BG11 medium with 50 µg/mL kanamycin sulfate as needed (135) to mid-log (OD_{730} ~0.5 – 0.6) at 50 µMol photons / m^2 / second continuous illumination and 120 rpm shaking with 0.8 mL/min air

bubbled through a 0.22 micron air filter in a growth chamber maintained at constant 30% humidity. Air was metered using a flow meter (Cole-Parmer). The air bubbled through the culture was additionally pre-humidified by passing through a side-arm flask of sterile dH_2O.

3.2.2 Assessing axenic status of bacterial strains

Axenic status of *Synechocystis* culture stocks was determined by T-RFLP to detect bacterial contaminants as described previously (136). Liquid cultures were prepared using sterile technique and cell pellets were collected via centrifugation for 5 minutes at 6,000xg. Decanted pellets were processed to extract genomic DNA using the Blood and Tissue DNeasy kit (QIAGEN) with indicated modifications for Gram-positive bacteria. The 16S rRNA gene was amplified from genomic DNA using Taq Master Mix PCR kit (QIAGEN) and universal bacterial primers: HEX-labeled 8F (AGA GTT TGA TCC TGG CTC AG) and unlabeled reverse primer 1392R (ACG GGC GGT GTG T) (137). Resulting amplicons were purified with QIAQuick PCR Purification Kit (QIAGEN) and digested with restriction endonuclease enzymes (138) HaeI, HhaI, MseI, and MspI (New England Biolabs). Digested fragments were analyzed with a 3730 capillary sequencer (Applied BioSystems) and sized via ROX 1000 ladder (ThermoFisher). Additionally, visual screening with light microscopy at 100x was used to detect non-bacterial contaminants. To the extent that contamination is detectable by these two methods, cultures were considered axenic if they did not have any non-*Synechocystis* peaks in resulting fragment spectra, and no non-*Synechocystis* cells were detected microscopically.

3.2.3 Modified crystal violet assay

The crystal violet assay was adapted to *Synechocystis* from methods described previously ('plastic binding assay') (91). Starter cultures were sub-cultured to 100 mL at $OD_{730} \sim 0.2$ and grown again to log phase as follows: for control cultures (no nutrient dilution), growth conditions were as described above; for experimental cultures, nutrient dilution was introduced by removing the water flask that humidified the air bubbled through the culture (described above), such that the culture flask would evaporate to ~84 mL volume over 24 hours, equivalent to a nutrient strength of approximately 1.20x BG11. Returning this culture to 1x BG11 at time=0 of biofilm assay (below) therefore introduces a shift from higher to lower nutrient condition.

Control and experimental cultures were pelleted by centrifugation at 6,000xg for 5 minutes, and resuspended in 1xBG11 to an OD_{730} of 0.05. Three mL of culture was added to each well of a 12-well plate (Corning Costar, Fisher Scientific) that contained thick (0.25-mm) glass coverslip as biofilm substratum (Fisher Scientific) that had been trimmed to fit vertically into the well using a diamond scribe (Ted Pella, Inc.). Plates with coverslips inserted, and with plate lids removed and inverted in cross-linker (Spectroline Spectrolinker XL-1500), were sterilized by UV radiation (254 nm) for 400 seconds at 1,500 $\mu W/cm^2$ (600 $mJoules/cm^2$). After inoculation, lids were sealed onto plates with Parafilm M and cellophane tape to minimize evaporation. Plates were incubated for 72 hours on a platform shaker at 72 rpm under 32 μMol photons / m^2 / second in a chamber humidified to 30%. Three wells per culture were normalized to % of WT positive control for each experiment. BG11 medium without inoculum was used as a blank.

Coverslips were removed and rinsed 10 seconds per side with a strong stream of BG11 from a squeeze bottle, and excess solution was wicked off by standing the coverslip edgewise on absorbent paper for 2 seconds. Coverslips were then stained by inserting in wells containing 4 mL of 0.01% aqueous crystal violet solution (w/vol) for 5 minutes in a separate tissue culture plate. Unbound stain was rinsed and wicked as above. Coverslips were dried in small weigh boats in ambient air overnight in the dark and used for qualitative assessment (imaging) or quantified by dissolving in 1 mL of DMSO with platform shaking for 20 minutes in the dark or until coverslip stain was removed (up to 45 minutes). Crystal violet absorbance was measured at 600 nm; the amount of absorbance is a proxy for quantifying the amount of cellular material bound to coverslips. The final culture OD_{730} of each well was also measured to correlate culture growth with biofilm growth.

3.2.4 Live-dead staining and imaging of biofilms

Biofilms were grown on glass coverslips as described in the crystal violet assay. 100 µL of BacLight live-dead stain (ThermoFisher) was prepared according to manufacturer's instructions was applied to biofilm and incubated for 15 minutes at room temperature in the dark. BacLight solution was wicked off as above and then the biofilm was placed on a chilled microscope slide on ice. 100 µL of 1.6% low-melt agarose in sterile isotonic solution (1%NaCl w/vol in dH_2O) was applied to the chilled coverslip. Coverslips with agarose overlay were attached to the interior of a small Petri dish with dental wax and then immersed in isotonic solution. Biofilms were imaged using a Leica TCS SP5 II with 10x or 63x DIC dipping lens. Sample fluorescence was excited by argon laser and live and dead stain collected through FITC and Texas Red filters, respectively.

Biofilm heights were calculated manually by measuring samples of interest using the pre-calibrated Z-axis of the SP5 II. For dual-species biofilm, log-phase WT *Synechocystis* cultures were prepared as usual, and then inoculated with stationary-phase *Pseudomonas putida* culture grown in LB broth to a 100:1 ratio of *Synechocystis:P. putida* ODs. Incubation of dual-species culture in flasks was continued as with *Synechocystis* growth conditions for 24 hours as described above to induce biofilm formation, and then the crystal violet assay was conducted as described previously.

3.2.5 Plasmid and Strain Construction

DNA manipulation was carried out using standard procedures (138). Suicide plasmids for replacing *Synechocystis* genes with a Km^R*sacB* cassette were constructed by four-part ligation into commercial vector pGEM 3Z (Promega), a pUC18 derivative. The Km^R*sacB* cassette from pPSBA2KS (139) contains markers for kanamycin resistance and sucrose sensitivity. PCR fragments of ~500 bp located upstream and downstream of each gene targeted for removal were amplified from the *Synechocystis* genome using primers from Table 3 to select locations of double homologous recombination flanking the gene of interest for each suicide vector. Flanking regions, pGEM 3Z, and the Km^R*sacB* cassette were stitched together by restriction digest and ligation. Briefly, NheI and EagI digested restriction sites were generated between the two flanking sequences to accommodate the digested Km^R*sacB* fragment, and BamHI and SphI (New England Biolabs) sites allowed insertion of these three fragments into the pGEM 3Z multi-cloning site. For example, I created the plasmid pΨ541 (for replacing *pilC* with Km^R*sacB*) by ligating digested PCR products amplified from upstream and downstream regions of *pilC* with digested Km^R*sacB* and pGEM-3Z. (For replacing *wzc*, BamHI and XbaI were used

to insert the Km^R*sacB* cassette, and SacI and SphI were used to insert the fragments to create pΨ546). Ligation reactions were transformed into competent *E. coli* (5-alpha, New England Biolabs) and transformants were screened by antibiotic selection and DNA sequencing.

Design of Km^R*sacB* suicide plasmids incorporated genomic context of each gene to avoid introducing polar effects of neighboring genes from altered putative promoter regions, as follows. For *sll1581*, the last 100 bp of the predicted open reading frame (orf) were left intact in order not to delete the region directly upstream of neighboring orf *sll1582*. Similarly, the putative promoter regions of *sll1581* and *ssr2843* overlap; therefore this region was not included in the replacement region in order to preserve native expression of orf *ssr2843* in *sll1581* mutants. For the remaining three mutant strains, both gene and upstream region (predicted promoter) were targeted for Km^R*sacB* replacement. For the intergenic region mutant, the genome coordinates from 1,418,681 bp to 1,418,995 bp between divergent orfs *slr2060* and *sll1956* were predicted to be a neutral site, as it did not show presence of predicted orf nor transcription activity, such as for non-coding RNA or small peptide encoding RNA not included in NCBI genome annotation according to (140).

3.2.6 Transformation and complementation

Mutants of *Synechocystis* were generated as previously described (69). Briefly, log-phase culture was centrifuged as above and cell pellet resuspended to 200 uL volume equivalent of OD_{730} = 2.5. Four µg of suicide vector was added to *Synechocystis* and incubated for 6 hours in BG11 without antibiotic, with intermittent shaking. The transformation reaction was plated onto a Nuclepore Track-etch membrane (Whatman)

on a BG11 agar plate. These were then incubated for 24 hrs at 30°C with 50 µmol photons/m^2/second. Following this incubation, membranes were transferred to a BG11 plate containing 50 µg/mL kanamycin and incubated for ~2 weeks until single colonies appeared. To ensure complete segregation of the mutants, colonies were re-streaked for isolation 3-5 times on BG11 with 50 µg/mL kanamycin. Kanamycin-resistant colonies were screened via PCR with primers internal to genes targeted for deletion to determine complete segregation.

Since natural competence in *Synechocystis* requires Type IV pili (101), I prepared electro-competent cultures of apiliate *pilC* mutants in order to transform them with complementation plasmids, as described previously (141, 142). Briefly, I centrifuged and resuspended cell pellets from 50 mL of log-phase *Synechocystis* culture in sterile 10% glycerol solution, with a final 500 µL volume. 60 µL aliquots of cells were mixed with 10 µL purified plasmid in up to 30 µL volume (H_2O, or 10 µL if in 10 mM TE buffer), using high concentrations of DNA (300 – 3000 ng/µL). Cells and DNA are added to 0.1 cm electroporation cuvettes and then pulsed with 12 kV/cm, 25 µF, 400 ohms setting (standard for electrocompetent *E. coli)*. Cells were resuspended in 900 µL BG11, transfer to test tubes with 2 mL additional BG11, and incubate as described previously until OD_{730} doubled. To select for transformants, cells were centrifuged and pellet resuspended in 500 µL supernatant for plating a range of volumes on selective medium (BG11 supplemented with 30 µg/mL streptomycin and spectinomycin). Complementation plasmids were created by amplifying gene of interest from *Synechocystis* genome via PCR, and cloning into expression vector pΨ568, a derivative of RSF1010 broad-host plasmid, created via restriction endonuclease digestion with AbaI and AbaII.

3.2.7 Isolation and analysis of outer membrane protein fractions

Cells were lysed and fractionated using standard methods (143). 15 mL volumes of culture were pelleted by centrifugation at 6,000xg for 5 minutes; cell pellets were stored at -80 °C. Pellets were resuspended in 1.2 mL of 50 mM ammonium bicarbonate buffer solution with HALT protease inhibitor (ThermoFisher) on ice. 600 µL of sample were added to 2 mL cryo-vials with 400 µL of 0.1 mm zirconium beads. Cells were lysed by bead-beating for 7 cycles; one cycle was comprised of 30 seconds beating at maximum speed, followed by 2 minute incubation on ice (Mini BeadBeater, BioSpec).

Whole cell lysates were fractionated using differential centrifugation. Lysates were transferred to new tubes. Unlysed cells were pelleted at 1,600xg for 5 minutes. Supernatants were transferred and total membrane fraction was pelleted at 16,000xg for 1 hour. Total membrane pellet was resuspended in 500 µL of 20 mM Tris pH 8 and 500 µL 0.8% Sarkosyl on ice, and incubated at 4°C with inversion for 90 minutes. Outer membrane fraction was pelleted at 16,000xg for 8-12 hours at 4°C. Supernatant was removed, and final pellet (enriched for outer membrane fraction) was resuspended in 50 µL of 20 mM Tris buffer pH 8. Samples were quantified via BCA assay (Sigma Aldrich). Volumes equivalent to equal protein (20 µg per well) were added to SDS loading buffer, heated at 100°C for 10 minutes, and loaded onto Mini-Protean TGX gradient acrylamide gels (4-20%) (BioRad Laboratories, Inc.) for PAGE. Protein bands were imaged via Coomassie stain.

3.2.8 Aggregation assay

100 mL of mid-log culture (OD_{730} of 0.5 – 0.6) was pelleted as previously and resuspended in either supernatant (negative control) or 0.8x BG11 (treatment condition)

and decanted into 100 mL glass graduated cylinders. The starting OD_{730} is measured and the standing cultures are incubated at 30 °C with illumination as described above. The final OD_{730} after 3-6 hours is measured by sampling 1 mL of culture from the 50 mL mark on the cylinder. Aggregation is reported as normalized percentage change in OD, as follows: [(Final OD – Starting OD) / Starting OD] x 100. Negative % aggregation in negative controls indicates that the culture density increased over time due to cell growth, and minimal aggregation occurred.

3.2.9 Cellulase treatment of aggregated cultures

Three mLs of aggregated cultures were transferred to 15 mm glass test tubes, and 100x stock preparations were added to final concentrations of 0.60 U / mL *Aspergillus niger* cellulase (Sigma-Aldrich), as described previously (72). An equal volume of water was added to a negative control culture. Cultures were mixed and incubated without shaking at 30°C in the light, as for cultivation conditions. After incubation, cultures were gently resuspended, and 1 mL aliquots were transferred to semi-micro cuvettes and allowed to settle for 1 hour.

3.2.10 Motility and phototaxis assay

Phototaxis assay was adapted from (104). Log-phase cultures were diluted to OD_{730} of about 0.25 and 10 µL spotted on motility agar (BG11 medium prepared in 0.5% Difco BactoAgar) in grid-lined square petri dishes such that inocula were oriented directly over grid lines. Plates were sealed in Parafilm M and incubated at 30°C and 30% ambient humidity under directional illumination (a dark box with a 30 µMol photons / m^2 /second light source at one end). Strains were graded as motile using qualitative assessment of colonies having blurred edges and having elongated away from grid line,

as compared to *pilC* negative control strain colony known to be amotile (104), which grows in a symmetrical disc centered on top of grid line and with crisp edges (Appendix B, Figure B.1). Alternatively, plates were streaked on motility agar for isolated colonies and placed in standard illumination; motile colonies were identified by larger size with hazy edges, and amotile colonies smaller with clearly defined edges.

3.2.11 Statistical analysis

Data were analyzed using two-tailed paired Student's t-test of at least three biological replicates, with alpha level at 0.05 for the null hypothesis (no difference between sample means). Differences between sample means were considered statistically significant if the resulting test statistic had a p-value <0.05.

3.3 Results and Discussion

3.3.1 Biofilm formation in outdoor PBR correlated to water hardness

WT *Synechocystis* cultures (SD100) were grown in a 4000 liter outdoor PBR. When cultures were inoculated into sterile growth medium prepared from hard (tap) water, I observed consistent and florid growth of green biofilms in the PBR (n = 3 biological replicates). Figure 3.1 presents representative images illustrating that the visible biofilm accumulated in characteristic stages from isolated colonies to thick confluent growth during one week of semi-batch PBR operation (Days 7-11). In subsequent rooftop PBR cultures with medium prepared with softened tap water, biofilms were no longer prevalent (n>3 biological replicates; data not shown). Under the conditions tested, my data are consistent with the hypothesis that biofilms containing *Synechocystis* form only when nutrients were reduced due to precipitation by hard water, and not present in nutrient replete conditions with no precipitation in softened tap water.

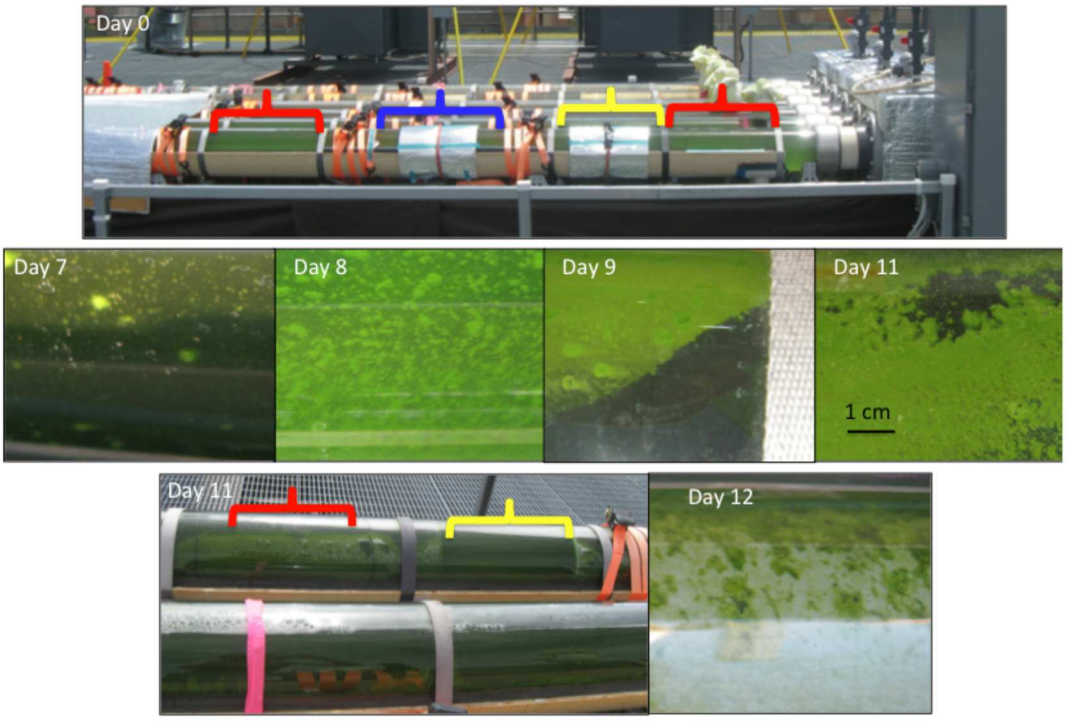

Figure 3.1. Macroscopic biofilm formation by *Synechocystis* cultures in outdoor PBR. Representative images of macroscopic biofilms from one PBR culture are shown growing in 4000 liter outdoor roof-top PBR inoculated with WT *Synechocystis* (n=3 biological replicates of PBR inoculation and operation without water softening step). Area marked with red bracket received full diurnal sun exposure. Area marked with blue bracket was continuously covered. Area with yellow bracket was only covered for the times of day with most intense illumination (2:30 – 3:30 p.m. daily). Reactor was operated in semi-batch mode, with lag phase corresponding to maintenance of culture density for the first week after inoculation (Day 0 -7).
Day 7 – Day 11: Macroscopic biofilm formation was observed in red bracket area of maximum illumination that conformed to typical stages of bacterial biofilm formation, starting with isolated colonies on day 7 (corresponding to day 2 of exponential planktonic growth); more isolated colonies on day 8; a confluent but thin lawn on day 9; and a thicker biofilm with some non-laminar shedding by day 11. Biofilm formation only occurred on surfaces receiving full diurnal sun exposure (red bracket); areas with no sunlight (blue bracket) or partial diurnal sunlight (yellow bracket) did not grow any macroscopic biofilms. On day 12, biofilms turned grey, corresponding with loss of planktonic culture density, and the experiment was terminated after 27 days operation.

3.3.2 Wild-type *Synechocystis* forms axenic biofilms when growth medium is diluted

The roof-top PBR construction enables biofilm sampling at the conclusion of experiments but not during operation; additionally, it is operated under conditions that are

not axenic. To assess axenic *Synechocystis* biofilm formation under controlled laboratory conditions, I adapted the crystal violet assay ("plastic binding assay" as described in (91)) typically used to study heterotrophic biofilm formation to *Synechocystis* biofilms. Specifically, I screened biofilm formation in a range of conditions including 0-120 rpm shaking, 4-50 umol photons/m^2/second, and a range of BG11 concentrations from 0.4x to 1.2x BG11, measured every 24 hours for 5 days (data not shown). Maximum biofilm formation as measured by crystal violet staining was determined to be 32 uMol photons/m^2/second at 30 °C, 72 rpm shaking, for 72 hours. It is noteworthy that unlike heterotrophic bacteria growth in batch mode in this assay, *Synechocystis* does not form biofilms unless shifted to diluted nutrient conditions via an evaporation and reconstitution process (see Materials and Methods), as shown in Figure 3.2, below. In Figure 3.3A, below, I verified that material stained with crystal violet was attached cells and extra-cellular material. In Figure 3.3B, below, scanning laser confocal microscopy revealed biofilms corresponding to these crystal violet data as isolated micro-colonies approximately 300 microns wide and 1-2 cells tall (n = 12 biological replicates).

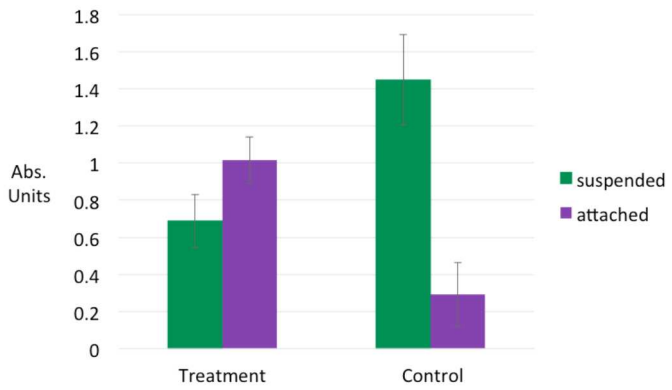

Figure 3.2. Adapted Crystal Violet Assay shows axenic biofilms require change in nutrient status. The crystal violet assay was adapted to include a growth medium dilution step (treatment) or no dilution step (control). Wild-type *Synechocystis* does not form axenic biofilms on glass coverslips under nutrient replete conditions (control) (p-value <0.05; N = 4 biological replicates per condition, 12 biofilm coupon samples per biological replicate).

3.3.3 *Synechocystis* requires cell surface structures to form biofilms

I genetically engineered knock-out mutations of genes required for *Synechocystis* cell surface structures that are related to biofilm formation in other bacteria, as identified by literature and bioinformatic search. Specifically, I used allelic exchange of the Km^R*sacB* marker to remove genes previously shown to be essential for pili (*pilC, slr0162-0163*), EPS (*wza, sll1581*), and S-layer (*sll1951*). I inserted the same marker at a neutral site in WT strain SD100 to create a kanamycin-resistant control strain SD525, in order to control for effect of growth under selection by kanamycin on biofilm formation. Three independent isolates of each fully segregated clone were confirmed by PCR and sequencing. I verified that *sll1581* and *sll1951* genes are not required for motility in SD500, a motile sub-strain of WT *Synechocystis* (Supplementary Figure B.1). Therefore, there are no motility-related changes upstream of the *pilC* mutation in the SD100 non-motile WT strain (104) that could potentially influence biofilm formation. The list of strains (by SD number) and plasmids (by pψ number) that were used in this study are

listed in Table 3.1; primers used are in Table 3.2. In Figure 3.4, below, both pili and S-layer are shown to be required for biofilm formation by *Synechocystis*, as measured by the modified crystal violet assay. The *wza* mutants appeared to have a growth defect under conditions used in the modified crystal violet assay (compare green bars in Figure 3.4). As growth and/or energy is required for biofilm formation in other bacteria (91), it could not be determined whether Wza-dependent EPS is required for biofilm formation by *Synechocystis*.

3.3A **3.3B**

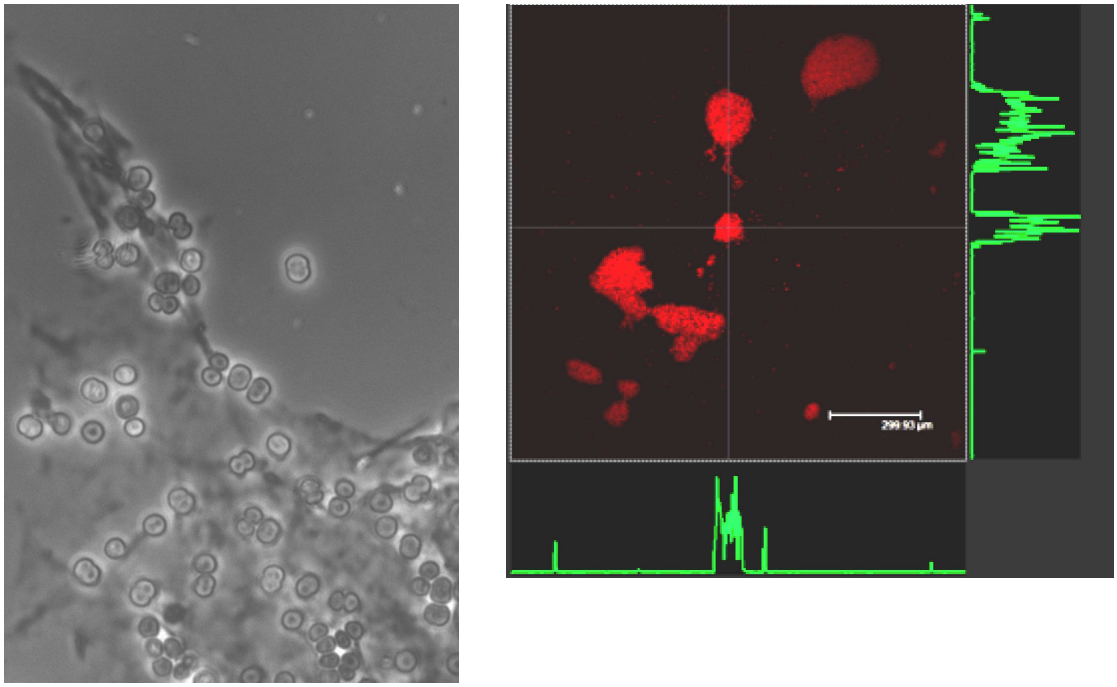

Figure 3.3. Microscopy confirms that absorbance measured in crystal violet assay is attached cells and extracellular material.
Figure 3.3A: Phase contrast (black-and-white) imaging with 100x objective lens was used to visualize biofilms grown on glass coverslips and then stained with crystal violet in the treatment condition; stained material corresponded to cells (~1.5 micron diameter) and extracellular matrix (ECM) (n=3 biological replicates). Control coverslips had no attached cells and no stained material (not shown).
Figure 3.3B: Scanning laser confocal microscopy was used to image auto-fluorescent cells in biofilms grown under treatment condition (without crystal violet staining) (n=12 biological replicates). Bar = 300 microns. Green Z-axis cross-sections of biofilms are shown in margins.

Table 3.1: List of strains and plasmids used in this study.

SD Number	Parent Strain	Mutation	Source
N/A	*Pseudomonas putida*	wild-type	Gift from Nielsen lab, ASU
SD100	WT Kazusa variant	wild-type	Gift from Vermaas lab, ASU
SD500	WT Paris variant	wild-type	Pasteur Cyanobacterial Collection
SD506	EPS-minus strain	*slr0977*	Fisher et al, 2013
SD515	Paris *wza*::KmR sacB	*sll1581*	This study
SD517	Kazusa *wza*::KmR sacB	*sll1581*	This study
SD519	Kazusa *pilC*::KmR sacB	*slr0162-0163*	This study
SD520	Paris *pilC*::KmR sacB	*slr0162-0163*	This study
SD522	Paris *s-layer*::KmR sacB	*sll1951*	This study
SD523	Kazusa *s-layer*::KmR sacB	*sll1951*	This study
SD525	Kazusa intergenic::KmRsacB	intergenic	This study
SD546	Kazusa *wzc*::KanSac	*sll0923*	This study
SD577	Kazusa *pilC*::KmR sacB + pPSI 568 *PilC*	*slr0162-0163*	This study
SD578	Kazusa *pilC*::KmR sacB + pPSI 568 *Wza*	*sll1581*	This study

pψ Number	Vector	Construct	Source
540	pGEM 3Z	wza up KanSac dn	This study
541	pGEM 3Z	pilC up KanSac dn	This study
543	pGEM 3Z	s-layer up KanSac dn	This study
545	pGEM 3Z	intergenic up KanSac dn	This study
546	pGEM 3Z	wzc up KanSac dn	This study
550	pGEM 3Z	wza complement	This study
552	pPSI 568	pilC complement	This study
553	pPSI 568	wza complement	This study
568	RSF1010	expression vector	Gift from Soo-Young Wanda
pPsbA2ks	pPSBA2	source of KanSac marker	Lagarde et al, 2000
540	pGEM 3Z	wza up KanSac dn	This study
541	pGEM 3Z	pilC up KanSac dn	This study

Table 3.2: List of primers used in this study.

Primer #	Primer name	Primer Sequence	Description
1	Up wza F NheI (Eag)	ggattggctagcattcatagcattcggccgatg	5' primer for upstream of wza
2	Up wza R SphI	cctggatacgacgcatgccatcatctaag	3' primer for upstream of wza
3	Dn wza F BamHI	gcttgcagggcataatttttggatccacaagattcc	5' primer for downstream of wza
4	Dn wza R NheI (stop)	ccaactttaagaaacaatgatgtagtcttagc tagcaccagtggttaaact	3' primer for downstream of wza
5	Up wzc F SacI	gcactgtccctatgcgagctcaagccagta	5' primer for upstream of wzc
6	Up wzc R BamHI	gcttgtaaggcaggggatccaccaact	3' primer for upstream of wzc
7	Dn wzc F BamHI (XbaI)	cgcttgatcacggatccatatctagaaataaa aaccagttcaga	5' primer for downstream of wzc
8	Dn wzc R Sph R	ggttcatcactcaaaagcatgctggcatcc	3' primer for downstream of wzc
9	Up s-layer F BamHI	gggcagtaagcgacgggatccagctcgtttaag	5' primer for upstream of s-layer
10	Up s-layer R Nhe!	ggatttaatctctaaatctgctagctaaagttacgg	3' primer for upstream of s-layer
11	Dn s-layer F NheI (Eag)	gcacttttcagacacttgctagcggccggggaaaa	5' primer for downstream of s-layer
12	Dn s-layer R SphI	ggttggtcttactatagcatgcaggtggtaacgga	3' primer for downstream of s-layer
13	Up pilC F BamHI	ccaatgctctgcggggatccttacgggaagatccg	5' primer for upstream of pilC
14	Up pilC R NheI	ggtcagatgattagggggctagcaccgaaaaacttatg	3' primer for upstream of pilC
15	Dn pilC F NheI (Eag)	gccgctagcgttgtgaagagagtacggccgcac	5' primer for downstream of pilC
16	Dn pilC R SphI	gcggcattcccaagtaaagcatgcgctctttaa	3' primer for downstream of pilC
17	pilC compl F NdeI	ccccctaatcatatgaccccaaactattaagc	5' primer for pilC
16	pilC compl R SalI	gtcacaagcaatcagtcgacagcagagc	3' primer for pilC
19	Up KanR F BamHI	gcctgcaagagaattttaataaccttggatcc gatcccaatcaa	5' primer for upstream of intergenic region
20	Up KanR R NheI	ggtataagttgttcagtttatttataccggag aaaccgctagcaataat	3' primer for upstream of intergenic region
21	Dn KanR F NheI (Eag)	gcaggctagcaacaacggccgcgaaggtttgaaag	5' primer for intergenic region
22	Dn KanR R SphI	gcaaaccaccttggcatgcgaaattaatcaacgggcagaa	3' primer for intergenic region

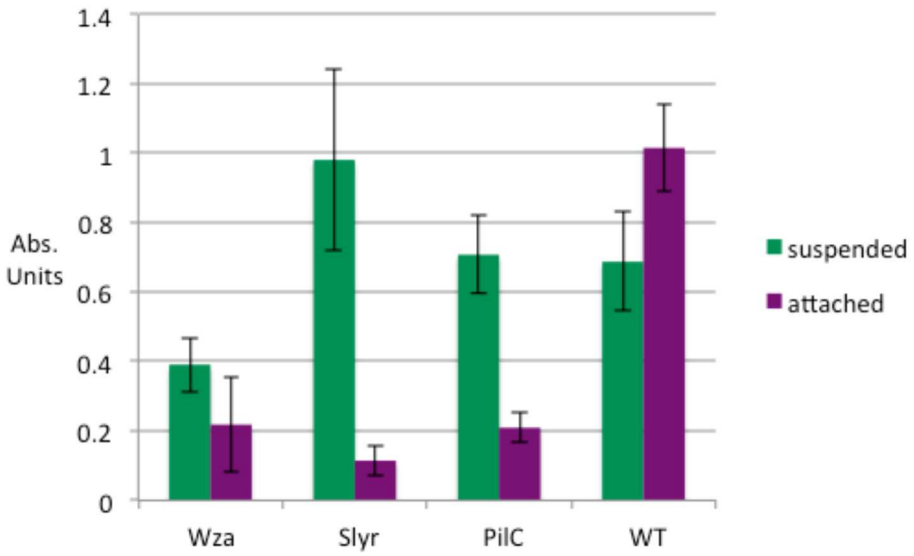

Figure 3.4. S-layer and pili are required for biofilm formation by *Synechocystis*.
Mutant and WT strains (see Table 3.1, above) were assessed using treatment condition as with Figure 3.2. Attached cells of mutant strains lacking S-layer (Slyr) or pili (PilC) were deficient compared to WT (p-value < 0.05 for all mutants. N = 4 biological replicates using two independently isolated clones of each mutant strain.) The *wza* mutant showed a growth defect under these conditions (green bars), so its biofilm status could not be directly compared with WT.

3.3.4 *Synechocystis* forms dual-species biofilms with *P. putida*.

One untested paradigm of mixed-species biofilm formation is that phototrophs are deficient in or unable to initiating biofilm formation, and occur in mixotrophic biofilms by joining communities that are established by heterotrophic microbes (23). However, when viewed macroscopically, roof-top PBR biofilm formation only occurred in illuminated areas (Fig 3.1); biofilm and planktonic community identity included diverse heterotrophic bacteria (clone library data not shown). The absence of visible heterotrophic biofilms in un-illuminated areas suggests that in mixed cultures that occur in this outdoor PBR, *Synechocystis* determines total biofilm growth, as *Synechocystis* is an obligate phototroph and does not grow in shaded areas.

To investigate, I grew axenic WT *Synechocystis* and *P. putida* cultures separately, and combined them to conduct dual-species biofilm analysis. I chose *P. putida* because it can grow on a multitude of fixed carbon sources (144) such as those making up the soluble microbial products (SMPs) of *Synechocystis* supernatants (136), and also is able to form biofilms (145). Cultures were combined in a 100:1 ratio of *Synechocystis*:*P. putida* cells/mL. This ratio was chosen to approximate environmental contamination of outdoor PBR *Synechocystis* cultures with heterotrophic bacteria, as being more relevant than a 1:1 ratio, for example.

In Figure 3.5, below, co-culture biofilms or attached single cells included *Synechocystis* and *P. putida*, or *Synechocystis* alone, but rarely *P. putida* alone (white arrow), as determined by auto-fluorescence and live-dead stain. Additionally I found the similar punctate structure occurring between axenic *Synechocystis* and axenic co-culture with *P. putida*. These preliminary data, while inconclusive, are consistent with the hypothesis that *Synechocystis* determines total biofilm formation and structure in axenic co-culture with *P. putida*, which could be occurring at the initiation, growth and/or maturation stages of biofilm formation. Additionally, the observation that no biofilm formation occurred in the roof-top PBR once the water softening step was implemented into the cultivation system process is consistent with the conclusion that the results with *P. putida* also apply to other heterotrophs, namely that in mixed cultures grown in autotrophic medium such as BG11, *Synechocystis* is driving biofilm formation in PBRs, not heterotrophs.

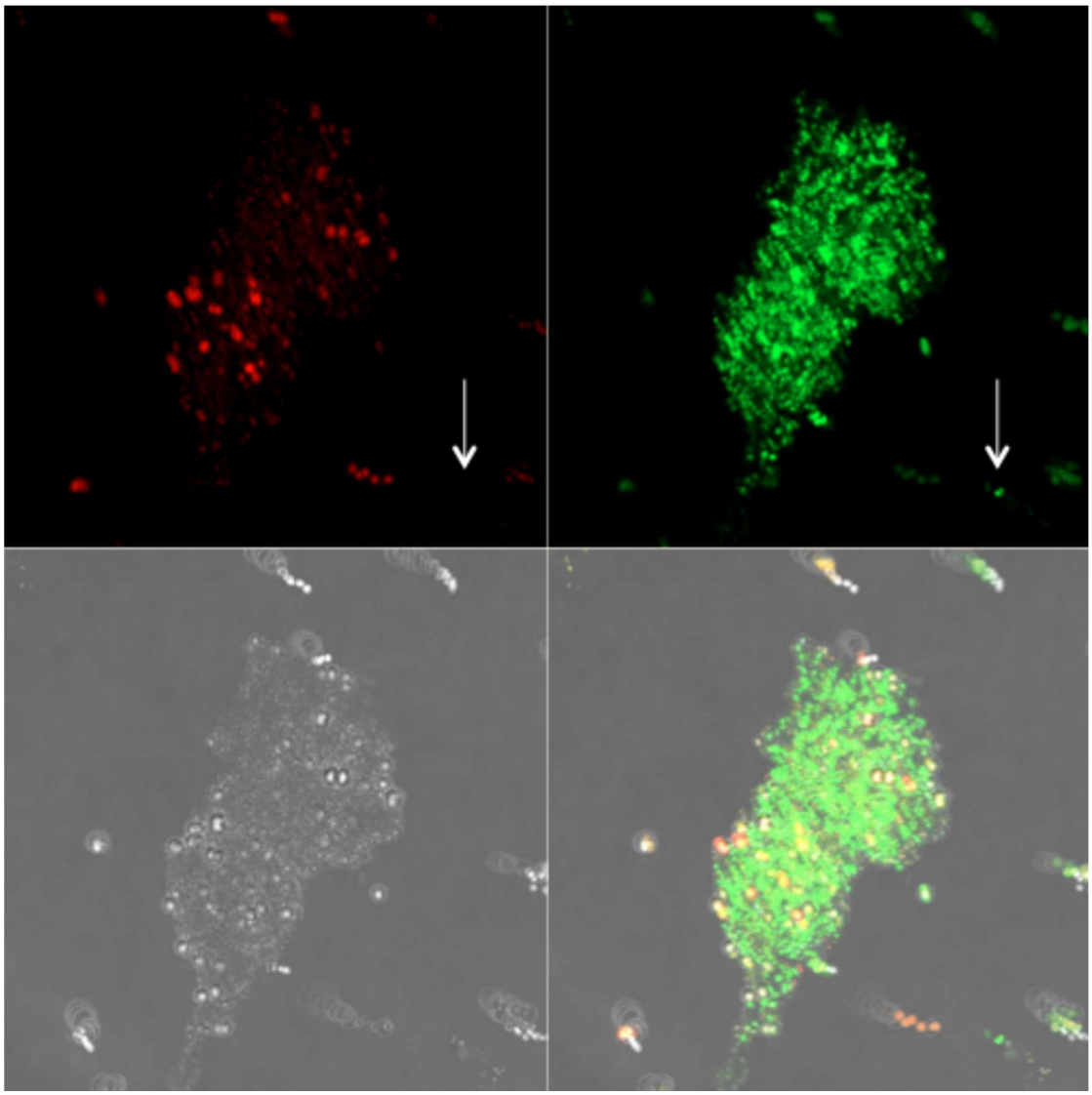

Figure 3.5. Co-culture of axenic *P. putida* and *Synechocystis* forms dual-species biofilms.
Biofilms imaged with a 40x objective dipping lens were induced as with treatment condition (dilution step), Figure 3.2. Shown is maximum projection of a Z-series stack of a dual species biofilm of *Synechocystis* and *P. putida* co-culture labeled with live/dead stain.
Red (upper left): All dead cells and live *Synechocystis* auto-fluorescence.
Green (upper right): All live cells.
Grey (lower right): Bright field image.
Yellow (lower left): Overlay of red, green, and bright field.
Isolated live *P. putida* can be identified by presence of green fluorescence in the upper left panel that does not correspond to red fluorescence in the upper right panel (white arrows).

3.3.5 *Synechocystis* aggregation requires cellular energy and is induced by change in nutrient status

Crystal violet data show that pili and S-layer are necessary but not sufficient for biofilm formation (Figure 3.4); presence of these structures do not cause WT cells to form biofilms unless some additional unknown factor is induced by nutrient dilution. An aggregation assay was developed to better understand both the environmental signals and molecular mechanisms of cell-cell binding in *Synechocystis*. Aggregation is related to biofilm formation in that it requires cell-cell binding and forms multi-cellular communities as flocs relevant to many of the same environmental and biotechnology applications (146, 147). Additionally, the amount of cellular material in biofilms grown on coverslips by *Synechocystis* was insufficient for commonly used biochemical assays for protein or RNA analysis. Therefore, I developed a rapid static aggregation assay to further characterize molecular mechanisms of cell binding by *Synechocystis.*

Wild-type *Synechocystis* cultures with a starting OD_{730} = 0.5 – 0.7 aggregate an average of 56% +/- 6% total biomass within 6 hours when shifted to reduced strength medium (0.8x BG11), compared to negative control cultures resuspended in supernatant (Figure 3.6, below), consistent with formation of biofilms (Figure 3.2, above). The role of cellular energy in aggregation was also investigated. Cultures induced for aggregation by shift to 0.8x BG11 remained suspended when incubated in the dark, or when the herbicide DCMU (3-(3,4-dichlorophenyl)-1,1-dimethylurea) was added to a 5 μM concentration in nutrient-diluted cultures incubated in the light. Dark conditions and

DCMU conditions both block electron transport for cellular energy generation (148, 149). When dark-incubated nutrient-limited cultures are shifted to illuminated conditions, they aggregate to the same degree as without dark incubation. Therefore, the aggregation phenotype requires cellular energy; i.e. it is not a passive sedimentation process facilitated by changes in electrostatic or hydrophilic cell-cell attraction due to change in nutrient status, for example, but requires active cellular energy production.

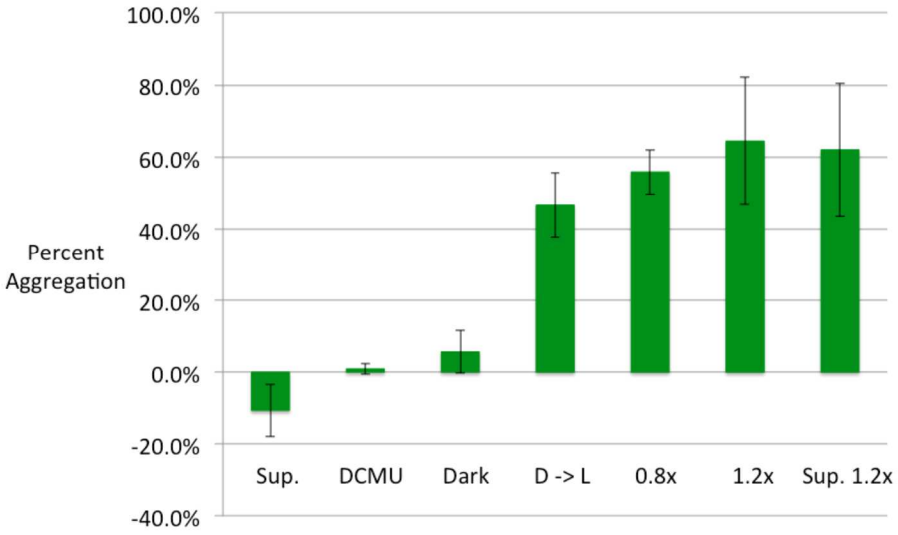

Figure 3.6. Wild-type aggregation requires cellular energy; is induced by change in nutrient status. All cultures were shifted to 0.8x BG11 to induce aggregation, unless otherwise indicated. Sup. = supernatant; negative control (cells were resuspended in supernatant). A negative % aggregation ('Sup.') indicated the culture increased in density and did not aggregate over the course of the experiment (~6 hours). DCMU = a.k.a. Diuron, an herbicide that inhibits cellular electron transfer. Dark = culture was incubated in the dark. D->L = 'Dark' culture shifted to light conditions. 1.0x and 1.2x = shifted to 1.0x or 1.2x BG11, respectively. Sup. 1.2x = the cells were resuspended in supernatant, and spiked with additional concentrated BG11 stock solutions for an approximate final concentration of 1.2x BG11 in supernatant.

3.3.6 Soluble microbial products do not influence aggregation

During the aggregation assay, conditioned supernatant is exchanged for fresh growth medium. In this step, the extracellular environment is modified in two ways: SMP are removed, and the osmotic/ nutrient / salt condition of the culture is altered. One or more of these signals could be influencing aggregation. For example, presence of SMP could inhibit cell-cell binding in supernatant negative controls, as was shown with *S. elongatus* (71), and/or removal of SMP could signal cells to induce aggregation through unknown mechanisms in treatment conditions, and/or change in nutrient status could induce aggregation in combination, either independently or in conjunction with SMP removal. I tested altering nutrient strength without removing SMP, which was accomplished by spiking 100 mL supernatant with microliter volumes of concentrated BG11 stock solutions to an estimated 1.2x BG11 final concentration. Aggregation when nutrient strength was increased by shift to fresh BG11 at 1.2x concentration served as a negative control. I found that aggregation in supernatant +1.2xBG11 was the same as that measured for aggregation with fresh 1.2xBG11. I conclude that removal of SMPs is not required for aggregation signaling or for mediating cell-cell binding.

3.3.7 Cell surface molecules modulate aggregation

In Figure 3.7 below, I compared aggregation phenotypes between WT and mutant strains under 0.8x BG11 conditions. The S-layer mutant had bi-modal aggregation phenotype: either a high level of aggregation (42% +/- 2%; n=2) or no aggregation (3% +/- 3%, n=2). This suggests that S-layer facilitates aggregation, but its absence can be overcome under commonly occurring yet unknown conditions. As the S-layer mutant is also deficient in biofilm formation, it is possible that S-layer is important for initial

attachment, and this plays a bigger role for attachment to glass than it does for cell-cell binding. Mutants lacking *wzc* had WT levels of aggregation, whereas mutants lacking *wza* had enhanced levels of aggregation. This is consistent with previously reported results showing that a *wza* mutant sediments more readily than a *wzc* mutant, which correlates to less cell-bound EPS in the *wza* mutant compared with the *wzc* mutant (25% vs 50%, respectively) (121). This suggests that capsular EPS production promotes dispersal of cells, and absence of EPS creates a super-binding phenotype due to increased facility of initiating cell-cell contact.

The *pilC* mutant strain was deficient in aggregation; complementation restored WT aggregation, indicating that any unknown spontaneous secondary mutations in the *pilC* mutant genome background did not contribute to the aggregation defect phenotype. The role of pili in aggregation may be due to facilitating cell-cell contact via glycoproteins and/or overcoming electrostatic or hydrophilic repulsion. PilC, as a cytoplasmic chaperone in PilA subunit export, may also facilitate export of an aggregant, either directly or through assembled hollow pili. In summary, my current model is that aggregation is energy-dependent, induced by changes in nutrient / salt / osmotic strength, but not removal of SMPs, in a process that requires pili, is facilitated by S-layer, and is reduced but not prevented by *wza*-dependent cell-bound EPS.

3.3.8 Characterization of cell surface biochemistry to identify putative aggregation molecules.

As with biofilm formation, pili and S-layer are necessary but not sufficient for aggregation by wild-type *Synechocystis*: an additional factor induced by change in growth medium status is required for aggregation to occur. I hypothesized that WT

Synechocystis is producing novel unknown adhesive molecule(s) (aggregant(s)) on its surface in response to changes in growth medium, causing aggregation. To detect these

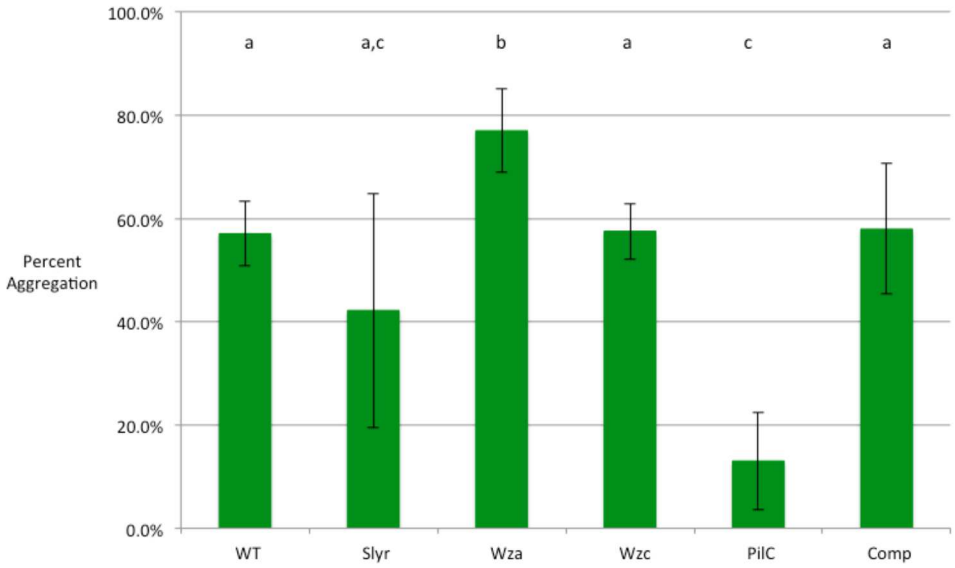

Figure 3.7. Cell surface structures modulate *Synechocystis* aggregation.
All cultures were shifted to 0.8x BG11. WT = wild-type. Wza, Wzc, PilC, Slyr = mutant strains lacking proteins indicated; Comp = complementation strain for mutant lacking PilC. For details on strain construction, see Table 3.2. Columns with different letters above them have statistically different amount of aggregation, p-value < 0.05.

putative aggregants, I isolated outer membrane protein fractions of WT and mutant strains under treatment and control aggregation conditions (four biological replicates per condition). Samples were split before loading on gels to include both boiled and unboiled preparations of proteins, as some proteins are heat labile. As seen in Figure 3.8, below, I did not identify any putative protein aggregants (adhesins) that were expressed at higher levels in the treatment (aggregated) cultures vs negative control, as determined by differential band patterns of Coomassie stained gels analyzed by SDS-PAGE. This result may indicate that aggregation is not mediated by synthesis of outer membrane proteins, although more definitive conclusion would require identification and quantitation of

specific outer membrane proteins under each growth condition, as proteins of more than one identity can co-migrate in a given band.

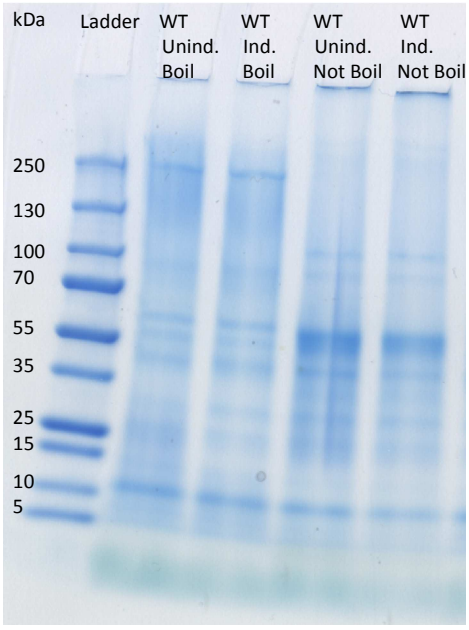

Figure 3.8. SDS-PAGE of outer membrane proteins shows no difference between aggregated and un-aggregated cultures.
Ind. = aggregation induced by shift to 0.8x BG11; Unind. = negative control cultures resuspended in supernatant. Boil = sample was boiled before loading onto gel; Not Boil = sample not boiled before loading onto gel.

3.3.9 Degree of cell aggregation is not affected by treatment with cellulase

Although previous reports did not detect cellulose in *Synechocystis* (127), c-di-GMP-dependent aggregation has been reported in this species (132), which is often correlated with cellulose-dependent aggregation, including for cyanobacteria (72, 128). Aggregated cells of the cyanobacterium *T. vulcanus* were visibly dispersed by treatment with cellulase, consistent with the role of cellulose in causing aggregation in this species (72). I used the cellulase assay described for *T. vulcanus* to test for role of cellulose in *Synechocystis* aggregation. As seen in Figure 3.7 below, I saw no dispersal of aggregated

cells in cellulase-treated cultures compared to a negative control. This result suggests that, unlike *T. vulcanus*, cellulose is not required for aggregation in *Synechocystis*. However, these data are preliminary and additional experiments testing the activity of the cellulase enzyme and for the presence of cellulose in extracellular matrices of cells are needed for definitive conclusions. It may be that additional aggregants such as proteins also contribute to aggregation in *Synechocystis*, or less likely, that cellulose plays no role in *Synechocystis* aggregation.

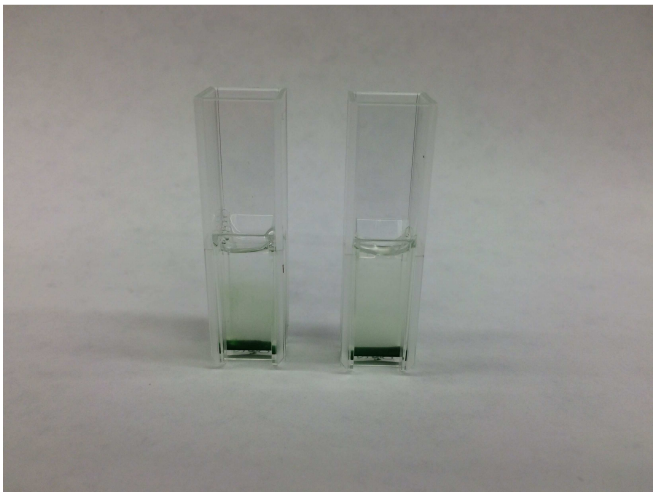

Figure 3.9. Cellulase treatment does not disperse aggregated *Synechocystis* cells. Aggregated wild-type cells were treated with cellulase (left) or an equal volume of cellulase-free buffer (right) and incubated overnight. 1 mL samples were transferred to cuvettes, and cell dispersal was measured by absorbance of suspended cells, as described previously, to evaluate role of cellulose in aggregation. No qualitative or quantitative effect of cellulase was detected (n = 4 biological replicates).

3.4. Conclusions

3.4.1 *Synechocystis* forms axenic biofilms using the modified crystal violet assay

These results show *Synechocystis* is able to form log-phase axenic biofilms (Fig. 3.2) and aggregates (Fig. 3.5). I conclude that *Synechocystis* is a suitable model organism for phototrophic biofilm formation, which addresses a significant gap in the field of microbiology. I also report the development of two rapid assays relevant to ecological

and biotechnological studies of axenic cell-cell binding under controlled laboratory conditions, namely a modified crystal violet assay and an aggregation assay, which enable comparative biological studies with the canon of axenic heterotrophic biofilm formation. I demonstrate the utility of these assays in performing mutational analysis of cell surface structures required for cell-cell binding under these two conditions, namely pili and S-layer, and show that dual-species biofilm microscopy is supported by these methods. These findings include the report of a non-biofouling strain of *Synechocystis*, the *pilC* mutant SD519, which would be advantageous for use as a feedstock strain in planktonic PBR or open ponds. Additionally, I used these assays to determine that change in nutrient status of WT *Synechocystis* cultures is one possible environmental signal for rapid, economical biomass harvesting method convenient to bioenergy applications. It is also worth noting that neither Wza nor S-layer are required for phototactic motility (Supplemental Figure B.1), indicating that *Synechocystis* uses some other source of extracellular material to facilitate movement across surfaces (106).

3.4.2 Mutational analysis supports novel role for Wza-dependent EPS in promoting dispersal of cells in planktonic cultures

Overall, my evidence supports a model of cell-cell binding that is regulated by two different mechanisms depending on growth status. During nutrient-replete planktonic growth, the negatively-charged EPS keeps cells distributed by electrostatic and possibly hydrophilic repulsion; this could benefit the cell by limiting self-shading that would otherwise be caused by sedimentation (121) or transient contact in cell suspensions (150). Under conditions of altered nutrient status, a second aggregation mechanism over-rides this cell-cell repulsion through unknown means that likely involves export of a non-

protein aggregant such as cellulose or other component in response to environmental signals, based on results in this study and also assuming similar mechanisms to those previously reported in other cyanobacteria. Overlaying of the capsular Wza-dependent EPS with an additional layer of new material may compensate for the electrostatic repulsion of Wza-dependent EPS by creating a physical bridge across intercellular distances, while also promoting cell-cell binding through electrostatic and/or hydrophilic attraction or adhesion by the new aggregant material. I note that, compared with heterotrophic bacteria, which use Wza-dependent Group 1 capsular EPS to promote biofilm formation, in *Synechocystis* and possibly other cyanobacteria such as *F. diplosiphon* (132), this cell surface structure prevents aggregation under nutrient replete conditions. If this trend holds true with study of additional cyanobacteria, it represents a new paradigm in bacterial biofilm formation, and illustrates how development of this understudied field of axenic phototrophic biofilm formation may yield interesting insights into molecular mechanisms of the divergent evolution of biofilm formation between phototrophs and heterotrophs, giving a new perspective on how pathogens like *E. coli* adapted biofilm formation as part of the infection process. An additional definitive comparison would be to assess the aggregation and sedimentation phenotypes of the *E. coli wza* mutant under similar conditions as for *Synechocystis* in this study.

Environmental signals inducing aggregation include both increase and decrease in nutrient strength (Figure 3.6), as well as in blue light (132). Whether these diverse environmental signals are part of the same pathway related to energy limitation, or are separate pathways to induce aggregation, is undetermined. Based on my results, I describe here one possible parsimonious molecular model for cell-cell binding during

Synechocystis aggregation. The cell regulates this phenotype in response to environmental change. Two-component signal transduction systems have been characterized as detecting and regulating response to diverse signals, including changes in nutrients, salt, and osmotic pressure (151-154); I propose that the environmental signals for aggregation are likely also detected by the cell through as-yet undetermined two-component system(s), which then activates the c-di-GMP-dependent aggregation pathway. Although the data reported here do not allow distinction between different stages of biofilm formation or aggregation, my results are consistent with a model of passive cell-cell contact facilitated by pili and S-layer, and inhibited by Wza-dependent EPS (Figure 3.7).

Over the course of 2-3 hours, transcriptional changes initiated by the two-component regulatory system induce energy-dependent synthesis and export of unknown adhesive molecule(s). This process does not require Wza/Wzc proteins (Figure 3.7) so it is not caused by increased export of polysaccharide analogs to *E. coli* Group 1 capsule or colanic acid. My preliminary data also contradict cellulose as the aggregant, as my cells were not dispersed upon treatment of cellulase, but additional control experiments are needed for definitive conclusions. PilC, a cytoplasmic chaperone of PilA export, may be directly required for exporting this putative aggregant, or indirectly enable aggregant export through Type IV pili, which enable transport of molecules related to cyanobacterial adhesion (71). As I did not detect differential expression of membrane proteins in aggregated cultures, my data support that the unknown aggregant may be a non-cellulose, non-colanic acid polysaccharide. Biochemical characterization of

supernatants and ECMs via total carbohydrate measurements are underway to test this theory.

3.4.3 Implications for naturally-occurring phototrophic biofilm formation

The extent to which other phototrophic microbes are able to initiate axenic biofilm formation during the modified crystal violet assay or other means remains to be tested. As photolithoautotrophs such as *Synechocystis* have one of the few metabolic profiles able to grow in environments without biotic resources such as fixed carbon and fixed nitrogen, it is possible that one of their ecological roles is colonizing surfaces that are initially uninhabitable by heterotrophic microbes (155). If so, it may be that many microbial phototrophs are able to initiate biofilm formation, though not necessarily under the same growth conditions described in this study.

The lack of macroscopic biofilms in shaded areas of the roof-top PBR, and the similarity of microscopic appearance of axenic *Synechocystis* biofilms on glass coverslips with dual-species biofilms co-cultured with *P. putida,* are preliminary evidence that phototrophs are driving the total biofilm formed in mixed cultures under those conditions. Whether this represents a generalizable paradigm to other growth conditions or phototrophs is undetermined; however, the assays and model organisms to study axenic phototrophic and defined synthetic community biofilms such as those described in this study are a useful tool to address these questions.

CHAPTER 4

COMPARATIVE TRANSCRIPTOMICS SUGGEST THAT AGGREGATION BY *SYNECHOCYSTIS* PCC 6803 IS CORRELATED WITH STRINGENT RESPONSE IN THE LIGHT

4.1 Introduction

Stringent response (SR) is one of several known highly conserved stress responses in bacteria that entails rapid coordinated shifts in multiple cellular pathways to adapt to environmental signals, including nutrient limitation (reviewed in (156)). Originally described in *E. coli*, the name SR refers to the stringency or restricted condition of reduced RNA synthesis under nutrient limitation in WT, in contrast to the so-called *rel*axed response in a *relA* mutant, which does produce RNA under nutrient limitation (157, 158). A universal feature and criterion of SR is use of secondary messenger (p)ppGpp or ppGpp, guanosine (penta or) tetra-phosphate. In heterotrophic bacteria, this metabolite interacts directly or indirectly with sigma factors (which are required for RNA polymerase activity) and other regulatory molecules to effect rapid large-scale synchronized changes in transcription levels. Levels of this poly-phosphorylated guanosine act as an alarmone, and are regulated in Gram-negative bacteria by the relative activities of a synthase RelA and a hydrolase SpoT (which also has limited (p)ppGpp synthase activity in response to other nutritional signals (159)). In *Firmicutes* and other Gram-positive bacteria such as *Bacillus subtilis*, (p)ppGpp regulates activity of RNA polymerases indirectly through controlling levels of purines, especially GTP (160).

Many bacteria, including *Synechocystis* (161) include both synthase and hydrolase activities as separate domains of a single protein, termed a RelA-SpoT homolog, or RSH (162). In *E. coli*, the activity of RelA is determined by conformational changes of the enzyme when bound to ribosomes lacking sufficient charged tRNA (163). While the *Synechocystis* RSH gene was able to complement (p)ppGpp synthase activity in an *E. coli* null mutant, the mechanism for (p)ppGpp regulation of cyanobacteria has not been characterized. Phylogenic analysis shows that essential motifs for mechanisms of action of (p)ppGpp in heterotrophs, such as by binding to ribosomes or modulating GTP levels, are not conserved in cyanobacteria (164, 165).

SR is an adaptive response to stress that confers survival advantage to the cell by down-regulating pathways related to so-called "house-keeping" functions of normal cell growth and proliferation, such as those regulated by sigma 70, while up-regulating pathways to activate stress responses, regulated by alternative sigma factors such as sigma S (RpoS), sigma 54 and sigma 32. The effect of SR in *E. coli* and other heterotrophic bacteria has been correlated with transition to stationary phase (156, 157, 166), as well as increased virulence of log-phase cells (167), including formation of multi-drug resistant persister cells (158) and induction of toxin-antitoxin bacteriophage defense mechanism (168). In the absence of SR, such as with mutant strains of *E. coli* lacking (p)ppGpp, cells will have the same proteomic profile in stationary phase as in exponential phase, causing much reduced survival rates in stationary phase compared to WT stationary-phase cells (169).

Genes and processes specifically affected by SR vary across different bacteria and growth conditions (158), but frequently include up-regulation of trans-translation (a

mechanism for rescuing stalled ribosomes due to amino acid shortage (170)) as well as amino acid biosynthesis and uptake, proteolysis, universal stress protein A (166), glycolysis and/or glycogen catabolism (171), and osmotic and other stress response genes, as well as some phage promoters (172). Genes down-regulated during SR are largely related to macromolecule biosynthesis, such as the afore-mentioned rRNA synthesis and elongation factors, DNA replication genes (173), and cell growth (fatty acids and peptidoglycans, for example) (174). In *E. coli* and also in Gram-positive bacteria, (p)ppGpp has also shown to directly interact with certain groups of proteins, including GTPases, thereby inhibiting their role in initiation or elongation of protein synthesis (175).

Environmental signals that induce SR include nutrient limitation and other stressors. Amino acid starvation is a nearly universal activator of SR across all bacteria studied thus far, with the exception of *Vibrio* spp. (156). Acid or alkaline stress response and heat shock have also been shown to induce SR in various bacteria (156). Whereas in *E. coli* and other species, amino acid starvation is sufficient for SR activation, in the oligotroph *C. crescentus*, SR required both amino acid starvation and also a second limitation of nitrogen or overall carbon supply (176). *R. sphaeroides*, an alpha-proteobacterium capable of anaerobic photosynthesis, induces SR upon shift from light to dark (177); *S. elongatus*, a cyanobacterium, also shows SR upon shift to dark (178). An auxotrophic mutant of *R. sphaeroides* had a SR when deprived of the amino acid leucine (177).

SR has been correlated with cell-cell binding as biofilm formation in many heterotrophic pathogens. This is consistent with the essential role of (p)ppGpp in

regulating a large portfolio of pathogenic phenotypes related to invasion, survival and persistence during infection of hosts by these bacteria, which may or may not include biofilm formation (179). In *E. coli*, biofilm formation is (p)ppGpp-dependent, but only under specific growth conditions (slow growth rate and also serine limitation) (180). Enterohaemorrhagic *E. coli* deficient in (p)ppGpp production loses adherence required for attaching to host cells, in addition to losing expression of pathogenicity islands required for invasion and destruction of host cells (181). Similarly, *Listeria monocytogenes relA* mutants were also deficient in both surface attachment and also virulence (182).

Similar to biofilm formation by pathogens, the generally non-pathogenic oligotrophic bacterium *C. crescentus*, which has a motile cell and an attached cell over the course of its life cycle, increases (p)ppGpp during transition to attachment as part of a larger regime change in physiology, including becoming competent for cell growth and division. Unlike other bacteria, higher (p)ppGpp levels during nutrient limitation correspond to the motile cells in this species, rather than the attached cells (183). *Myxococcus xanthus*, which feeds on other bacteria for its primary food source, has a feedback mechanism that allows it to continue to form (p)ppGpp-dependent fruiting bodies (multicellular aggregates) even when amino acids are not limiting (184).

Generalizing from these results in heterotrophs, the mechanisms and conditions of (p)ppGpp-dependent cell-cell binding to vary by species and are part of a larger physiological adaptation to the specific lifestyles of the bacteria. Therefore, it is plausible that aggregation or other forms of cell-cell binding is not a requirement of SR under all conditions. Consistent with this view, a study of the cyanobacterium *S. elongatus*

showed that SR occurs when shifted to dark conditions (178); aggregation was not a phenotype reported as part of this study, or other studies of SR in *Anabaena* PCC 7120 and *R. sphaeroides* (185) (164, 165). Cyanobacteria include a circadian rhythm to coordinate global gene expression in anticipation of predictable 24-hour cycles of light and dark (186, 187); these studies also do not report aggregation upon shift to dark conditions, which also support that aggregation is not a requirement of SR in cyanobacteria.

While circadian rhythm induces transcriptional changes in advance of nightfall, SR is induced after shift to darkness in *S. elongatus*, and the degree of SR did not correlate with the timing of the internal clock mechanism of entrained cultures (178), suggesting that SR and circadian rhythm are regulated separately in *S. elongatus*. This would be beneficial in that it would allow *S. elongatus* to activate SR during unpredictable shifts to dark caused by changes in daytime weather conditions, for example. Growth in dark conditions is similar to stationary phase for phototrophs, which use light as a primary energy source: dense cultures create light-limiting conditions due to self-shading of cells (150, 188, 189), resulting in reduced translation and switch to maintenance-level heterotrophy from rations of limited glycogen stores (190). Since aggregation results in self-shading, it may be that one of the consequences of aggregation is dark-induced SR, which would reverse the cause-and-effect paradigm such that the stringent stress response is an effect of aggregation, rather than the cause. Alternatively, since SR occurs in the dark in phototrophs, whereas aggregation occurs in the light, it may be that aggregation in does not engender a SR at all in these phototrophs.

As described previously, several species of cyanobacteria have been reported to have c-di-GMP dependent aggregation and biofilm formation in response to a variety of environmental factors including wavelengths of light, temperature, and salinity (128, 132); these studies did not report on whether SR was activated in aggregated cultures. I serendipitously identified a condition of sterile-filtered, autoclaved, room-temperature supernatant as inducing rapid floating floc formation (3 hours); the rapidity and degree of aggregation suggested a strong regulatory response that could be profiled more effectively than the slower 6 hour aggregation reported in Chapter 3.

Here I report preliminary transcriptomic evidence supporting the conclusion that aggregation is correlated with SR in the light in *Synechocystis*. I compared my RNA seq results of genes differentially expressed between aggregated and control *Synechocystis* cultures to 50 conserved genes identified as related to SR in *S. elongatus* due to being differentially expressed across at least two of three different comparisons of wild-type and mutant (*relA* mutant, (p)ppGpp-constitutive mutant) cultures under dark and light conditions. Additionally, I grouped the list of differentially expressed *Synechocystis* genes according to predicted function, and report anticipated outcomes for SR as indicated by genes that are differentially expressed across diverse bacteria during SR (such as down-regulation of ribosomal RNA genes and up-regulation of certain stress response genes) for both aggregated and control conditions. I discuss the implications of my findings for improved understanding of cyanobacterial physiology under natural conditions and for biofuel applications.

4.2 Materials and Methods

4.2.1 Aggregation of cultures

Synechocystis wild-type cultures were grown as described previously. Exponentially growing cultures (OD_{730} ~ 0.8) were harvested by centrifugation at 6000xg for 20 minutes. Control cultures were resuspended in sterile-filtered supernatant. For aggregated cultures, the supernatant was sterile-filtered, autoclaved for 15 minutes, returned to 30 °C by shaking in ice bath, and then returned to cultures. Cell suspensions were then transferred to 100 mL glass cylinders and incubated statically with illumination until aggregation occurred (3 hours).

4.2.2 Isolation, sequencing and analysis of RNA transcriptomes

Aggregated and unaggregated cultures (15 mL per sample) were transferred directly to RNA Protect Bacteria reagent according to manufacturer's instruction (QIAGEN). RNA Protect treated cells were then pelleted by centrifugation at 6,000xg for 5 minutes, decanted, and stored at -80 °C. Cells were lysed by enzymatic digestion method and RNA was isolated using the RNeasy purification kit (QIAGEN) according to manufacturer's instructions. RNA elutions were treated with DNase I (Rapid-Out, Thermo-Fisher) and assessed with an Agilent 2100 BioAnalyzer; all RNA had an RNA integrity number (RIN) score of at least 7 except for Control Sample 1, which had a RIN score of 5.8.

RNA was fragmented to 200 bp using a Covaris 220 shearing instrument before automated reverse transcription and cDNA library amplification on an Apollo 324 robotic liquid handling platform (IntegenX) using a Single Primer Isothermal Amplification kit (NuGEN). Illumina-compatible adapters and barcodes were ligated to the cDNA using

the KAPA DNA Library Preparation Kit (KAPA Biosystems). cDNA libraries were amplified using Hifi Library Amplification kit (Kapa Biosystems), and quantified via BioAnalyzer and qPCR. Libraries are multiplexed and denatured according to Illumina instructions. The NextSeq System platform (Illumina) was used to perform high output sequencing (1x75 base pairs, 400 million reads) for a predicted sequencing depth (clustered with other libraries) of approximately 2080x coverage of the *Synechocystis* genome (~3.6 MB).

RNA-seq reads for each sample were quality checked using FastQC v0.10.1. FASTA and .gtf files of *Synechocystis* PCC 6803 substrain GT for genome sequence and annotation references were accessed from Ensembl (191), release 29, bacterial collection 10 (192). A series of sequence quality control metrics were generated on the .BAM files by RNA-SeQC v1.1.8 (193). Reads were aligned to the reference genome using TopHat v. 2.1.1 (194) and Cufflinks v2.2.1 was used to report FPKM values (fragments per kilobase of transcript per million mapped reads) and read counts (195). FPKM for differential expression was used in edgeR package from Bioconductor v3.2 in R 3.2.3 (196). A multi-dimensional scaling (MSD) plot was drawn by plotMDS, in which distances correspond to leading log-fold-changes between samples. False discovery rates were corrected for statistical significance from multiple comparisons using Benjamini–Hochberg adjustment. Pathway enrichment with DAVID v 6.7 (197, 198) was used to identify affected pathways in expression data from the Gene Ontology database (GO Terms) (199).

Differentially expressed genes with p-values < 0.05 were selected; each of these entries have at least a 4-fold change in expression level between control and treatment

samples. This list of candidate differentially expressed entries was further manually curated by BLASTP search of entries using default parameters to assign predicted functions. Additionally, entries that did not show consistent expression trend between condition and treatment replicates (i.e. inconsistent / overlapping FPKM ranges between treatment and control conditions) were excluded from the set of potentially biologically significant differentially expressed transcripts. The final lists of genes were grouped according to biological function (Table A.1).

4.3 Results and Discussion

4.3.1 Genes predicted to be up-regulated during stringent response

In Figure 4.1, I anticipate that if aggregated cultures are undergoing stringent response, then I should see a larger number of gene entries in the Aggregated section of Figure 4.1A, and in the Control section of Figure 4.1B. I discuss each of those predictions separately. First, in Figure 4.1A (below), I found strong evidence supporting the conclusion that aggregated *Synechocystis* cultures have undergone SR, based on up-regulation of several genes central to SR phenotype in bacteria; namely *hpf*, *uspA,* and also *trnY*. Up-regulation of ribosome hibernation promotion factor *hpf* in aggregated *Synechocystis* cultures (Table A.1, p-value = 0.03) was also reported in *S. elongatus* cultures under all three comparisons correlating with elevated (p)ppGpp. This factor causes (p)ppGpp-dependent dimerization and inactivation of ribosomes by promoting dimerization during SR in a variety of Gram-positive and Gram-negative bacteria (200, 201). In *S. elongatus*, up-regulation of *hpf* correlated with direct measurement of increased (inactivated) ribosome dimers and a 2-fold decrease in protein synthesis; Δ*hpf* mutants did not form ribosome dimers.

Up-regulation of *uspA*, coding for universal stress protein (Table A.1, p-value = 0.0007), was also detected in aggregated cultures. *uspA* is found in all domains of life and is upregulated in response to a number of stressors, including activation by (p)ppGpp during SR (202). In *E. coli*, high levels of (p)ppGpp cause de-repression of *uspA* by the repressor FadR under conditions of severe starvation (166). *uspA* was not reported for SR in *S. elongatus*, which may be due to the fact that SR was induced by shift to dark, rather than nutrient-specific condition. Additionally, UspA has been implicated in response to UV stress and DNA damage conditions (203), which may be negatively regulated in phototrophs in dark conditions (but not aggregation conditions in the light), although this has not been addressed in the literature. Up-regulation of *trnY*, for biosynthesis of tRNA (Table A.1, p-value = 4E-4) was also found in aggregated *Synechocystis* cultures. Amino acid biosynthesis and import is one of the hallmarks of SR, as activation of SR is tied to a molecular mechanism of amino acid starvation in characterized bacterial systems, and up-regulation of amino acid synthesis is a logical adaptive response to amino acid limitation.

4.1A

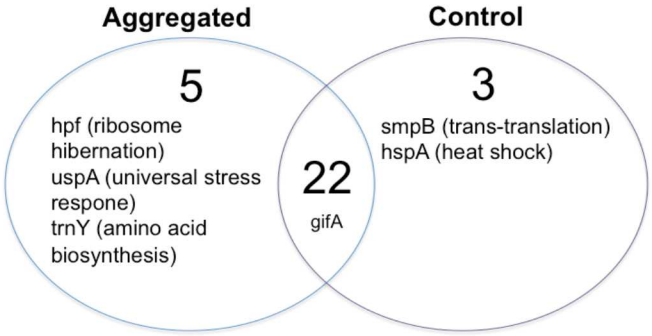

4.1B

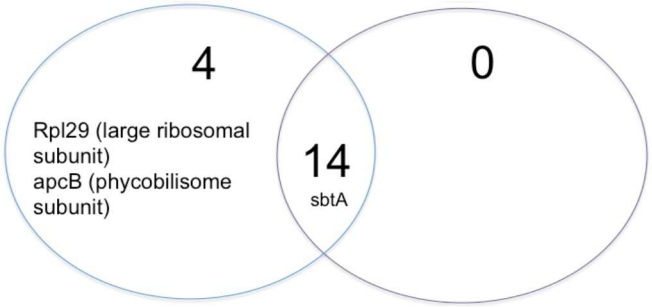

Figure 4.1: Incidence of *Synechocystis* genes predicted to be differentially expressed during stringent response, grouped by experimental condition.
Figure 4.1 summarizes the results of Table A.1, which is a list of *Synechocystis* gene expression results for 50 homologs identified as differentially expressed during stringent response in other bacteria. These homologs were curated from RNA seq data of *S. elongatus* genes differentially regulated under at least 2 of 3 comparisons in WT and two mutant strains under dark and light conditions. Additionally, genes reported in the literature as widely conserved parts of stringent response were also included. In Figure 4.1A, RNA seq results are reported for all homologs in Table A.1 predicted to be up-regulated during stringent response, and are grouped according to whether they are up-regulated in aggregated cultures (left), control cultures (right) or unaffected by growth condition (middle, intersection). Similarly, Figure 4.1B reports results for homologs predicted to be down-regulated. Entries of specific interest in each category are listed in text under the total number of entries in that category.

Additional supporting evidence that is consistent with SR while not directly tied to (p)ppGpp-dependent mechanisms included up-regulation of homologs for iron citrate uptake (*fecB,* p-value 0.03) and also for thioredoxin (*trxA*, p-value 0.04) which is used to regulate redox levels such as during transition from photosynthesis to respiration (204, 205). Furthermore, most of the genes grouped under biomolecule export, cell wall biogenesis, secondary metabolite production, and DNA replication (Table A.1, categories

5, 13, 15, and 16) were down-regulated in aggregated cultures (19 genes) vs control (6 genes), consistent with predictions for SR. As most genes in *Synechocystis* contribute to multiple categories of function, the role assignments in Table A.1 are somewhat arbitrary, so these findings are inconclusive without additional information determining their specific role, if any, in SR.

Overall, only 3 of the 7 genes in *S. elongatus* reported to be up-regulated by (p)ppGpp across all three comparisons tested are conserved in the *Synechocystis* genome; of these 3 genes, only one was also up-regulated in aggregated *Synechocystis* cultures, namely *hpf*. Not coincidentally, the other 4 *S. elongatus* genes were annotated as hypothetical and did not exist as homologs in *Synechocystis*; likewise, many hypothetical genes up-regulated in aggregated *Synechocystis* cultures (Table A.2) did not exist as homologs in *S. elongatus*, suggesting that hypotheticals not conserved between these two closely related cyanobacterial species may represent variation in how they customize their SR mechanism. Other genes up-regulated in *S. elongatus* in all SR conditions tested include transcription of glutamate synthase inactivator *gifA*. In contrast, this study showed *gifA* genes were not differentially regulated between aggregated and control cultures of *Synechocystis* (p-value = 0.1, Table A.1). The function of GifA is a repressor of glutamine synthase (206) under certain conditions, including increased role of ammonium as a nitrogen source (207). In this study, the *gifA* result suggests that aggregated cultures of *Synechocystis* are experiencing lowered /decreased ammonium status, which is consistent with up-regulation of an ammonium permease (uptake) gene in aggregated cultures (Table A.2, Category 3, *amt1*, p-value = 0.046).

Some of these results contradicted the conclusion that aggregated cultures undergo SR. Specifically, two genes related to translation went against trends consistent with SR: *smpB* (p-value = 0.045), which relates to trans-translation (ribosome recovery mechanism during SR (208)) was higher in control cultures (Figure 4.1A). Similarly, the gene for the large ribosomal protein, *rpmC* (p-value = 0.0075) was higher in aggregated cultures of *Synechocystis* (Figure 4.1B), whereas SR would predict reduced ribosomal protein synthesis under this condition. In the results with *S. elongatus*, genes for trans-trans mechanisms or ribosomal proteins were not reported as differentially expressed. The authors indicated that SR of heterotrophic bacteria includes translation-regulating mechanisms on a variety of time-scales, from rapid action of (p)ppGpp directly on ribosome translation activity (209, 210), to slower effects of reducing transcription of ribosomal proteins via modulating activity of sigma factors. The molecular mechanisms of cyanobacterial (p)ppGpp on activating SR is unknown, but given the results of *S. elongatus* SR transcriptomes, it's possible that the higher transcription of 50S ribosomal protein in aggregated *Synechocystis* cultures and trans-translation in control cultures was due to slower response of these regulatory mechanisms during SR. Additionally, the control cultures up-regulate larger numbers of stress response genes (19 in control vs 6 in aggregated condition, Table A.2, category 4 and category 11) that may also have mechanisms for conserving translation resources.

4.3.2 Genes predicted to be down-regulated during stringent response

In Figure 4.1B, the difference in my predicted results of down-regulated genes from those in *S. elongatus* could be attributed to use of nutrient status instead of dark conditions for inducing SR. Specifically, *S. elongatus* shows down-regulation of *sbtA*

expression in the dark vs the light in wild-type, and also down-regulated in a (p)ppGpp$^+$ constitutive mutant in the light vs control WT in the light, but up-regulated in the dark (WT) vs a *relA* mutant in the dark. If *sbtA* expression levels were only affected by (p)ppGpp as part of SR, then it should have down-regulated in all three comparisons. The fact that it is not down-regulated in WT in the dark compared to the *relA* mutant in the dark suggests that *sbtA* expression is responding to illumination status, in addition to SR. SbtA is a bicarbonate transporter whose expression is light-dependent (211), consistent with this analysis. In *Synechocystis*, *sbtA* was not differentially regulated between aggregated and control cultures (Figure 4.1B). Similarly, *hspA* correlated with increased (p)ppGpp with 2 of 3 comparisons in *S. elongatus* but not in the (p)ppGpp-constitutive mutant in the light; this gene is known to be strongly down-regulated in the dark in *S. elongatus* (212) and likely requires additional dark-induced factors for its regulation. *hspA* was upregulated in my control culture (Table A.1, p-value = 0.005).

4.3.3 Genes related to the illumination status of aggregated cultures

I sought to better characterize the illumination status of aggregated vs control cultures, to determine whether self-shading of aggregated cells was causing dark conditions sufficient to induce SR. In a previous study, *cmpB* (*slr0041*, bicarbonate transport permease) is down-regulated nearly 12-fold in *Synechocystis* within 1 hour in the dark (213); while this gene was down-regulated in aggregated cultures in my study, it was not to a statistically significant degree (p-value = 0.15, data not shown), suggesting that either that the degree of aggregation was insufficient to create darkness through self-shading in most of the cells, or that the cells were harvested before maximum reduction of this transcript level due to darkness. Additionally, *psbA2* has been previously shown to

be up-regulated 6-fold *Synechocystis* within 15 minutes of shift from dark to light (214, 215); my results do not support significant difference in *psbA2* levels between treatment and controls (p-value = 0.65; data not shown). I conclude that my aggregated cultures were not self-shaded to a degree sufficient to create dark conditions, relative to control cultures. I note that aggregated cultures may however experience lower light than controls, based on up-regulation of 6 genes coding for light-harvesting pigments (216, 217) (Table A.1, category 12: phototrophy).

4.4 Conclusions

4.4.1 *Synechocystis* undergoes SR during aggregation in the light

The biological purpose of SR is to provide survival adaptation during stress. In *S. elongatus*, it has been characterized as induced to maintain viability in the dark when energy and nutrients are rationed. These findings provide preliminary evidence that *Synechocystis* also undergoes SR during change in nutrient status in the light, most likely nutrient limitation, as indicated by up-regulation of ribosome hibernation promotion factor *hpf,* universal stress response transcript *uspA*, and other genes consistent with SR phenotype. Since aggregation is light-dependent, and dark-condition genes such as *hspA* and *cmpB* were not up-regulated in aggregated cultures, I conclude that the SR was not due to light limitation caused by self-shading of cells in aggregated cultures. While many of these results did not correlate with the patterns of gene expression in *S. elongatus* SR, especially in genes predicted to be down-regulated (Figure 4.1), I find that most of these inconsistencies can be attributed to the use of dark conditions rather than nutrient status to induce *S. elongatus* SR. This is the first evidence of a WT cyanobacterium undergoing SR in the light upon change in nutrient status, which is consistent with SR due to nutrient

limitation in heterotrophic bacteria, and consistent with the cause and effect paradigm of aggregation occurring as a result of stress.

4.4.2 The role SR and aggregation in natural environments

In *Enterococcus faecalis*, a *Firmicutes*, loss of (p)ppGpp regulation affects secondary carbon metabolism; evidence supports use of basal fluctuations in (p)ppGpp levels to respond to minor changes in external and internal carbon fluxes for cellular fitness, not just survival (218). In *Beta-* and *Gamma-proteobacteria* (including *E. coli*), levels of (p)ppGpp are not biphasic in activating physiological responses, but rather occur along a gradiation (158), with SR only occurring at higher levels of (p)ppGpp when other homeostasis mechanisms for restoring amino acid levels, such as the leucine-responsive protein pathway, have failed (158). I have shown previously in Chapter 3 that *Synechocystis*, upon shift to reduced nutrient strength, undergoes sedimenting aggregation in about 6 hours, whereas autoclaved nutrients (this study) induce rapid, floating flocs of aggregation in just 3 hours. If so, then the degree of aggregation can serve as an indicator of not just the presence or absence of SR, but also the severity of the response. It is assumed that the difference in floating versus sedimenting aggregated cells comprises a difference in rate and quantity of aggregation, but not type of aggregation.

Migration of cyanobacteria through the water column is a normal part of their seasonal adaption, forming blooms on lake surfaces in spring and benthic layers in the winter (219, 220). Aggregation into buoyant flocks during transition to spring season is part of this process of migration. One of the predicted benefits of aggregation under nutrient limitation in cyanobacteria is that both sedimentation or floating flocculation promote migration of cells through the water column to new locations with improved

nutrient status; presumably the degree of aggregation is tuned to the degree of nutrient limitation, such that severe nutrient stress promotes increased travel distance.

4.4.3 Suggested future work

It is noteworthy that in cyanobacteria, dark conditions (and SR) do not entail aggregation, whereas SR under nutrient limitation in the light is accompanied by aggregation. These results suggest that aggregation is regulated separately from SR, which is different than the cause-and-effect paradigm that aggregation is the result of stress response such as SR. If a (p)ppGpp-null mutant of *Synechocystis* is unable to aggregate under nutrient limitation despite having the full complement of c-di-GMP-dependent genes known to be needed for cellulose-dependent aggregation, that would suggest that the SR regulatory circuits include an optional on-off switch for aggregation; identification of this switch in bacteria would be beneficial for both basic and applied science in synthetic biology of biofuels and medicine. Alternatively, if this mutant were able to aggregate, this would contradict interpretation of aggregation as part of a conserved stress response like SR. Additional studies with such a (p)ppGpp-null mutant would help to refine understanding of how stress from nutrient limitation is distinct from regulatory pathways of stresses that engender SR. Additional elements to include in these proposed experiments would be using differential RNA sequencing (separate sense and anti-sense transcriptomes), as a previous study identified 314 non-coding RNAs, 866 genes potentially regulated with anti-sense RNA, in addition to the identification of small-peptide RNAs, all of which have had their transcriptional start sites mapped, but whose roles in biological function are understudied (140). Finally, mutational analysis of

hypothetical genes or other genes found to be differentially regulated in this study would be valuable.

In addition to increasing understanding of the basic science of cyanobacterial physiology, aggregation is also useful as an indicator of culture health for biofuel feedstock cultivation systems. SR could likewise be engineered to activate a reporter molecule such as green fluorescent protein to *rsh* transcription, enabling PBR engineers to more easily monitor stress response in cultures or in engineering strain metabolism, even when aggregation does not occur. These findings suggest that one strategy to begin this work would be comparing transcriptomes of dark condition vs cultures with altered nutrient status in *Synechocystis* to help clarify the minimum core of genes conserved in SR between these two conditions. In general, identifying which environmental conditions result in SR with and without aggregation will help cultivation system engineers and strain engineers to capitalize on the whole range of metabolic capabilities and growth conditions biocompatible with this versatile, highly adaptive organism.

CHAPTER 5

SYNTHETIC ECOLOGY FOR QUANTITATIVE PREDICTION OF ANTI-CONTAMINATION STRATEGIES IN BIOFUEL-PRODUCING CULTURES OF *SYNECHOCYSTIS* PCC 6803

5.1 Introduction

To fulfill the promise of microalgal biofuels as a carbon-neutral, renewable alternative to fossil fuels, cultures must be grown at unprecedented scale, while maintaining low cost; for recent reviews, see (221-223). Current approaches to maintaining healthy and productive biofuel feedstock cultures at large scale draw from modern industrial agriculture techniques, including use of selective growth conditions, antibiotics, and co-culture techniques. For example, in open ponds of microalgae, fish are introduced in order to reduce predation by zooplankton (224). Co-culture of 'refuge' species also protects more vulnerable macro-algae feedstock cultures from predation (225). Deliberate co-culture of multiple microalgal feedstocks in open ponds in order to increase biomass production and reduce grazing by zootrophs (*Daphnia pulex)* have also been used (226).

Synthetic ecology is an emerging specialty in microbiology (reviewed in (227-229)). Capabilities and interest have accelerated in recent years due to advances in next-generation sequencing, bioinformatics, and synthetic biology. Methods for synthetic ecology include rational design of defined minimal or representative microbial consortia to simulate naturally occurring populations. Recent ecosystems to be studied include natural systems such as the human gut (230), and engineered systems such as bioreactors

(226, 229, 231). A literature search did not identify any studies to dae that attempt to model naturally occurring PBR contamination using an artificial microbial consortium.

Synechocystis has been engineered previously to secrete elevated levels of long-chain fatty acids such as laurate (20). These strains were cultivated in a 4000-liter rooftop photobioreactor (PBR) as a test-bed for industrial-scale production of this J8 jet-fuel precursor (232). Decrease in laurate yield corresponded with increase in growth of heterotrophic bacteria in the PBR (hereafter referred to as heterotrophs) (233). These heterotrophs were able to grow using soluble microbial products (SMP) of *Synechocystis* for fixed carbon and nitrogen, as well as consuming laurate (136).

The objective of this pilot study was to test the proof-of-concept of whether it is possible to accurately and reproducibly model the bacterial PBR contaminome under controlled laboratory conditions in order to predict optimal PBR operation. The approach I used was to build a statistical model using an artificial Defined Consortium of heterotrophic bacteria, and see if the model predictions were still accurate when other contaminant species were used. Specifically, I built a regression model using a Defined Consortium comprised of a set of 40 axenic isolates of heterotrophic bacteria, and tested model predictions using novel Consortia. In this test case, I chose to optimize levels of three chemical additives that I hypothesized would be effective in mitigating the accumulation of heterotrophic bacteria while allowing *Synechocystis* to flourish, namely alkalinity, sodium chloride, and the antibiotic kanamycin.

In addition to building and testing these models, I performed a set of experiments to better inform the interpretation of the model results. First, I conducted a laurate time-course assay to test whether levels of salt, kanamycin, and/or pH predicted to be optimal

by the model were sufficient to protect the presence of laurate in deliberately contaminated *Synechocystis* cultures. I also screened a panel of mutant *Synechocystis* strains previously shown to lack cell surface structures (99, 101, 102, 104, 121) to investigate the effectiveness of genetic means of reducing contaminant food sources in the PBR supernatant. Finally, I used Illumina-generated 16S rRNA gene sequence data and PICRUSt metagenomic prediction (234) to assess Consortia community structure and function for improved understanding of PBR contaminome ecology, thereby informing improved contaminant mitigation strategies suggested by my results.

5.2 Materials And Methods

5.2.1 Defined consortia:

All isolation and propagation of bacterial cultures was conducted axenically at 30 °C and 24-hour illumination, with shaking or aeration of liquid cultures, unless otherwise indicated. Axenic status of *Synechocystis* culture stocks was determined via microscopy, and also T-RFLP, as follows: liquid cultures were prepared using sterile technique and cell pellets were collected via centrifugation for 5 minutes at 6,000xg. Decanted cell pellets were processed to extract genomic DNA using the Blood and Tissue DNeasy kit (QIAGEN) with indicated modifications for Gram-positive bacteria. The 16S rRNA gene sequence was amplified from genomic DNA using Taq Master Mix PCR kit (QIAGEN) and universal bacterial primers: HEX-labeled 8F (AGA GTT TGA TCC TGG CTC AG) and unlabeled reverse primer 1392R (ACG GGC GGT GTG T) (137). Resulting amplicons were purified with QIAQuick PCR Purification Kit (QIAGEN) and digested with restriction endonuclease enzymes (138) HaeI, HhaI, MseI, and MspI (New England Biolabs). Digested fragments were analyzed with a 3730 capillary sequencer (Applied

BioSystems) and sized via ROX 1000 ladder (ThermoFisher). To the degree that these methods are able to detect contamination, cultures were considered axenic if they did not have any non-*Synechocystis* peaks in resulting fragment spectra.

Heterotrophic bacteria for Defined Consortia were assembled from diverse sources, including non-axenic cultures grown in shake flasks or PBRs (150) cultivating WT *Synechocystis* parent strain (136) or fatty-acid secreting mutant SD304, a kanamycin-resistant version of SD277 (20). Ten of the strains of Consortium 1 were isolated by growth on BG11 agar plates (135) supplemented with sodium laurate as sole organic carbon source. Colonies with varying appearances were preferentially selected to increase likelihood of sampling diverse phyla. Isolated colonies were re-streaked repeatedly as needed to generate axenic stocks, which were then propagated on LB agar plates (138). Single colonies were used to inoculate LB liquid growth medium and incubated overnight at 30 °C with shaking. Samples of liquid culture were frozen at -80 °C with sterile 10% glycerol.

Additional sources of heterotrophs for Defined Consortium 1 included Tempe Canal, an open-air fresh water body fed by Arizona watershed surface and ground water (235), including the Verde and Salt River watersheds (sample site latitude 33.4217; longitude -111.927). Bacteria from water and soil samples from Tempe Canal were harvested via centrifugation at 6,000xg for 15 minutes, resuspended in 100 mL of log-phase *Synechocystis* culture, and incubated for 7 days to ensure heterotrophs chosen for Consortia were viable under experimental conditions. The culture was then centrifuged as above and the cell pellets were used to inoculate LB agar plates. Colonies with diverse phenotypes were propagated on new LB agar plates until axenic.

For Defined Consortium 2, all 40 isolates were sampled from non-axenic *Synechocystis* cultures grown in PBRs or flasks, and isolated on LB agar plates as above.

5.2.2 16S rRNA gene sequencing and BLAST identification of Defined Consortia Isolates:

Axenic cultures of each of the 80 isolates for the two Defined Consortia were grown overnight in LB liquid medium. 1 mL samples were harvested as described above. To identify species, 16S rRNA was prepared and purified as described above using unlabeled primers. Sequencing reactions were prepared and purified using standard procedures (138). 16S rRNA sequences were determined via Applied Biosystems 3730 capillary sequencer. Species identities of nearest related OTU were assigned by BLASTN search of NCBI Microbe database using default parameters (236). All BLAST identity scores were at least 99% (data not shown).

Community analysis of Consortium growth in *Synechocystis* supernatants was performed as described previously (136), in accordance with Earth Microbiome Project guidelines (237). Genomic DNA was isolated from cell pellets as described above. The V4 regions of 16S rRNA gene libraries were amplified using bar-coded 806f and 515r primers (238). The resulting 16S rRNA gene libraries were analyzed via Illumina MiSeq 2000 platform. Sequence data were analyzed using QIIME software package version 1.8.0 using default parameters, unless noted otherwise. Sequences were clustered in OTUs having 97% similarity with uclust (239). Representative sequences for each OTU were classified using the RDP classifier version 2.2 (240) and retrained on the Greengenes (241) database v. 13.8 pre-clustered at 97% identity. Representative sequences were aligned with PyNAST v. 1.2.2 (242) and a phylogenetic tree was

constructed with FastTree (243) for use in phylogenetic diversity calculations. Singletons and chimeras (244) were removed, and sample sets were normalized via rarefaction. I modified taxonomy plot data at genus level for each sample by aggregating all genera at less than 6% relative abundance for that sample into an 'Other' category.

5.2.3 Selection of mitigation factors and levels

Factors (salinity, antibiotic, and alkalinity) were chosen for applicability to large-scale microbial biofuel cultures. High factor levels were empirically determined using viability and growth-rate screens, such that the final statistical model would encompass the complete range of additive concentrations biocompatible with laurate-producing *Synechocystis* strains (the biocompatible sample space).

Kanamycin (kan) was chosen as a representative antibiotic because its activity is not affected by salinity or alkalinity, nor is it photo-degraded. All 80 heterotroph isolates of the two Defined Consortia were screened on LB agar plates supplemented with 50 μg/mL of kanamycin; both Consortia contained 10 kan-resistant isolates and 30 kan-sensitive isolates (data not shown). To establish the range of kan concentrations to be tested in the statistical model, kan-resistant *Synechocystis* biofuel strains were grown in a serial dilution from 0-400 μg/mL kanamycin in 100 mL of BG11 liquid media; 200 μg/mL was selected as the high level of kan concentration as it showed no growth rate defect compared to the negative control (data not shown).

Similarly, *Synechocystis* is naturally salt-tolerant (2), able to grow in liquid BG11 cultures with up to 0.8 M added NaCl (data not shown); sea water on average is ~0.6 M salinity. I selected 0.6 M as the high level of added NaCl concentration with robust

growth rate by laurate-secreting strain SD304, and because of its relevance to seawater cultivation.

Synechocystis is also naturally alkaliphilic, with optimal growth in BG11 between pH 7 and 8.5, and reasonably robust growth up to pH 11 (150, 245). I screened biocompatibility of *Synechocystis* strains in BG11 liquid buffered with a variety of common cell culture buffers. I observed *Synechocystis* growth in BG11 media at pH 7.5 buffered with TES (pKa of 7.4); Tricine buffered to pH 8.5 (pKa of 8.1); and CHES buffered to 9.5 (pKa of 9.3) (data not shown) as similarly rapid to growth in unbuffered BG11. All buffers were at 10 mM concentration.

5.2.4 Factorial Analysis, Regression and Model Testing in Rich Media.

I prepared 15 bottles of sterile liquid LB media (100 mL each) with levels of the three additives in different combinations of concentrations according to the conditions indicated for Tubes 1-17 in Table 5.1 (uncoded levels). Three mL samples of each type of medium were transferred to 17 sterile test tubes. Data for a total of three biological replicates were generated using Defined Consortium 1; each replicate was performed using consortium isolates that were freshly inoculated from freezer stocks to LB agar plates.

Table 5.1: Central composite design of a 2^3 full factorial augmented with center points and axial points.

		Coded Levels			Uncoded Levels		
Category	**Tube #**	**Added NaCl**	**Kan. sulfate**	**pH (10 mM buffer)**	**Added NaCl, Molar**	**Kan. sulfate, ug/mL**	**pH (10 mM buffer)**
Full Factorial	1	1	1	1	0.51	170.67	9.20
	2	1	1	-1	0.51	170.67	7.80
	3	1	-1	-1	0.51	29.30	9.20
	4	1	-1	-1	0.51	29.30	7.80
	5	-1	1	1	0.09	170.67	9.20
	6	-1	1	-1	0.09	170.67	7.80
	7	-1	-1	1	0.09	29.30	9.20
	8	-1	-1	-1	0.09	29.30	7.80
Center points	9	0	0	0	0.30	100.00	8.50
	10	0	0	0	0.30	100.00	8.50
	11	0	0	0	0.30	100.00	8.50
Axial points	12	-1.414	0	0	0.00	100.00	8.50
	13	1.414	0	0	0.60	100.00	8.50
	14	0	-1.414	0	0.30	0.00	8.50
	15	0	1.414	0	0.30	200.00	8.50
	16	0	0	-1.414	0.30	100.00	7.50
	17	0	0	1.414	0.30	100.00	9.50

Each of the 40 isolates of Defined Consortium 1 freezer stocks were streaked on LB agar plates and incubated for 2 days at 30 °C. Samples of an isolated colony from each stock were propagated overnight in 40 separate 3-mL cultures of LB liquid medium without additives. The growth of each of the 40 liquid cultures was estimated by measuring absorbance units at OD_{600}. To prepare the Consortium, different volumes of each of the 40 axenic cultures were combined in a single new test tube such that each strain contributed to approximately 1/40 the total OD_{600} in the new tube. The final mixed population of heterotrophs in the new tube comprised Defined Consortium 1. The same process was applied to isolates 41-80 to create Defined Consortium 2 when needed.

The Defined Consortium was mixed to a 1 mL volume at an OD_{600} of 1.0, and used as an inoculum for Tubes #1-17 at a starting OD_{600} of 0.001 (representing the combined contribution of all 40 isolates). The 17 tubes were incubated for 24 hours as previously and the OD_{600} of each tube was recorded. These data were direct inputs for statistical analysis (they were not normalized or transformed before analysis).

5.2.5 ANOVA, Regression Analysis, and Testing of Model in LB broths.

The response variable was combined growth of the heterotroph contaminants in Defined Consortium 1, as measured by absorbance at OD_{600} at 24 hours. ANOVA and regression using least squares fitting were performed on coded units using Minitab 16 statistical software (246). Trials were blocked by replicate, and linear and second-order factors and interactions were analyzed. ANOVA output (not shown) was used to generate a response regression model with factor levels measured in coded units (Equation 1, below).

Model adequacy checking by normal probability plot of residuals, and plots of residuals vs run order and fit values corresponded with acceptable levels (247) (not shown). In Figure 5.3, a surface response plot corresponding to Equation 1 is shown were generated using the surface plot function in JMP Pro 12 (248). In Table 5.2, below, model predictions of the total OD_{600} after 24 hours were generated for 4 different growth conditions using the Minitab OptiPlot function to solve the regression (Equation 5.1, Results and Discussion).

Table 5.2: Optiplot heterotroph growth response predictions from regression.

Y = OD_{600} (heterotroph growth absorbance units)	**Added Salt, Molar**	**Kanamycin sulfate, ug/mL**	**pH (10 mM buffer)**	**Y predicted (heterotroph growth absorbance units at OD_{600})**	**Y lower (95% confidence interval, absorbance units at OD_{600})**	**Y upper (95% confidence interval, absorbance units at OD_{600})**
Max	0	56.6	7.5	5.92	5.07	6.8
Min	0.6	200	8.73	-1.14	-2.00	0.04
Y=3.0	0.3	150	9.5	3.0	2.62	3.71
Y=0.01	0.58	200	7.5	0.01	-0.77	0.33

To test model predictions, I prepared media and Defined Consortium 1 as described above, for two replicates, as well as Defined Consortium 2 for two replicates. To test the model using an Undefined Consortium, 1.5 liters of Tempe Canal Water (TCW) was collected and pelleted via centrifugation at 6,000xg for 20 minutes at room temperature. The supernatant was decanted and the cell pellets resuspended in 100 mL of LB plain liquid. A 2 mL aliquot was pelleted and frozen for subsequent community analysis ('TCW' Figs. 5.1 and 5.5). The culture was grown for 24 hours and another 2

mL aliquot was removed ('UC1' Figs. 5.1 and 5.5.). This LB inoculum served as one replicate of an Undefined Consortium, and was used to inoculate the model test media to a starting OD_{600} of 0.001, as with Defined Consortia. The two replicates for the Undefined Consortia were sampled from the same location on different dates (January 30th and August 20th 2015, respectively).

5.2.6 Factorial analysis of heterotroph mitigation in *Synechocystis* cultures and supernatants.

Synechocystis cultures were grown as described above in BG11 media prepared with levels of additives corresponding to 17 conditions in Table 5.1 in the same manner as for LB media described above. *Synechocystis* supernatants were prepared using axenic 100 mL cultures of SD305, a kanamycin-resistant *Synechocystis* strain previously engineered to secrete fatty acids (20). These cultures were grown to log-phase (OD_{730} of ~ 0.5) in BG11 liquid without additives. Log-phase cultures were sterile-filtered through 0.22 micron SteriCup filtration units (MilliPore), and salt, kanamycin and buffer solutions were added axenically to create test conditions described as listed in Table 5.1, Tubes 1-17. These tubes were then inoculated with Defined Consortium 1, prepared as described above, to a starting heterotroph OD of 0.001, and incubated for 6 days. Every 24 hours, cfu dilutions were propagated on LB agar plates in order to measure cfu/mL.

5.2.7 Growth of consortia in supernatants of mutant *Synechocystis* cultures.

Synechocystis strains (Table 3.2) lacking pili (*pilC*, SD519), EPS (*slr0977*, SD506) and S-layer (*sll1951*, SD523) (69, 99, 104) were prepared as described in Chapter 3. Supernatants of these strains were prepared and inoculated with Defined Consortium 1, with no additives present, and incubated as described above for 6 days.

Heterotroph cfu/mL were measured from Day 6 by propagating supernatant samples on LB agar plates and counting subsequent colony formation after incubation at 30 °C for 2 days. The $\log_{10}$ of cfus/mL for each strain was calculated and growth of Defined Consortium 1 in supernatants from mutant strains was reported by normalizing to the same measurement in wild-type strains (Figure 5.5, below)

5.2.9 Laurate time course assay

Supernatants of *Synechocystis* strain SD305 were inoculated with Defined Consortium 1, or with an Undefined Consortium. Additive levels for the treatment flasks were the same as those levels predicted by Eq. 5.1 to minimize heterotroph growth in LB over 24 hrs ('Min'), namely 0.6 M added NaCl, 200 ug/mL kan, and pH 8.73 (10 mM Tricine, pKa of 8.1; Table 5.2). The negative control had 0 M added NaCl, 0 μg/mL kan, and pH 7.5 (10 mM TES, pKa of 7.4). A positive control for laurate stability had the same levels of additives as negative controls, but with no Consortium added, in order to test whether *Synechocystis* supernatant alone was able to degrade laurate under these conditions, for example due to presence of beta-oxidation enzymes released from cells.

All flasks contained 100 mL culture volume and were spiked with a laurate stock solution to a starting concentration of 100 mg/L (100 ppm) at the start of the time course (Day 0 data). Every 24 hrs, 10 mL of culture from each flask was removed and laurate was collected via hexane extraction as described previously (20). Briefly, 10 mL culture was combined with 10 mL hexane in Oak Ridge tubes, with 0.2 g NaCl and 200 μL of 1 M H_2PO_4. Tubes were shaken at 200 rpm for 30 minutes at 37 °C. Extracted laurate was then collected by centrifugation at 20,000xg for 20 minutes, with supernatant transferred to gas chromatograph sample vials stored at -80 °C until measured. Laurate was

quantified via FID-GC on a Shimadzu GC 2010. Laurate peak areas were calibrated via measurement of dilution series of sodium laurate standards of known concentrations. Heterotroph cfu/mL were measured at each time point by plating on LB agar plates as described above (Defined Consortium 1), or by flow cytometry (Undefined Consortium 1). For flow cytometry, 1 mL of culture was centrifuges at 6,000xg for 5 minutes, decanted, and cell pellet resuspended in isotonic neutral buffered formalin 10% (1xPBS, pH 7.7), and fixed for 24 hours at 4 °C. After fixation, cells were again collected by centrifugation as above, and then resuspended in sterile isotonic saline and stored at 4 °C. To count cells, samples were labeled with 5 μM SytoX green nucleic acid stain (Invitrogen). Green labeled counts/mL were compared with a dilution series of samples of known labeled cell concentration as determined by fluorescence microscopy hemocytometer. Flow cytometer model BD Accuri C6 Plus Flow Cytometer from BD Biosciences was used with native software. Flow cytometry data and laurate data are biological replicates (n=2 flasks per condition). Cfu data are reported as technical replicates (3 measurements of one flask per condition).

5.2.10 KEGG ortholog trait markers and their taxonomic distribution.

Candidate gene markers for tolerance to additives were initially identified from literature search (Table 5.3). Taxonomic distributions of putative orthologs were identified using STRING 10 database (1,678 bacteria) (249). As an example of how STRING data are reported: the NhaA protein functions as Na^+:H^+ anti-porter in *E. coli* to provide tolerance to excess NaCl; other genes in the *nha* operon such as *nhaR* code for regulatory/accessory proteins. To perform the search, 'NhaA' search term from the organism *E. coli* (no sub-species specified) was used to query the STRING 10 database

with default parameters. The top relevant search result was selected. Under 'Occurrence' view, taxonomic distribution of the ortholog was displayed for 29 different bacterial clades on the vertical axis, with the number of taxa per clade ranging from 1 (*Gemmatimonas aurantiaca*; others) to 411 (*Firmicutes*), as shown in the Appendix, Figure B.2. The number of clades containing at least one species with a putative NhaA ortholog sequence alignment score of 80 bits or higher were counted up, and then divided by number of total clades (29 clades) to generate %S scores reported in Table 5.3. Scores below 60 bits are considered possibly weak or spurious orthology as a rule of thumb according to the STRING website. Functional partners reported with NhaA were not considered for calculating %S. The %S STRING scores for all trait marker orthologs in Table 5.3 were assessed using the same tree of 29 clades.

Taxonomic distributions of a given marker were estimated using the Occurrence view from the STRING database (Appendix B Figure B.2). Taxonomic distribution of kanamycin phosphatase markers were not available in STRING, as kanamycin phosphatase activity does not require protein-protein interactions required for curation in the STRING database. I therefore used KEGG taxonomy view to ascertain the distribution of K19300, which was found in multiple taxa across many phyla (*Enterobacteraceae, Alpha-, Beta,* and *Gamma-Proteobacteraceae, Firmicutes* and *Actinobacteria*; data not shown). I conclude this marker also has wide taxonomic distribution.

5.2.11 Predictive Metagenomic analysis using PICRUSt.

QIIME 16S rRNA gene sequence data was used as input for PICRUSt software in order to curate a master file (not shown) of all unique KEGG (250) orthologs (6908

orthologs total) predicted to occur in the total pool of all sequenced Consortia samples. Twenty KEGG orthologs for trait markers of interest were identified. Identification was initiated by searching the master file for the KEGG ortholog numbers corresponding to orthologs identified by literature search. Additional markers coding for the same trait mechanism were found by using the KEGG definition search terms such as those listed in Table 5.3 ('Adaptive mechanism').

The final comprehensive list of 20 KEGG markers was used as input for searching predicted metagenomes of abundant OTUs per sample (at least 10% total abundance per sample) as PICRUSt (234) output. Table 5.3 was redacted to exclude most markers that were not found in abundant OTU metagenomes (Fig. 5.6); all trait mechanisms from the original 20 markers are still represented in the redacted list of 15 markers.

The most recent version of PICRUSt available uses GreenGenes v. 13.5; therefore QIIME analysis was repeated using closed reference OTU picking using GreenGenes v13.5 in order to correlate exact OTU numbers (one number per unique 16S rRNA gene sequence) with their corresponding metagenomic prediction outputs from PICRUSt. Because QIIME groups OTU abundance by genus, potentially including contributions from more than one unique sequence per genus abundance, I sorted PICRUSt outputs by most abundant OTU number per sample. For all abundant genera of interest, there was one unique OTU number (unique 16S nucleotide sequence from Illumina dataset) contributing to >90% of the total genus abundance. Metagenomic prediction data for each OTU in Fig. 5.6 are for these unique abundant OTU numbers for each genus.

Five of the KEGG markers of interest were not found in the PICRUSt precalculated metagenomics file for GreenGenes v13.5 (IMG v4), "KEGG Orthologs": K18095 (*mexY*), K18145 (*adeA*), K18324 (*acrD*), K19299 (*nptIII*) and K19300 (*nptII*). These KEGG orthologs were likely not part of the IMG v 4 database at the time the file was created (M. Langille, personal communication, PICRUSt users online forum). I therefore used BLASTN (239) of the Microbe database for each of the 11 most abundant OTU 16S sequences to identify the most closely related species with a fully sequenced genome in the KEGG Organisms database. For all species except two, the % identity between the 16S sequence data and KEGG organism was at least 98% for the full sequence length (not shown). For *Acinetobacter* it was 96%; for *Cloacibacterium*, it was 93%. Presence of these five KEGG orthologs was then assessed for these 11 abundant OTUs by searching the resulting KEGG organisms databases for each of the 5 KEGG markers.

5.3 Results And Discussion

5.3.1 Illumina sequence data show identity but not abundance of contaminant phyla is relatively conserved across Consortia

In Figure 5.1, I used the freshwater lake sequence database (FWLSD) (1) as a reference for approximating the global bacterial meta-community of freshwater microalgae cultivation system contaminomes, due to niche similarities (mesophilic, fresh water, illuminated, aerobic, and relatively oligotrophic). Compared to the FWLSD, the LB outgrowth (UC1) of Tempe Canal Water (TCW) was enriched for *Gamma-proteobacteria* phylotypes, with reduced levels of *Bacteroidetes* phylotypes. Defined

Consortium 1 appears to most closely resemble FWLSD in terms of identities, with 6 of 7 phylotypes at the phylum level occurring in both populations.

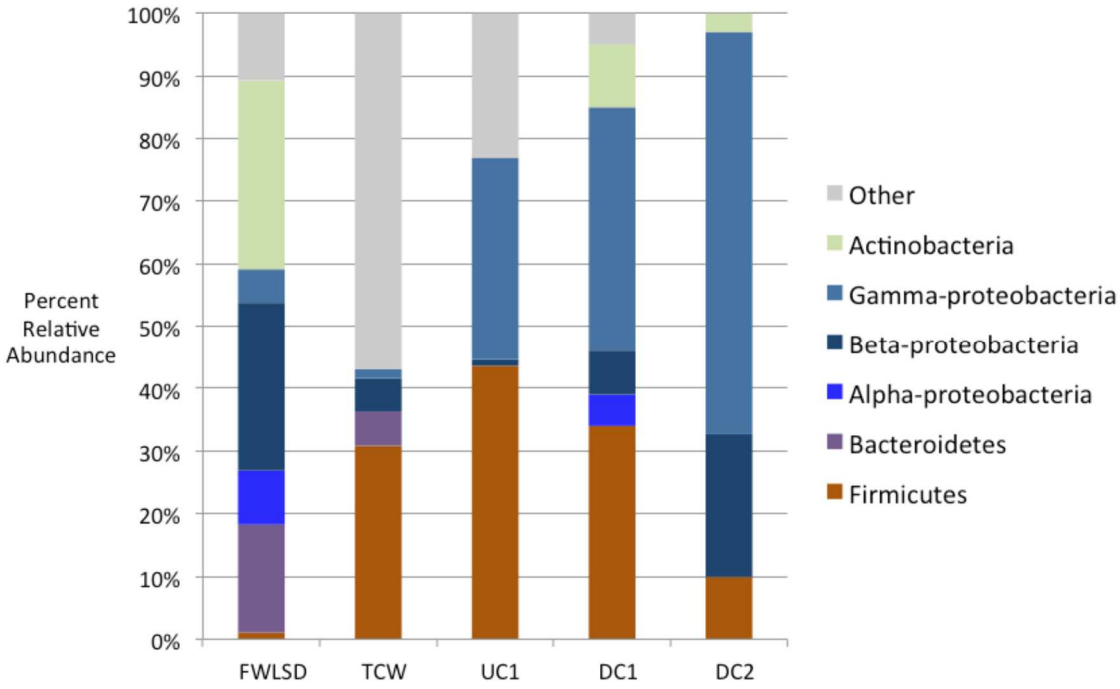

Figure 5.1. Model Consortia capture most phyla identities but not relative abundances of related populations. FWLSD = Fresh Water Lake Sequence Database (1). TCW = Tempe Canal Water. UC1 = Undefined Consortium 1, created by propagating TCW in LB broth for 24 hours to use as a contaminant inoculum. DC1 and DC2 = Defined Consortia 1 and 2, comprised of 40 isolates each of heterotrophic bacteria.

Relative abundances are less conserved, with major differences such as higher *Firmicutes* and lower *Beta-proteobacteria* in DC1 than TCW. The higher incidence of *Firmicutes* in UC1 can be attributed to the source TCW being higher in *Firmicutes* as well, whereas lack of *Bacteroidetes* could be due to competitive growth disadvantage during LB propagation (compare TCW and UC1 for *Bacteroidetes*, for example). The absence of *Bacteroides* from both Defined Consortia could be due to slower growth rate in rich medium compared to other isolates. For example, it is present at 5.5% abundance in TCW, has only trace occurrence in the subsequent LB outgrowth culture UC1 that

supports rapid growth by certain phyla, but then subsequently regains higher abundance (21.9% +/- 12.0%) when inoculated into *Synechocystis* supernatants which engender slower growth rates (NC1 and NC2). Thus *Bacteroidetes* is competitive in relatively oligotrophic environments (Tempe Canal Water; supernatants) compared to rich medium (LB broth). Studies show this phylum specializes in lake conditions associated with high dissolved organic carbon and a role in degrading organic biopolymers, such as in periods following cyanobacterial blooms (1, 251).

5.3.2 Model predicts amount of heterotroph growth in LB broths independent of which contaminant species are present.

I curated axenic heterotroph isolates to create artificial Defined Consortia. The amount of phylogenic diversity sufficient to generate a statistically significant regression (Equation 5.1, below) in LB media as calculated by ANOVA was determined empirically; 10 isolates per Defined Consortium were insufficient (data not shown), likely due to absence of kan-resistant isolates. Additional factors not included in the experimental design may be influencing the growth response, and also contribute to lack of fit of the regression. For example, growth rate under the conditions measured would likely influence the OD_{600} growth response. The Defined Consortium 1 isolates have a slower average growth rate in LB plain broth than Defined Consortium 2 (not shown). The faster growth rate of Consortium 2 would be especially relevant during the most rapid part of the growth curve, which is log phase. In the model testing (Figure 5.2), the 'Max' test condition is in linear phase, and the 'Min' and '0.01' conditions are in lag phase, whereas the '3.0' condition is closest to logarithmic phase. This may explain why the '3.0' condition of relatively faster-growing Defined Consortium 2 exceeded model

OD_{600} predictions, as the model was generated using the slower-growing Defined Consortium 1.

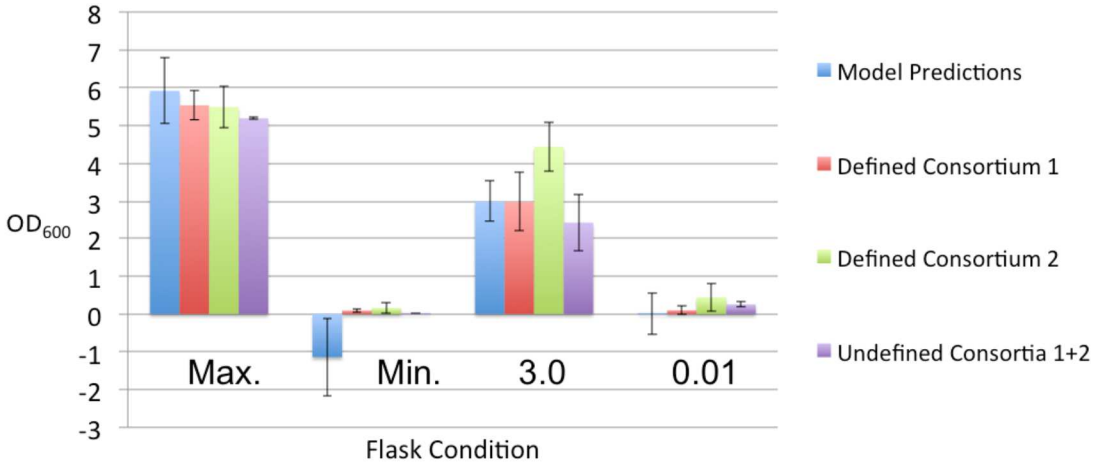

Figure 5.2. Regression model predicts heterotroph growth of diverse Consortia in LB media. Regression (Equation 5.1) was solved to calculate predictions of contaminant growth for 4 conditions shown in Table 5.2: 'Max', 'Min', '3.0', and '0.01'.
Model predictions (blue bars) were generated using Defined Consortium 1 (three biological replicates); error bars represent calculated 95% confidence intervals of each prediction. Model predictions were then tested using 2 biological replicates each of Defined Consortium 1 and 2 (red and green bars), and one replicate each of two different Undefined Consortia (purple bars)

Growth rate is likely an additional factor contributing to amount of growth, As a result, I would predict that only Consortia that fall within a certain range of growth rates would fit my model predictions when tested. In fact, I tested several additional Undefined Consortia (3 and 4) that did not meet model predictions; one of them had a very slow growth rate for undetermined reasons; the other was too small a sample size and lacked any kanamycin-resistant strains (data not shown).

5.3.3 Quantitative modeling yields non-intuitive results for contaminant mitigation

I generated a statistically significant regression, shown in Equation 5.1, below. Linear terms for salt (NaCl) and *Kan* were significant, as well as second-order terms kan^2 and pH^2 (p-value < 0.01). The salt*kan interaction was also significant (p-value < 0.05). The

linear term for pH was not statistically significant (-0.16*pH; p-value = 0.072). The R^2 predicted value for this regression is 82.9%. The term Y refers to total Consortium growth as measured by absorbance units at OD_{600}.

Eq. 5.1: $Y = 3.28 – 1.36\ (salt) – 0.75(kan) – 0.44(kan^2) + 0.31(pH^2) – 0.22(salt*kan)$.

When examining the regression model as a whole, I identified some non-intuitive results that illustrate the benefit of this quantitative approach for studying combinations of additives. Specifically, I anticipated that the condition for minimum amount of heterotroph growth would correspond to the maximum level of all three additives. While this holds true for levels of kan (200 μg/mL) and salt (0.6 M) predicted by the model (Table 5.2, 'Min'), it is not the case for pH (8.73, instead of the maximum 9.5), since the pH^2 term has a positive coefficient in the regression. I tested at n=3 with Undefined Consortia that growth in 0.6 M NaCl, 200 ug/mL kan and pH 9.5 did result in higher OD than that for the 'Min' condition, as the model predicted (data not shown). This is an especially surprising result considering that the pH of the source environments for isolates and Undefined Consortia is pretty close to pH 8.73: bench-top PBRs average approximately pH 8.5-9.5 under non-carbon-limited operating conditions, and the pH of Tempe Canal Water was measured as 8.2 +/- 0.5 at ~25 °C (n=2 daytime measurements in August and April). In general, Consortia growth should be more robust under conditions similar to those from which they were isolated; my results contradict this.

Furthermore, as noted previously, NaCl anti-porter activities (which provide tolerance to both alkalinity and sodium; see Table 5.3) are pH-sensitive; NhaA in *E. coli* has a maximum anti-port activity at pH 8.5 (252) and declined at higher pH levels. This means that the combination of 0.6 M NaCl and pH 9.5 should be even more effective at

suppressing heterotroph growth compared to pH 8.73, as the Na^+ : H^+ antiporters required for such growth would be deactivated, but this is not the case, as correctly predicted by the model.

One possible explanation for the observation that more alkalinity (pH 9.5 vs. pH 8.73) results in unexpectedly higher heterotroph growth could be due to the fact that batch growth in LB liquid medium results in very dense cultures (~10^9 cells/mL), which tends to cause anaerobic fermentation due to oxygen limitation, driving acidification of the growth medium that greatly exceeds the buffering capacity (253). This acidification then arrests growth, which would mean that starting at a higher pH of 9.5 would enable more growth before becoming limited by acidification of the medium. This loss of buffering capacity in dense cultures may also explain why there is no statistically significant interaction term between salt and pH in the regression (i.e. no salt*pH term in Eq. 5.1), despite overlapping adaption mechanisms for these two additives.

Another interesting attribute of the model is the synergistic interaction between NaCl and kanamycin, even though PICRUSt data show that none of the mechanisms for trait markers in abundant OTUs are present against both salt and kanamycin (Table 5.3, below). Instead, this synergy may be due to the cell's requirement to import H^+ for both ATP synthesis and Na^+ export. Markers found in abundant treatment OTUs, namely kanamycin phosphatase (K19300), use ATP as a co-factor; various Na^+:H^+ anti-porters also confer tolerance by importing H^+. The biological consequence would then be that kanamycin is more effective in the presence of NaCl because the Na^+ export competes for importable H^+ resources with ATP synthase needed for kanamycin deactivation. As a

result, NaCl and kan combined have a synergistic effect (and interacting regression term) in suppressing heterotroph growth.

5.3.4 Surface response model identifies opportunities for cultivation system engineers to make strategic decisions for customizing operation parameters

Although this model is for growth in LB media rather than *Synechocystis* cultures, the interaction between salt and kanamycin illustrates the general utility of statistical modeling for optimizing cultivation conditions. For example, to achieve a predicted OD_{600} of 0 absorbance units (at 24 hours' growth), engineers could either use 0.6 M NaCl with 31.5 μg/mL kan, or 0.13 M NaCl and 200 μg/mL kan. Kanamycin is much more expensive to purchase than NaCl, so the first option could reduce cost without sacrificing total contaminant mitigation under the conditions tested. Alternatively, if cultivation system materials are not chemically compatible with high salt concentrations, the second option would be preferred as kanamycin is more chemically benign. Green contour lines in Figure 5.3 (below) help to identify additional opportunities for strategic decision-making across a given heterotroph growth outcome.

Unlike with growth in LB broth, factorial analysis of heterotroph growth data in *Synechocystis* supernatants did not result in a statistically significant regression (data not shown). However, growth differences among certain growth conditions (Flask 1 and Flask 8) were significantly different (not shown). I therefore proceeded with studies of these two flask conditions to evaluate performance of additives with regard to net biofuel yield and metagenomic analysis of Consortia.

5.3.5 Additives protect laurate in deliberately contaminated *Synechocystis* supernatants

In Figure 5.4, below, I observed that in the absence of additives, heterotroph growth and laurate decay occurred within 24 hrs in *Synechocystis* supernatants. In presence of additives, heterotrophs did not increase above starting concentration until Day 3, when laurate levels also began to drop. Control flasks with no heterotrophs (or additives) retained initial laurate concentration for 6 days (not shown), demonstrating that the protective effect of additives was due to the inhibition of heterotroph growth.

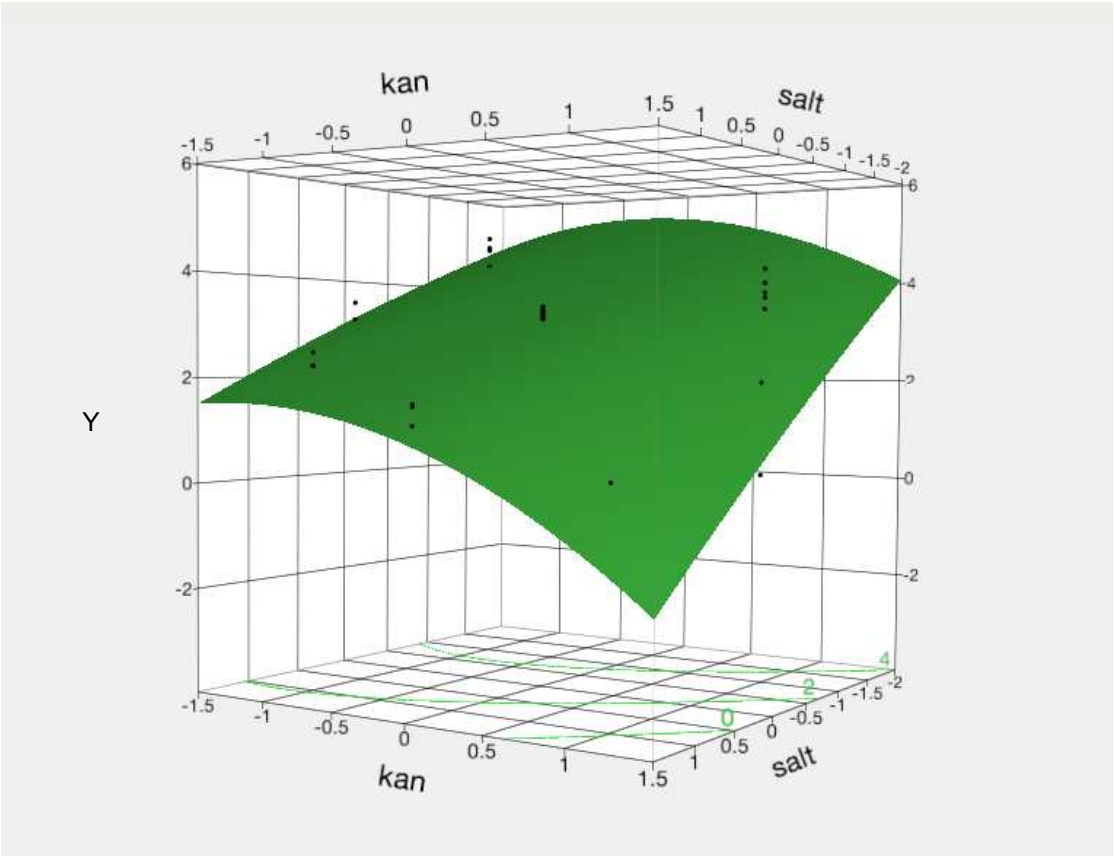

Figure 5.3. Surface response plot of interaction between NaCl and Kanamycin.
Heterotroph growth response Y on the z-axis is in absorbance units at 600 nm, OD_{600}.
kan = coded levels of Kanamycin added; salt = coded levels of added NaCl. Data points (black) are response surface plus residuals. Green contour lines of orthogonal projection are cross sections of the response surface through points of constant OD_{600} value (values indicated with green numbers) across varying combinations of NaCl and kanamycin levels. The pH for this plot was set to coded level = 0, corresponding to uncoded level of pH = 8.5

5.4A

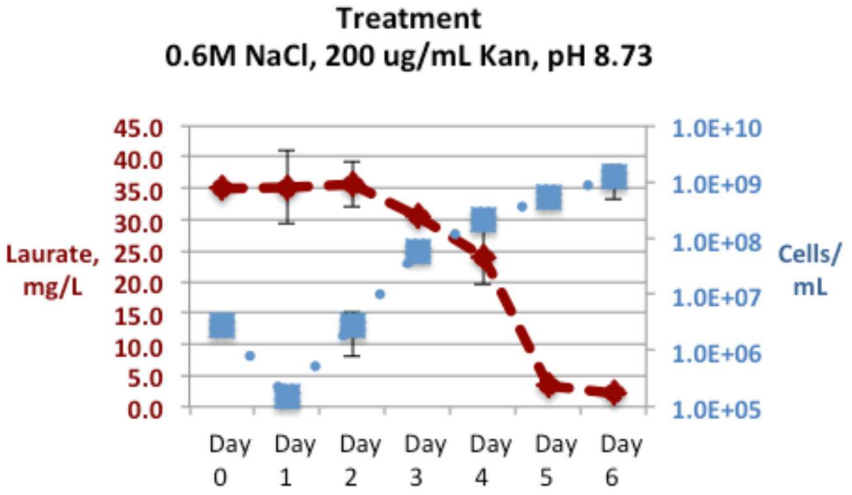

5.4B

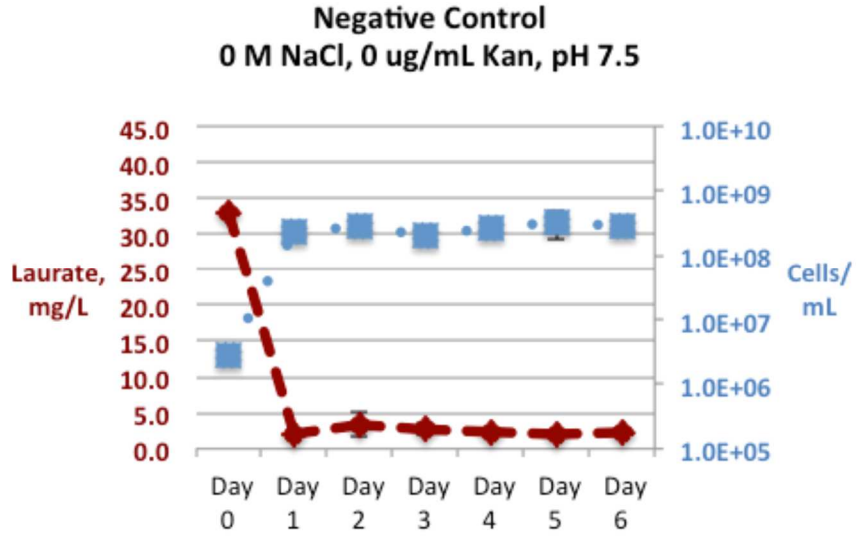

Figure 5.4. Laurate time-course assay using Defined Consortium 1 in *Synechocystis* supernatants. Treatment condition in 5.4A corresponds to levels of additives predicted to correspond to Minimum heterotroph growth in LB media according to regression model (Eq. 5.1, Table 5.2). Cfu/mL = colony forming units per mL of culture as measured on LB plain agar plates; shown in blue dotted lines on the right vertical axes. Laurate mg/L = laurate concentration as measured by gas chromatography, shown in red dashed lines on the left vertical axes.

5.3.6 Amount of Consortia growth is the same in WT and mutant *Synechocystis* supernatants

In Figure 5.5, below, I compared the relative amount of contaminant growth in supernatants of mutant *Synechocystis* strains with that of WT strains by comparing ratios of the $\log_{10}$ of cfus/mL for each condition. If cell surface structures of WT strains such as pili, EPS, or S-layer contributed to growth of Consortia, such as by contributing to SMPs (136), then I would predict that these normalized ratios would be less than the 100% negative control ratio between supernatants of WT cultures. My preliminary data (n=2 biological replicates, Defined Consortium 1) indicate that these mutant strains phenocopy WT in terms of total contaminant growth, suggesting that these surface structures do not substantially contribute to total supernatant SMP.

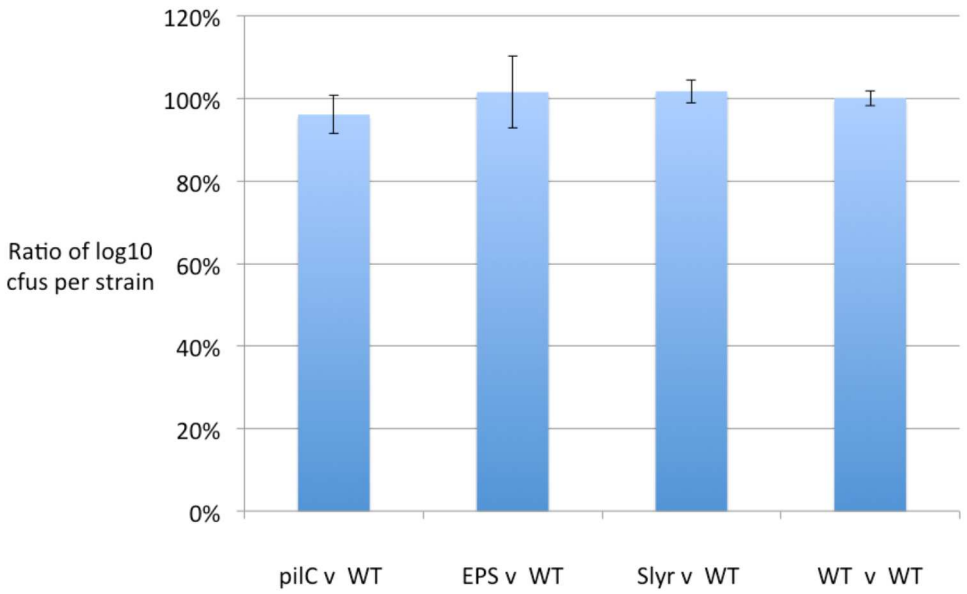

Figure 5.5. Amount of Consortia growth is the same in WT and mutant *Synechocystis* supernatants. Supernatants of *Synechocystis* strains (Table 3.2) lacking pili ('PilC', *slr0162-0163*, SD519), EPS (*slr0977*, SD506) and S-layer ('Slyr', *sll1951*, SD523) were prepared as for WT (SD525) and used to propagate Defined Consortium 1 (two biological replicates). These mutants lack the cell surface structures indicated, which may contribute to total SMPs in the supernatants that comprise the contaminant food supply. Log_{10} ratios of contaminant growth in mutant vs WT supernatants were

5.3.7 Study of community structure and function for ecological insight into regression model

I wanted to better understand my result in Figure 5.2; specifically, how it was possible to quantitatively predict the amount of contaminant growth in LB liquid media across different bacterial species. I formulated two possible hypotheses to explain this result. Hypothesis 1, the 'superbug' hypothesis, predicts that the reason I measure the same OD_{600} for a given condition across multiple Consortia is because of the presence of ubiquitous isolate(s) with a competitive growth advantage under all the conditions tested. As a result, I would measure the same OD_{600} across different Consortia because I was repeatedly measuring the growth of the same 'super-bug(s)' for all Consortia and conditions.

Hypothesis 2, which I termed the 'ubiquitous function' hypothesis, is based on the premise that bacteria have encountered salt stress, pH stress and antibiotics across all different environmental niches throughout the course of evolution, such that genes conferring salt tolerance, for example, are widely conserved across diverse phyla, and are somewhat modular, able to function relatively independently of the genomic context of a particular species. This hypothesis is an application of the Unified Neutral Theory of Hubbell, which states that traits not selected for in a given environment are ecologically equivalent, or neutral (254, 255).

Hypothesis 1 predictions can be tested by analyzing the community structure, and Hypothesis 2 can be tested by examining community function. Accordingly, I used 16S Illumina sequencing of the 16S rRNA genes and also PICRUSt metagenomic prediction to analyze community structure and function. For these analyses, I used Consortium

samples generated during the laurate time course assay at Day 0 and Day 6 (start and end points).

5.3.8 16S Illumina sequence data show that contaminant identities are not predicted by growth condition

In Figure 5.6, below, I show the relative abundances of OTUs for each growth condition. Hypothesis 1 predicts the presence of a single 'superbug' OTU as predominantly abundant across diverse Consortia. I can see many unique OTUs in the treatment condition replicates TR1 and TR2, which are very diverse and different between the two different Consortia, and the same is true for negative control replicates NC1 and NC2 across Consortia. I therefore reject the 'super-bug' hypothesis.

5.6A

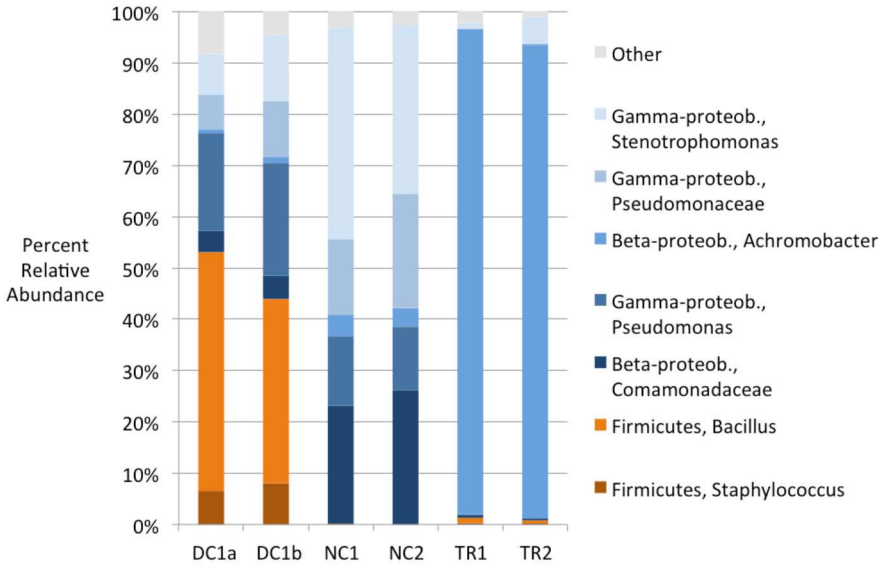

5.6B

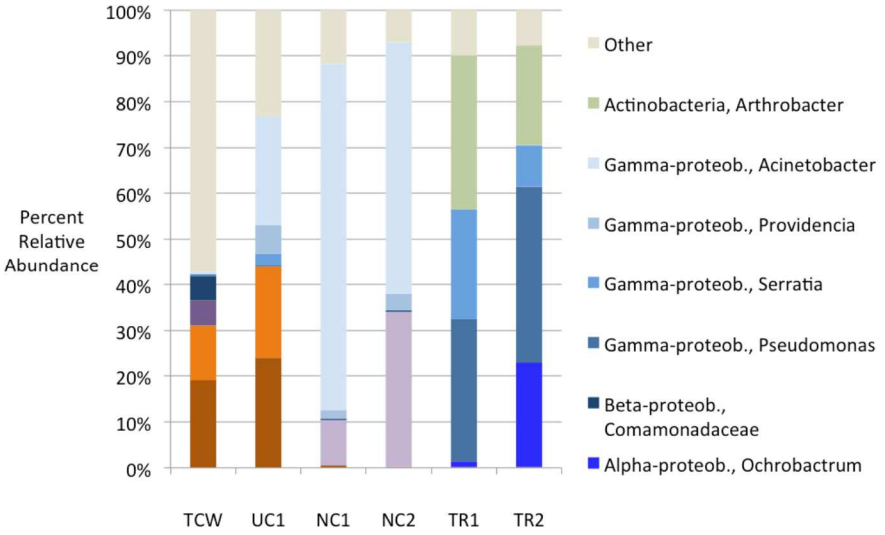

Figure 5.6. Community structure of Consortia from laurate time-course assay.
16S rRNA gene sequencing of samples from Day 0 and Day 6 time points of laurate time course assay from Defined Consortium 1 (Figure 5.6A, above) and Undefined Consortium 1 (Figure 5.6B, below) were analyzed using QIIME. Each different colored segment shows the abundance contributed by a unique 16S rRNA gene sequence, but is identified at the *Phylum* level for familiarity. The relative abundance is listed as percentage of total abundance per sample, normalized to 100%. For 5.6A and 5.6B, NC1 and NC2 = negative control replicates sampled at end of time course (Day 6); TR1 and TR2 are corresponding treatment replicates.
5.6A: DC1a and DC1b are replicates of Defined Consortium 1 inoculum used at time point 0 days.
5.6B: TCW = Tempe Canal Water sample before LB outgrowth. UC1 = Undefined Consortium 1, comprised of TCW after LB outgrowth, used as inoculum at time point 0 days.

5.3.9 PICRUSt metagenomic predictions indicate that growth in presence of additives predicts type and quantity of trait markers

In order to test Hypothesis 2, I performed three steps. First, I used literature search and PICRUSt software to curate a list of trait markers that are relevant to rapid, physiological adaptations to the presence of these additives on timescales relevant to the duration of my experiments. I identified 15 markers, shown in Table 5.3, below. Second, I used the STRING database to describe the phylogenic distribution of these markers, to test the prediction of Hypothesis 2 that they would be widely distributed across the bacterial domain. I show in Table 5.3, below, that this prediction is consistent with STRING phylogeny data, with an average %S score of 76.7%. In step 3, I used PICRUSt to predict occurrence of these markers in abundant contaminant OTUs identified from my Illumina sequence data.

Metagenomic prediction shows growth in additives is predicted by a 'minimum core' of 7 trait markers across unrelated phylotypes.

I used PICRUSt to assess the presence of trait markers for OTUs that were most abundant (>10% relative OTU abundance per sample) in both treatment and negative controls. I assessed both the total number of markers between conditions, and also the types of markers present for each growth condition. As seen in Figure 5.6, I found that abundant OTUs in all samples for treatment conditions had at least 7 markers, whereas those in negative controls had no more than 6. When the number of markers was weighted by the total relative abundance of OTUs for all samples within a growth condition, I found that 60% of all abundant treatment OTUs had 7 markers, whereas OTUs in negative controls were about 1/3 each of 4, 5, or 6 markers (Figure B.3).

Table 5.3: KEGG ortholog trait markers and their phylogenic distribution.

Additive	Adaptive mechanisms	Organism	Ortholog	KEGG Number	% clades (%S Score)
NaCl	Compatible solute biosynthesis	*Synechocystis* (2)	*stpA*	K05978	69%
NaCl	Compatible solute transport	*Synechocystis* (2)	*ggtA*	K10112	100%
NaCl, pOH	Na^+:H^+ anti-porter	*Synechocystis* (3)	*nhaA*	K03313	53.3%
NaCl, pOH	monovalent cation:H^+ antiporter	*E. coli* (4)	*mrpA (ybaL, mnhA)*	K03316 (K03455, K05565)	100%
NaCl, pOH	Ion homeostasis K^+:H^+ anti-port	*Synechocystis* (2)	*ktr, kdpA*	K01546	62.1%
pOH	H^+ transporting ATPase	*E. faecalis* (5)	*atpH (atpB)*	K02113 (K02108)	75.9%
Kan	aminoglycoside 3'-phosphotransferases	*S. aureus* (6)	*Aph3-II; (aph3'III)*	K19299, (K19300)	N/A
Kan, pOH	multidrug / efflux transport protein	*E. coli* (3)	*mdfA, cmr*	K08160	41.4%
Kan	Aminoglycoside /multi-drug efflux	*E. coli* (7)	*acrD*	K18324	93.1%
Kan	Aminoglycoside / multi-drug efflux	*P. aeruginosa* PAO1 (8-10)	*mexY*	K18095	93.1%
Kan	Aminoglycoside / multi-drug efflux	*A. baumannii* (7)	*adeA*	K18145	79.3%

Additives are color-coded, with different molecular mechanisms for a given additive indicated by different shades within each color. Markers conferring tolerance to NaCl are in shades of orange; markers related to import of H^+ (as hydronium) are colored in shades of brown; and markers related to Kanamycin (Kan) resistance are shown in shades of blue. %S score refers to prevalence of ortholog in bacterial domain, calculated using STRING database.

5.7A

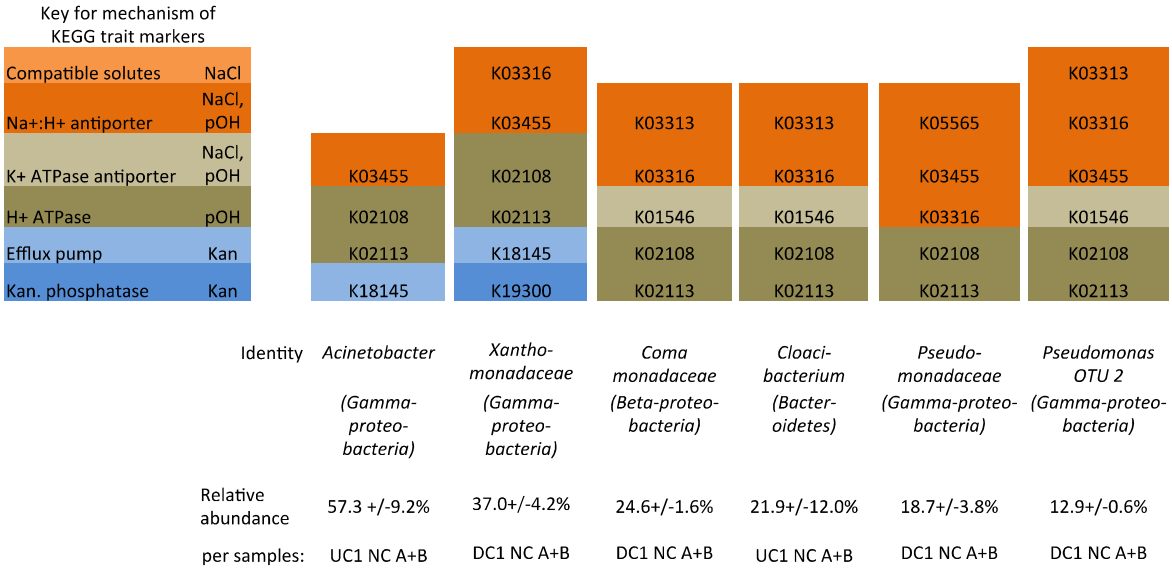

5.7B

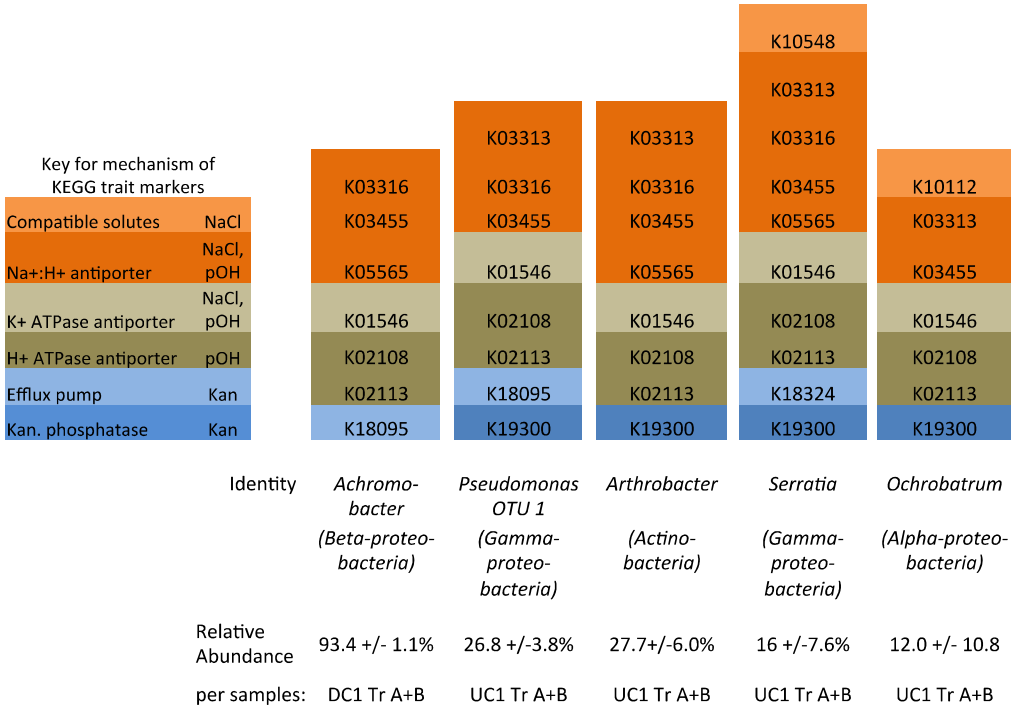

Figure 5.7. PICRUSt data of community function of Consortia from laurate time-course assay. PICRUSt data correspond to the abundant unique 16S rRNA sequences and identities in Figure 5.6. Abundances are given as replicate averages of the samples indicated. Figure 5.7A corresponds to identities from negative control conditions (above), and Figure 5.7B corresponds to identities from treatment conditions (below).KEGG ortholog markers are described in Table 5.3, with the same color-coding.

While it's not surprising that selective growth conditions in the treatment samples would enrich for strains carrying kanamycin resistance genes, for example, it is noteworthy that such markers would be largely absent from abundant OTUs in negative control strains, because these markers are widely distributed across diverse taxa. This is not fully explained by relative growth advantage of strains with fewer markers under permissive growth conditions, as strains abundant in negative control samples still carry an average of 5 markers. Thus while trait markers are important for determining community structure under different growth conditions, other factors are also important in predicting Consortia ecology.

As shown in Figure 5.7, marker type was also predicted by growth condition. In treatment conditions, all abundant OTUs had a minimum core of 1 kan-resistance marker (blue), 3 H^+ importers (brown), and 3 Na^+ ion adaption markers (orange). No abundant OTUs in the negative control samples had this minimum core of markers; four of six abundant OTUs in negative controls were missing a kan-resistance marker, and most had fewer H^+ import and Na^+ export markers. As a positive control for my analysis pipeline, all strains showed the presence of F-type ATPase genes (K02113 and K02108; *atpBH*), which code for highly conserved bi-directional protein complex subunits of cellular respiration that can either import H^+ or alternatively synthesize ATP using a proton gradient.

Because the regression coefficients of the quantitative model are based on coded units (see Table 5.1), the magnitude between different terms and factors can be directly compared to facilitate interpretation of model predictions at different levels of additives within the sample space tested. Accordingly, the model predicts that the single most

significant factor in mitigating heterotroph growth is the added NaCl, because it has the largest negative coefficient. This is consistent with the PICRUSt data (Fig. 5.6), which shows that the difference in number of KEGG markers between treatment and control abundant OTUs is largely due to differences in markers related to Na^+ ion (shades of orange and light brown).

These results are consistent with the reported ubiquitous and modular function of these markers. Ion homeostasis and salt and nutrient stress responses that are relevant to the time scales and mechanisms in this study include physiological changes in water-borne pathogenic bacteria such as in *E. coli* and *Vibrio cholera* that must survive immune response during host infection, but also persist in external environments such as waterways during transmission between hosts (3). For example, the Na^+:H^+ anti-porter NhaS3 from *Synechocystis* was able to restore salt tolerance in an *E. coli* mutant lacking its native sodium anti-porter activity (256). In another study, bacterial biofilms colonizing the surface of sea lettuce macroalgae (*U. australis*) (257) showed that only 15% of bacterial species were conserved across sea lettuce biofilm samples, but nearly 70% of samples had the same set of core functional genes. Importantly, bacteria with the same core of functional genes may be taxonomically distant, forming a smaller 'guild' of unrelated phyla that are competent for biofilm formation that occur within the larger bacterial microbiome exposed to sea lettuce surfaces.

The Ubiquitous Function hypothesis does not preclude a role for microbial interactions influencing Consortia ecology. Previous studies have shown that stochastic elements (such as random immigration of species from a larger meta-community into a smaller niche microcosm) and deterministic elements (such as heterogeneous niche

micro-environments), are not mutually exclusive (254, 255). For example, studies of root-associated soil fungi (254) and termite gut bacteria (255) found that deterministic elements (soil pH; termite foregut and hind-gut microenvironments, respectively) were important predictors of microbial communities.

Especially in *Synechocystis* supernatants, it may be that the growth differences shown in Figure 5.4 could either be due to differences in growth rate in oligotrophic medium, and/or microbial interactions that may not occur in LB broth. An interaction specifically involving cyanobacteria has also been identified: *Prochlorococcus*, which is abundant in open oceans, relies on other ocean-dwelling microbes to detoxify hydrogen peroxide generated by solar energy absorbed by organic compounds (258). *Bacteroidetes*, which was detected in TCW (Figure 5.1) and which are reported to be most abundant in fresh-water lakes after cyanobacterial blooms because of their ability to biodegrade complex polysaccharides and other biopolymers, may enable other heterotrophs to thrive (1).

However, although many synthetic ecology studies focus on microbial interactions, a systematic test of cultures of aqueous samples were shown to be dominated by competition for nutrients rather than cooperative interactions such as syntrophies in oligotrophic medium (beech leaf media) (259). Additionally, if microbial interactions such as syntrophies are important predictors of contaminant growth in *Synechocystis* cultures, then I would not see a single OTU dominating the total heterotroph abundance in a given sample, which is what I observed in the Treatment Condition of Defined Consortium 1 (Figure 5.6A), where 95% of total abundance is occupied by a single genus of *Achromobacter*.

5.4 Conclusion

These results show that levels of additives were largely able to predict the amount of Consortia growth in LB broth, independent of which species were present (Figure 5.2). Augmenting experimental design to control for the effect of growth rate and pH levels, such as with automated logging and/or utilizing chemostatic/turbidostatic experimental conditions, would enhance model accuracy, especially in relatively oligotrophic growth medium of *Synechocystis* cultures. I also demonstrated that NaCl, kanamycin, and alkalinity protect laurate for 3-4 days in deliberately contaminated *Synechocystis* supernatants by suppressing the growth of contaminants. *Synechocystis* mutants with altered cell surface structures did not impact the amount of Consortia growth. Engineering feedstock strains to produce fewer SMPs, such as by deletion of *wzc*, which has been shown to result in 50% reduction of released exopolysaccharides compared to wild-type *Synechocystis* (121), may enable an additional genetic means of contamination management.

Preliminary metagenomic and community abundance data support the conclusion that traits rather than species are the key determination of community structure for selective growth condition in the presence of NaCl, kanamycin and alkalinity, which supports my hypothesis that function and not structure is what predicts the bacterial PBR contaminome under these conditions. This model should be tested using direct gene expression measurements with additional diverse Consortia.

I conclude that these data are consistent with a ‘minimum core’ of markers occurring in a guild of unrelated contaminant species predicts growth in the presence of additives, which is based on the premise that unrelated species with similar traits are

ecologically equivalent during competitive growth (257). I did not see much overlap between abundant species identities in treatment flasks between Consortia drawn from a single 'meta-community' of heterotrophs (both Defined and Undefined Consortia included species from Tempe Canal Water). I did find that growth condition was a good predictor of a core set of functional genes, namely of 7 KEGG markers present in all abundant treatment OTUs (Figure 5.7). Bacterial phyla vary widely in their genetics and physiology; it is challenging to meaningfully capture this diversity using only a small, defined consortium. However, my study indicates that the traits necessary to grow as contaminants in the presence of one or more of these commonly used additives are widely represented, such that much of the increase in phylogenic diversity between these Defined and Undefined Consortia is functionally redundant to the response variables of interest in this study (contaminant growth and laurate consumption in the presence of different combinations of these additives).

5.4.1 Results suggest knowledge of genetic regulation and molecular mechanisms of additive tolerance to inform strategic combinations of additives.

Figure 5.4 showed that additives protect laurate consumption by inhibiting growth of heterotrophic bacteria. Na^+ toxicity is due to competitive binding with K^+-dependent enzymes (2). This is tied to mechanisms of resistance: ion homeostasis regulation, such as increasing cytoplasmic concentration of K^+ relative to Na^+, will improve resistance to added NaCl present in the growth medium. As described previously, this is coupled with H^+ transport, such that several trait markers provide 'two for the price of one' benefit to the contaminants that harbor them: NhaA confers tolerance to NaCl and alkalinity, and MdfA confers tolerance to NaCl and kanamycin (Table 5.3). Knowledge of such

overlapping adaptive mechanisms would inform more strategic selection of combinations of additives that each require a separate adaption mechanism. I predict that selection of additives requiring mutually exclusive adaptations would be the most effective in suppressing contaminant growth, especially in oligotrophic media, where energy or nutrient sources needed for synthesizing adaptive molecules may be in shorter supply.

5.4.2 Ecological models suggest 'probiotic' approach for long-term management of PBR ecology.

In the field of ecology, a long-standing objective has been to develop model that is able to explain, much less predict, both the identities and abundances of species in a given niche. Theories including r/K strategies (260, 261), the Unified Neutral Theory (262), and niche theory (255, 263) have undertaken quantitative predictions to explain biodiversity across taxonomic domains, geographies, and scales, with preliminary data able to test and support some but not all of the predictions of these various models (264), due in part to difficulty of modeling these parameters experimentally.

One elaboration of neutral theory, termed the lottery hypothesis, predicts that the structure of a community for a given niche is largely determined by whichever species within an ecologically equivalent group has immigrated there first (265). This hypothesis was supported by a study of two closely related coral reef goby fish (*G. histrio* and *G. erythrospilus*): once one goby species inhabited a coral niche, it could not be displaced by the other goby species (266).

Although the experimental design used was not intended to test such ecological models, my findings were consistent with the theory of ecological equivalence. The Lottery Hypothesis is also supported by the theory of ecological equivalence. It is

possible, therefore, that the PBR contaminome also conforms to the predictions of the Lottery Hypothesis. If so, it would have implications for longer-term community structure, namely that, like goby fish, contaminants that become abundant during initial PBR start-up will likely be most abundant for longer experiments, such as repeated 'runs' or cultures within a single PBR. This raises the exciting possibility of proactively "immunizing" a cultivation system with a beneficial or benign Consortia to establish a healthy and productive niche microcosm, thereby reducing the ability of additional detrimental heterotrophs from the environment to colonize feedstock cultures.

These results have shown that quantitative predictions yielding non-intuitive insights can be generated using an artificial Consortia to simulate the bacterial PBR contaminome under controlled lab conditions. To my knowledge, this is the first study showing the effectiveness of artificial Consortia to study PBR contamination, and the first study quantifying contribution of multiple interacting factors in suppressing PBR contaminants. The value of quantitative prediction of contamination is highly valuable for both ecological insight, and also for economic modeling of cost-to-benefit for synergistic application of more costly antibiotic used with less expensive salt and alkalinity, and how these variables influence biofuel yield.

I conclude that this study has been successful proof-of-concept showing the utility of combining DNA sequence analysis, artificial consortia and statistical modeling in generating quantitative and ecological insights into studying the PBR contaminome under controlled lab conditions, which meets my goal for this project. This platform is modular and versatile; it is readily compatible with experiments at larger scales and longer durations, and applied to other contaminant Consortia such as cyanophage or eukaryotes.

Finally, I note that the ease of monitoring laurate production as a response variable, and the natural tolerance to commonly-used additives for suppressing contaminants at industrial scales, makes a laurate secreting strain like this *Synechocystis* mutant an ideal candidate as a model organism for the study of the synthetic ecology of PBR contamination under controlled conditions.

CHAPTER 6

SUMMARY, PERSPECTIVE, AND OUTLOOK

6.1 Research trajectory and decision checkpoints

This study was initiated on the strength of addressing two separate but related knowledge gaps in the field of microbiology: one, an apparent dearth of studies in the literature characterizing axenic phototroph biofilms, and two, the relevance of these biofilms to the larger ongoing research initiative in producing biofuels from phototrophs. Regarding the state of the literature, I originally (and naively) thought that the under-developed state of axenic phototroph biofilm research relative to its scientific importance was likely due to the "silo-ing" of medical microbiology and environmental microbiology / engineering into two different disciplines, each with a distinct set of methodologies. As phototrophs belonged in the latter category, I reasoned, axenic biofilm studies, a technique largely restricted to the former category, were not historically a priority. Thus, I presumed (incorrectly) that applying familiar previously established methods from my studies of heterotrophic bacteria to a model phototroph, *Synechocystis*, would enable a substantive contribution to advancing the field of phototroph microbiology. This presumption was initially bolstered by preliminary data collected within the first few months of research showing axenic biofilm formation using the crystal violet assay.

However, I had great difficulty reproducing those preliminary results reliably in subsequent years. Important clues (and key motivation not to abandon this project) came from very thick and repeatedly occurring green biofilms growing in the roof-top photobioreactor that replaced themselves with each reactor run and caused great difficulty among PBR engineers for their continued removal and prevention (Figure 3.1).

Discovery that using softened water in the preparation of the growth medium abated biofilm formation in the roof-top PBR provided an important avenue of investigation into nutrient signals being required for *Synechocystis* to form biofilms. I recapitulated this finding at lab scale when a humidification flask was inadvertently omitted from a crystal violet assay experiment, causing starter culture evaporation that increased nutrient strength, which was then decreased when cultures were resuspended in 1.0x BG11. Thus, with additional screening of additional growth parameters such as illumination levels, temperature, shaking, evaporation rate, and others for optimization of this modified crystal violet assay, I was able to demonstrate with statistical significance that exponentially growing *Synechocystis* forms axenic biofilms in response to changes in nutrient status.

At this point there was some suggestive evidence that a new paradigm in biofilm research had potentially been uncovered, since studies previously characterizing heterotrophs describe their ability to form biofilms in nutrient replete media using this assay, whereas *Synechocystis* cannot. If this *Synechocystis* phenotype also holds true for other phototrophs, it could certainly be a major contributing factor to why so few studies of axenic phototroph biofilms have been published: previous researchers, including myself, had only assessed phototroph biofilms in nutrient replete media, leading to negative (and unpublished) results. However, the crystal violet assay grows cultures in batch mode, during which time, increase of heterotroph (and phototroph) culture densities certainly drive nutrient limitation, along with many other stress signals typical of stationary phase. One could argue that the difference may be in terms of degree: whereas growing in batch mode would create condition of nutrient limitation gradually over the

course of the growth curve, rapid dilution of growth medium such as used in the adapted crystal violet assay for *Synechocystis* may engender some sort of stress response driving biofilm formation. Alternatively, perhaps the differences in metabolism between phototrophs and heterotrophs resulted in different thresholds of sensitivity to nutrient limitation during batch growth. Clearly, more information was needed.

Taking the advantage of *Synechocystis* cultivation in a defined growth medium BG11, I then proceeded to screen individual nutrients (phosphate, divalent cation metals, nitrogen, carbon) at various dilutions, which did seem to increase biofilm formation compared to nutrient-replete condition, but not reproducibly enough to demonstrate statistical significance (data not shown). Furthermore, confocal microscopy revealed that *Synechocystis* biofilms were rarely more than a monolayer (similar to a few other model organisms for heterotroph biofilm studies); the scarcity of cellular material generated by the modified crystal violet assay limited the ability to biochemically characterize these biofilms. Therefore, I developed an aggregation assay using nutrient limitation, and was able to determine that aggregation, which, like biofilm formation, requires cell-cell binding, could be induced by change in nutrient status, and was dependent on bioenergy. However, I was still unable to identify the signals driving aggregation, whether nutrient limitation, or salt or osmotic stress that accompanies changes in nutrient strength, or other signal(s).

More information was needed to uncover the environmental conditions and genetic regulation of these phenotypes; for example, how they related to conserved stress responses that occur during nutrient limitation, such as stringent response. Additionally, although my library of mutants with altered cell surface structures demonstrated that the

requirement for pili and S-layer for biofilm formation was conserved across heterotrophic and phototrophic species, I was unable to detect the presence of a hypothesized aggregant that enabled cell-cell binding through preliminary measurements of outer membrane proteins and treatment with cellulase. I elected to perform an RNA seq transcriptome experiment in order to be able to correlate internal regulatory changes with the incidence of aggregation, to better understand how *Synechocystis* was interpreting and responding to its environment.

The results of this RNA seq experiment provided strong preliminary evidence that aggregation was occurring in the context of stringent response (SR), based primarily on comparison of stringent response RNA seq data from a related cyanobacterium, *Synechococcus elongatus*. Interestingly, *S. elongatus* undergoes SR upon shift to darkness (without aggregation), whereas *Synechocystis* aggregation is dependent on light. While these RNA seq data would need to be confirmed with additional lines of evidence such as measurements of (p)ppGpp levels and assessment of deletion mutant SR and aggregation phenotypes, the results are consistent with SR being linked to nutrient limitation and aggregation in heterotrophic bacteria, and suggests than in bacteria with a phototrophic metabolism such as *S. elongatus* and *Synechocystis*, light limitation is analogous to nutrient limitation in heterotrophs. This is logical because in heterotrophs, certain nutrients such as carbohydrates are also the cell's energy supply; thus SR response across all metabolic profiles could be under the umbrella of energy limitation. Indeed, one of the hallmarks of SR is down-regulation of translation, because synthesis of ribosomes is a very energy-intensive process, comprising 30-50% of cellular energy.

In addition to providing an important clue linking aggregation, SR and nutrient/light limitation, this study was also very useful for suggesting that in cyanobacteria, while aggregation occurs with SR (in the light), SR does not necessarily engender aggregation (in the dark), demonstrating that aggregation is regulated separately from SR. While I did not identify the specific environmental signal responsible for either aggregation or SR due to change in nutrient status, results suggest that I did make progress by determining that there are two distinctly regulated (though obviously related) signals and pathways between aggregation and SR, which helped to guide proposed experiments to elucidate these pathways in the Conclusion of Chapter 4.

The final area of investigation returned to the starting point of Chapter 3, namely the *Synechocystis* cell surface and how it related to the productivity of the roof-top PBR. I investigated whether my library of mutants with missing cell surface structures, in addition to having benefits related to a non-biofouling phenotype, might also lend a genetic means of enhancing laurate yield by contributing less fixed carbon and nitrogen for consumption by contaminants in the supernatant, compared to parent strains that shed these cell surface structures into the growth medium. I additionally screened for the effectiveness of salt, antibiotic and alkalinity in suppressing the growth of laurate-consuming heterotrophic bacteria. While these mutants did not provide any detected benefit regarding growth of contaminants, this study did demonstrate the effectiveness of combining statistical modeling and artificial contaminant consortia to model the PBR contaminome in the lab, and generate quantitative and qualitative predictions. These findings suggested improving strategies for mitigating contamination in the roof-top PBR

by choosing combinations of additives or conditions informed by molecular mechanisms of tolerance of tolerance and/or growth by contaminants (discussed in more detail below).

6.2 Interpretation of findings in the context of current paradigms of heterotrophic bacterial biofilm formation

At the conclusion of this research topic, I revisited my original speculation about the dearth of studies of axenic phototrophic biofilms. Was this truly a "low-hanging fruit" on the tree of microbiology research, that is easy to study but had simply been neglected previously, or is the paucity of publications an indication that phototrophs engender a new paradigm in bacterial biofilm formation, and thus a more challenging topic to "harvest"? One of the more interesting findings in my studies of axenic *Synechocystis* aggregation was that the mutant *wza*, which makes only 25% of the cell-bound EPS of WT cells under nutrient replete conditions (121), has a super-binding phenotype when shifted to reduced nutrient strength. Furthermore, unlike WT, *wza* mutants settle out of solution in standing nutrient-replete cultures.

In the Chapter 3 Conclusion, I described a model of cell-cell binding in *Synechocystis* that is regulated by two different mechanisms depending on whether nutrient status was replete or not, and that the role of Wza-dependent EPS in *Synechocystis* under nutrient-replete conditions seemed to be related to keeping the cells in suspension (cell-cell repulsion). This represented a new (and opposite) role for Wza-dependent EPS, which previously had only been described as contributing to increased cell binding in heterotrophs. Additionally, this new feature would explain why, unlike the heterotrophs I and others had previously studied with the crystal violet assay, *Synechocystis* required a shift to nutrient deplete conditions, which might have led many

researchers to conclude from preliminary data in nutrient replete conditions that phototrophs cannot form biofilms by themselves. The fact that diverse species of cyanobacteria have EPS that share the common feature of being negatively charged due to presence of uronic acids and sulfate groups uncommon in other bacteria (110, 111, 115) suggest that the role of EPS in keeping cyanobacteria dispersed under nutrient replete conditions may be widely conserved, and indeed represent a new paradigm that distinguishes phototrophs from heterotrophs in how they use EPS, and thus the requirement of nutrient limitation to shift to a cell-binding phenotype. Furthermore, it may explain why *Synechocystis* only forms a monolayer or so during biofilm formation, similar to *C. crescentus*, which cannot bind to itself due to special surface properties, and only forms a monolayer (though a very strong one), on glass coverslips. If this reasoning is correct, it would suggest that the different role of S-layer in biofilm formation (essential) vs aggregation (not essential but does contribute) may be due to different mechanisms of adhesion between these two phenotypes. Using the modified crystal violet assay to screen additional phototrophic bacteria is necessary to address these questions.

6.3 Follow-up studies to extend the most significant findings of this research

How do I put these phenotypic differences in the context of the divergent lifestyles and metabolisms of these bacteria, and what do these differences tell us about the evolution of biofilm formation and its role in bacterial pathogenesis? An exciting recent discovery that could be used to study these questions was the identification of a non-photosynthetic group of bacteria, termed *Melainabacteria*, assigned to the *Cyanobacteria* phylum based on genome sequence (41). This discovery is in line with all other phyla known to contain phototrophs also containing non-phototrophic members;

related studies in this area recommend cyanobacteria be assigned a new class termed *Oxyphotobacteria*. Although this bacterium cannot yet be cultured axenically in the lab, it could provide an important missing link in comparative biology studies of the function and evolution of biofilm formation between cyanobacteria and heterotrophs. For example, if a feature was found that was conserved between *Melainabacteria* and *Synechocystis* biofilm formation but not found in the much more recently evolved *E. coli*, it may enable identification of novel molecular targets for therapeutic treatment of infections that would not be identified when comparing biofilm mechanisms between closely related bacterial pathogens such as *S. enterica* and *E. coli.* Additionally, *Melainabacteria* is a heterotrophic fermenter, and fermentation metabolism predates the evolution of photosynthesis. This could provide the tools needed to study how the evolution of metabolism and the evolution of biofilm formation interacted, a potentially rich and under-studied area related to basic science and applied bioremediation.

Another area for future development relates to the crystal violet assay. Perhaps because of its cell-cell repulsion phenotype, *Synechocystis* did not form very thick or extensive biofilms using the adapted crystal violet assay, which is different from the results of this assay with heterotrophs. Thus, it may be necessary to develop additional formats for harvesting larger amounts of biofilm for biochemical and transcriptome analysis, instead of relying on the related aggregation assay. The glass tube format of the roof-top PBR worked very well for growing thick green biofilms, which could be due to the much larger culture volume, and/or the semi-chemostatic mode of operation. A bench-top-scale version of similar glass-tube format compatible with microscopy may be beneficial for studying biofilm structure over time. The company Biosurface Technology

Corporation has previously made customized, autoclavable reactors for the study of epilithic mixed species phototrophic biofilms, and would be a good resource for developing a customized reactor for planktonic format axenic phototrophic biofilms (267). This would be beneficial both for biofilm PBR applications, and developing the basic biology of phototrophic biofilms. Because heterotrophic bacteria get their energy from nutrients (inside the reactor), whereas phototrophs get their energy from light (outside the reactor), the available designs for off-the-shelf biofilm reactors are not ideal for phototrophs. Based on the information presented in this dissertation, some form of customized biofilm reactor will likely be essential for the development of *Synechocystis* or similar bacterium as a model organism for axenic phototrophic biofilm formation to reach its full potential, in line with heterotrophic biofilm research. These methods should be developed in parallel with study of biofilm formation by other phototrophs, such as nitrogen-fixing cyanobacteria.

Finally, I return to the topic of synthetic ecology of the PBR contaminome. The challenge of managing PBR ecology is perhaps the most daunting and significant challenge in large-scale production of microbial biofuels, and likely requires a multivariate approach combining anti-contamination strategies wih more "probiotic" approaches of engineered polycultures for a total ecology management system (268). Engineering the niche of the PBR for healthy and productive feedstock cultures means developing multiple mutually compatible approaches fundamentally different than industrial microbiology historically using sterilization and antibiotics to maintain pure cultures, but provides opportunities to substitute environmentally sound approaches to replace intensive use of antibiotics. These studies highlighted the importance of

developing contaminant-management strategies that are informed by understanding the molecular mechanisms and genetic regulation of heterotroph physiology.

A promising idea attempted in my lab previously is the use of nutritional immunity to selectively enrich *Synechocystis* growth at the expense of contaminants. Nutritional immunity comes from the field of medical microbiology and describes the strategy of the host to sequester essential nutrients (often metals) to limit the growth of pathogens; pathogens have also been shown to use the same strategy to out-compete other microbes in the host microbiome (reviewed in (269-271). The utility of this approach in managing contamination of microbial biofuel cultures has been recently reported in several strains (272), such as engineering *E. coli* to use melamine as a sole nitrogen source, or yeast to use phosphite as a source of phosphorous, both of which are metabolic capabilities not widely found in nature. This has the added advantage of providing a method of biocontainment of engineered feedstocks, as sources of melamine and phosphite are rare in the environment.

Future studies should be conducted to combine the techniques of nutritional immunity, along with engineered probiotic consortia and strategic combinations of additives. This project would require several stages, including development of a nutritional immunity system for *Synechocystis* based on an essential nutrient that is not released in appreciable quantities into the supernatants of growing cultures, or whose uptake by contaminants can be repressed in some controlled way. Next, a group of genetically tractable heterotrophs that are beneficial or at least benign when grown in co-culture with *Synechocystis* would need to be identified. Such a probiotic consortia may benefit culture health in a number of ways, including increased stability of the PBR

ecosystem against environmental perturbations, potentially including the ability to resist colonization by additional heterotrophs, as well as providing *Synechocystis* with CO_2 from heterotroph respiration. These probiotic strains could then be engineered to have reduced SMPs, such as with a *wzc* mutation that was shown in *Synechocystis* to have reduced production of RPS. Finally, these probiotic candidates would be engineered to have a similar nutritional immunity and additive tolerance profile as *Synechocystis*, but without competing with *Synechocystis* for other limiting nutrients.

With this example, I have returned to the opening theme of nature-inspired design, and the overlap in human endeavors of microbiology between topics of medicine and of sustainability, derived from the remarkable capacity of bacteria to encompass a huge diversity of metabolisms while reusing the structural format of a single cell; and so conclude this dissertation.

WORKS CITED

1. **Newton RJ, Jones SE, Eiler A, McMahon KD, Bertilsson S.** 2011. A guide to the natural history of freshwater lake bacteria. Microbiol Mol Biol Rev **75:**14-49.

2. **Hagemann M.** 2011. Molecular biology of cyanobacterial salt acclimation. FEMS Microbiol Rev **35:**87-123.

3. **Padan E, Bibi E, Ito M, Krulwich TA.** 2005. Alkaline pH homeostasis in bacteria: new insights. Biochim Biophys Acta **1717:**67-88.

4. **Swartz TH, Ikewada S, Ishikawa O, Ito M, Krulwich TA.** 2005. The Mrp system: a giant among monovalent cation/proton antiporters? Extremophiles **9:**345-354.

5. **Nyanga-Koumou AP, Ouoba LI, Kobawila SC, Louembe D.** 2012. Response mechanisms of lactic acid bacteria to alkaline environments: a review. Crit Rev Microbiol **38:**185-190.

6. **Woegerbauer M, Zeinzinger J, Springer B, Hufnagl P, Indra A, Korschineck I, Hofrichter J, Kopacka I, Fuchs R, Steinwider J, Fuchs K, Nielsen KM, Allerberger F.** 2014. Prevalence of the aminoglycoside phosphotransferase genes aph(3')-IIIa and aph(3')-IIa in Escherichia coli, Enterococcus faecalis, Enterococcus faecium, Pseudomonas aeruginosa, Salmonella enterica subsp. enterica and Staphylococcus aureus isolates in Austria. J Med Microbiol **63:**210-217.

7. **Rosenberg EY, Ma D, Nikaido H.** 2000. AcrD of Escherichia coli is an aminoglycoside efflux pump. J Bacteriol **182:**1754-1756.

8. **Masuda N, Sakagawa E, Ohya S, Gotoh N, Tsujimoto H, Nishino T.** 2000. Contribution of the MexX-MexY-oprM efflux system to intrinsic resistance in Pseudomonas aeruginosa. Antimicrob Agents Chemother **44:**2242-2246.

9. **Brock TD, Freeze H.** 1969. Thermus aquaticus gen. n. and sp. n., a Nonsporulating Extreme Thermophile. J Bacteriol **98:**289-297.

10. **Ishino S, Ishino Y.** 2014. DNA polymerases as useful reagents for biotechnology – the history of developmental research in the field. Front Microbiol **5:**465.

11. **Coker JA.** 2016. Extremophiles and biotechnology: current uses and prospects. F1000Research **5:**F1000 Faculty Rev-1396.

12. **Rittmann BE.** 2008. Opportunities for renewable bioenergy using microorganisms. Biotechnol Bioeng **100:**203-212.

13. 2016, posting date. Energy Information Administration. U.S. Department of Energy. [Online.]

14. **Song Y, Peng R, Hensley DK, Bonnesen PV, Liang L, Wu Z, Meyer HM, Chi M, Ma C, Sumpter BG, Rondinone AJ.** 2016. High-Selectivity Electrochemical Conversion of CO2 to Ethanol using a Copper Nanoparticle/N-Doped Graphene Electrode. ChemistrySelect.

15. **Brasier MD, Antcliffe J, Saunders M, Wacey D.** 2015. Changing the picture of Earth's earliest fossils (3.5-1.9 Ga) with new approaches and new discoveries. Proc Natl Acad Sci U S A **112:**4859-4864.

16. **Rittmann BE.** 2008. Opportunities for renewable bioenergy using microorganisms. Biotechnol Bioeng **100:**203-212.

17. **Rippka R, Coursin T, Hess W, Lichtle C, Scanlan DJ, Palinska KA, Iteman I, Partensky F, Houmard J, Herdman M.** 2000. Prochlorococcus marinus Chisholm et al. 1992 subsp. pastoris subsp. nov. strain PCC 9511, the first axenic chlorophyll a2/b2-containing cyanobacterium (Oxyphotobacteria). Int J Syst Evol Microbiol **50 Pt 5:**1833-1847.

18. **Pagani I, Liolios K, Jansson J, Chen IM, Smirnova T, Nosrat B, Markowitz VM, Kyrpides NC.** 2012. The Genomes OnLine Database (GOLD) v.4: status of genomic and metagenomic projects and their associated metadata. Nucleic Acids Res **40:**D571-579.

19. **Liu X, Fallon S, Sheng J, Curtiss R, 3rd.** 2011. CO2-limitation-inducible Green Recovery of fatty acids from cyanobacterial biomass. Proc Natl Acad Sci U S A **108:**6905-6908.

20. **Liu X, Sheng J, Curtiss R, 3rd.** 2011. Fatty acid production in genetically modified cyanobacteria. Proc Natl Acad Sci U S A **108:**6899-6904.

21. 2011. Microbiology by numbers. Nat Rev Micro **9:**628-628.

22. **Davey ME, O'Toole GA.** 2000. Microbial Biofilms: from Ecology to Molecular Genetics. Microbiology and Molecular Biology Reviews **64:**847-867.

23. **Roeselers G.** 2007. Microbial Ecology of Phototrophic Biofilms: Roeselers, G., Doctoral Thesis, Delft University of Technology. Guus Roeselers.

24. **Charpy L, Palinska KA, Casareto B, Langlade MJ, Suzuki Y, Abed RM, Golubic S.** 2010. Dinitrogen-fixing cyanobacteria in microbial mats of two shallow coral reef ecosystems. Microb Ecol **59:**174-186.

25. **Battin TJ, Besemer K, Bengtsson MM, Romani AM, Packmann AI.** 2016. The ecology and biogeochemistry of stream biofilms. Nat Rev Micro **14:**251-263.

26. **Lu H, Yang L, Zhang S, Wu Y.** 2014. The behavior of organic phosphorus under non-point source wastewater in the presence of phototrophic periphyton. PLoS One **9:**e85910.

27. **Overmann J, van Gemerden H.** 2000. Microbial interactions involving sulfur bacteria: implications for the ecology and evolution of bacterial communities. FEMS Microbiol Rev **24:**591-599.

28. **Swingley WD, Meyer-Dombard DR, Shock EL, Alsop EB, Falenski HD, Havig JR, Raymond J.** 2012. Coordinating environmental genomics and geochemistry reveals metabolic transitions in a hot spring ecosystem. PLoS One **7:**e38108.

29. **Daniel H. Buckley JMM, Michael T. Madigan, Kelly S. Bender, David A. Stahl, Thomas Brock.** 2014. Brock Biology of Microorganisms, 14th edition ed. Pearson.

30. **Bryant DA, Frigaard N-U.** 2006. Prokaryotic photosynthesis and phototrophy illuminated. Trends Microbiol **14:**488-496.

31. **Bryant DA, Costas AM, Maresca JA, Chew AG, Klatt CG, Bateson MM, Tallon LJ, Hostetler J, Nelson WC, Heidelberg JF, Ward DM.** 2007. Candidatus Chloracidobacterium thermophilum: an aerobic phototrophic Acidobacterium. Science **317:**523-526.

32. **D'Amelio ED, Cohen Y, Des Marais DJ.** 1987. Association of a new type of gliding, filamentous, purple phototrophic bacterium inside bundles of Microcoleus chthonoplastes in hypersaline cyanobacterial mats. Arch Microbiol **147:**213-220.

33. **Jungblut AD, Hawes I, Mackey TJ, Krusor M, Doran PT, Sumner DY, Eisen JA, Hillman C, Goroncy AK.** 2016. Microbial Mat Communities along an Oxygen Gradient in a Perennially Ice-Covered Antarctic Lake. Appl Environ Microbiol **82:**620-630.

34. **Bryantseva IA, Gorlenko VM, Kompantseva EI, Achenbach LA, Madigan MT.** 1999. Heliorestis daurensis, gen. nov. Sp. Nov., An alkaliphilic rod-to-coiled-shaped phototrophic heliobacterium from a siberian soda lake. Arch Microbiol **172:**167-174.

35. **Pages A, Grice K, Vacher M, Welsh DT, Teasdale PR, Bennett WW, Greenwood P.** 2014. Characterizing microbial communities and processes in a modern stromatolite (Shark Bay) using lipid biomarkers and two-dimensional distributions of porewater solutes. Environ Microbiol **16:**2458-2474.

36. **Bebout BM, Garcia-Pichel F.** 1995. UV B-Induced Vertical Migrations of Cyanobacteria in a Microbial Mat. Appl Environ Microbiol **61:**4215-4222.

37. **Suosaari EP, Reid RP, Playford PE, Foster JS, Stolz JF, Casaburi G, Hagan PD, Chirayath V, Macintyre IG, Planavsky NJ, Eberli GP.** 2016. New multi-scale perspectives on the stromatolites of Shark Bay, Western Australia. Sci Rep **6:**20557-20563.

38. **Knoll AH.** 2015. Paleobiological Perspectives on Early Microbial Evolution. Cold Spring Harb Perspect Biol **7:**a018093.

39. **Dupraz C, Visscher PT.** 2005. Microbial lithification in marine stromatolites and hypersaline mats. Trends Microbiol **13:**429-438.

40. **Hamilton TL, Bryant DA, Macalady JL.** 2016. The role of biology in planetary evolution: cyanobacterial primary production in low-oxygen Proterozoic oceans. Environ Microbiol **18:**325-340.

41. **Shih PM, Hemp J, Ward LM, Matzke NJ, Fischer WW.** 2016. Crown group Oxyphotobacteria postdate the rise of oxygen. Geobiology.

42. **Albarracin VH, Gartner W, Farias ME.** 2016. Forged Under the Sun: Life and Art of Extremophiles from Andean Lakes. Photochem Photobiol **92:**14-28.

43. **Pringault O, Garcia-Pichel F.** 2004. Hydrotaxis of cyanobacteria in desert crusts. Microb Ecol **47:**366-373.

44. **Vitek P, Camara-Gallego B, Edwards HGM, Jehlicka J, Ascaso C, Wierzchos J.** 2013. Phototrophic Community in Gypsum Crust from the Atacama Desert Studied by Raman Spectroscopy and Microscopic Imaging. Geomicrobiology Journal **30:**399-410.

45. **Beraldi-Campesi H, Garcia-Pichel F.** 2011. The biogenicity of modern terrestrial roll-up structures and its significance for ancient life on land. Geobiology **9:**10-23.

46. **Baqué M, de Vera J-P, Rettberg P, Billi D.** 2013. The BOSS and BIOMEX space experiments on the EXPOSE-R2 mission: Endurance of the desert cyanobacterium Chroococcidiopsis under simulated space vacuum, Martian atmosphere, UVC radiation and temperature extremes. Acta Astronautica **91:**180-186.

47. **de Vera JP, Dulai S, Kereszturi A, Koncz L, Lorek A, Mohlmann D, Marschall M, Pocs T.** 2014. Results on the survival of cryptobiotic cyanobacteria samples after exposure to Mars-like environmental conditions. International Journal of Astrobiology **13:**35-44.

48. **Janchen J, Feyh N, Szewzyk U, de Vera JPP.** 2016. Provision of water by halite deliquescence for Nostoc commune biofilms under Mars relevant surface conditions. International Journal of Astrobiology **15:**107-118.

49. **Syed MA, Henshaw PF.** 2003. Effect of tube size on performance of a fixed-film tubular bioreactor for conversion of hydrogen sulfide to elemental sulfur. Water Res **37:**1932-1938.

50. **Tian X, Liao Q, Zhu X, Li J, Wang H.** 2010. Characteristics of a biofilm photobioreactor as applied to photo-hydrogen production. Bioresour Technol **101:**977-983.

51. **Wigglesworth-Cooksey B, Cooksey KE.** 2005. Use of fluorophore-conjugated lectins to study cell-cell interactions in model marine biofilms. Appl Environ Microbiol **71:**428-435.

52. **Lardon L, Helias A, Sialve B, Steyer J, O B.** 2009. Life-cycle Assessment of biodiesel production from microalgae. Environmental Science and Technology **43:**7.

53. **Yang WF, Zhao WW, Liu YP, Hu HY, Pei XW, Wu Y, Zhou F.** 2016. The effect of wetting property on anti-fouling/foul-release performance under quasi-static/hydrodynamic conditions. Progress in Organic Coatings **95:**64-71.

54. **Garcia M, Stupak M, Perez M, Blustein G.** 2015. Transitioning to nontoxic antifouling paints. Pigment & Resin Technology **44:**116-121.

55. **Fay F, Carteau D, Linossier I, Delbury M, Vallee-Rehel K.** 2013. Joint-action of antifouling substances in copper-free paints. Colloids and Surfaces B-Biointerfaces **102:**569-577.

56. **Dafforn KA, Lewis JA, Johnston EL.** 2011. Antifouling strategies: History and regulation, ecological impacts and mitigation. Marine Pollution Bulletin **62:**453-465.

57. **Roeselers G, Zippel B, Staal M, van Loosdrecht M, Muyzer G.** 2006. On the reproducibility of microcosm experiments - different community composition in parallel phototrophic biofilm microcosms. FEMS Microbiol Ecol **58:**169-178.

58. **Gosse JL, Chinn MS, Grunden AM, Bernal OI, Jenkins JS, Yeager C, Kosourov S, Seibert M, Flickinger MC.** 2012. A versatile method for preparation of hydrated microbial-latex biocatalytic coatings for gas absorption and gas evolution. J Ind Microbiol Biotechnol **39:**1269-1278.

59. **Wang YZ, Liao Q, Zhu X, Tian X, Zhang C.** 2010. Characteristics of hydrogen production and substrate consumption of Rhodopseudomonas palustris CQK 01 in an immobilized-cell photobioreactor. Bioresour Technol **101:**4034-4041.

60. **Behrendt L, Schrameyer V, Qvortrup K, Lundin L, Sorensen SJ, Larkum AW, Kuhl M.** 2012. Biofilm growth and near-infrared radiation-driven

photosynthesis of the chlorophyll d-containing cyanobacterium Acaryochloris marina. Appl Environ Microbiol **78:**3896-3904.

61. **Dickson DJ, Ely RL.** 2013. Silica sol-gel encapsulation of cyanobacteria: lessons for academic and applied research. Appl Microbiol Biotechnol **97:**1809-1819.

62. **Masse A, Pringault O, De Wit R.** 2002. Experimental study of interactions between purple and green sulfur bacteria in sandy sediments exposed to illumination deprived of near-infrared wavelengths. Appl Environ Microbiol **68:**2972-2981.

63. **Cairns LS, Hobley L, Stanley-Wall NR.** 2014. Biofilm formation by Bacillus subtilis: new insights into regulatory strategies and assembly mechanisms. Mol Microbiol **93:**587-598.

64. **Hermans K, Roberfroid S, Thijs IM, Kint G, De Coster D, Marchal K, Vanderleyden J, De Keersmaecker SC, Steenackers HP.** 2016. FabR regulates Salmonella biofilm formation via its direct target FabB. BMC Genomics **17:**253-267.

65. **Wright DJ, Smith SC, Joardar V, Scherer S, Jervis J, Warren A, Helm RF, Potts M.** 2005. UV irradiation and desiccation modulate the three-dimensional extracellular matrix of Nostoc commune (Cyanobacteria). J Biol Chem **280:**40271-40281.

66. **Sharif DI, Gallon J, Smith CJ, Dudley E.** 2008. Quorum sensing in Cyanobacteria: N-octanoyl-homoserine lactone release and response, by the epilithic colonial cyanobacterium Gloeothece PCC6909. ISME J **2:**1171-1182.

67. **Mikkelsen H, Duck Z, Lilley KS, Welch M.** 2007. Interrelationships between colonies, biofilms, and planktonic cells of Pseudomonas aeruginosa. J Bacteriol **189:**2411-2416.

68. **Mohamed HE, van de Meene AM, Roberson RW, Vermaas WF.** 2005. Myxoxanthophyll is required for normal cell wall structure and thylakoid organization in the cyanobacterium Synechocystis sp. strain PCC 6803. J Bacteriol **187:**6883-6892.

69. **Fisher ML, Allen R, Luo Y, Curtiss R, 3rd.** 2013. Export of extracellular polysaccharides modulates adherence of the Cyanobacterium synechocystis. PLoS One **8:**e74514.

70. **Jiang GH, Ohtaguchi K.** 2006. Kinetics of biofilm formation of a cyanobacterium on bioreactor surfaces. Journal of Chemical Engineering of Japan **39:**453-460.

71. **Schatz D, Nagar E, Sendersky E, Parnasa R, Zilberman S, Carmeli S, Mastai Y, Shimoni E, Klein E, Yeger O, Reich Z, Schwarz R.** 2013. Self-suppression of biofilm formation in the cyanobacterium Synechococcus elongatus. Environ Microbiol **15:**1786-1794.

72. **Kawano Y, Saotome T, Ochiai Y, Katayama M, Narikawa R, Ikeuchi M.** 2011. Cellulose accumulation and a cellulose synthase gene are responsible for cell aggregation in the cyanobacterium Thermosynechococcus vulcanus RKN. Plant Cell Physiol **52:**957-966.

73. **Karatan E, Watnick P.** 2009. Signals, regulatory networks, and materials that build and break bacterial biofilms. Microbiol Mol Biol Rev **73:**310-347.

74. **Berne C, Ducret A, Hardy GG, Brun YV.** 2015. Adhesins Involved in Attachment to Abiotic Surfaces by Gram-Negative Bacteria. Microbiol Spectr **3**.

75. **Vogeleer P, Tremblay YD, Mafu AA, Jacques M, Harel J.** 2014. Life on the outside: role of biofilms in environmental persistence of Shiga-toxin producing Escherichia coli. Front Microbiol **5:**317.

76. **Diez-Garcia M, Capita R, Alonso-Calleja C.** 2012. Influence of serotype on the growth kinetics and the ability to form biofilms of Salmonella isolates from poultry. Food Microbiol **31:**173-180.

77. **Laverty G, Gorman SP, Gilmore BF.** 2014. Biomolecular Mechanisms of Pseudomonas aeruginosa and Escherichia coli Biofilm Formation. Pathogens **3:**596-632.

78. **Heindl JE, Wang Y, Heckel BC, Mohari B, Feirer N, Fuqua C.** 2014. Mechanisms and regulation of surface interactions and biofilm formation in Agrobacterium. Front Plant Sci **5:**176.

79. **Hoffman MD, Zucker LI, Brown PJ, Kysela DT, Brun YV, Jacobson SC.** 2015. Timescales and Frequencies of Reversible and Irreversible Adhesion Events of Single Bacterial Cells. Anal Chem **87:**12032-12039.

80. **Sauer K.** 2003. The genomics and proteomics of biofilm formation. Genome Biol **4:**219.

81. **Gerstel U, Romling U.** 2001. Oxygen tension and nutrient starvation are major signals that regulate agfD promoter activity and expression of the multicellular morphotype in Salmonella typhimurium. Environ Microbiol **3:**638-648.

82. **Teschler JK, Zamorano-Sánchez D, Utada AS, Warner CJA, Wong GCL, Linington RG, Yildiz FH.** 2015. Living in the matrix: assembly and control of Vibrio cholerae biofilms. Nature reviews. Microbiology **13:**255-268.

83. **O'Toole GA, Kolter R.** 1998. Initiation of biofilm formation in Pseudomonas fluorescens WCS365 proceeds via multiple, convergent signalling pathways: a genetic analysis. Mol Microbiol **28:**449-461.

84. **Romling U, Sierralta WD, Eriksson K, Normark S.** 1998. Multicellular and aggregative behaviour of Salmonella typhimurium strains is controlled by mutations in the agfD promoter. Mol Microbiol **28:**249-264.

85. **Sutrina SL, Griffith MS, Lafeuillee C.** 2016. 2-Deoxy-d-glucose is a potent inhibitor of biofilm growth in Escherichia coli. Microbiology **162:**1037-1046.

86. **Kuttler C, Hense BA.** 2008. Interplay of two quorum sensing regulation systems of Vibrio fischeri. J Theor Biol **251:**167-180.

87. **Leao PN, Engene N, Antunes A, Gerwick WH, Vasconcelos V.** 2012. The chemical ecology of cyanobacteria. Nat Prod Rep **29:**372-391.

88. **Romero M, Diggle SP, Heeb S, Camara M, Otero A.** 2008. Quorum quenching activity in Anabaena sp. PCC 7120: identification of AiiC, a novel AHL-acylase. FEMS Microbiol Lett **280:**73-80.

89. **Valentini M, Filloux A.** 2016. Biofilms and Cyclic di-GMP (c-di-GMP) Signaling: Lessons from Pseudomonas aeruginosa and Other Bacteria. J Biol Chem **291:**12547-12555.

90. **Toyofuku M, Inaba T, Kiyokawa T, Obana N, Yawata Y, Nomura N.** 2015. Environmental factors that shape biofilm formation. Biosci Biotechnol Biochem **80:**7-12.

91. **Bodenmiller D, Toh E, Brun YV.** 2004. Development of surface adhesion in Caulobacter crescentus. J Bacteriol **186:**1438-1447.

92. **Barnhart MM, Chapman MR.** 2006. Curli biogenesis and function. Annu Rev Microbiol **60:**131-147.

93. **Krasowska A, Sigler K.** 2014. How microorganisms use hydrophobicity and what does this mean for human needs? Frontiers in Cellular and Infection Microbiology **4:**112.

94. **Montagud A, Gamermann D, Fernandez de Cordoba P, Urchueguia JF.** 2015. Synechocystis sp. PCC6803 metabolic models for the enhanced production of hydrogen. Crit Rev Biotechnol **35:**184-198.

95. **Yu Y, You L, Liu D, Hollinshead W, Tang YJ, Zhang F.** 2013. Development of Synechocystis sp. PCC 6803 as a phototrophic cell factory. Mar Drugs **11:**2894-2916.

96. **Bolhuis H, Cretoiu MS, Stal LJ.** 2014. Molecular ecology of microbial mats. FEMS Microbiol Ecol **90:**335-350.

97. **Cole JK, Hutchison JR, Renslow RS, Kim YM, Chrisler WB, Engelmann HE, Dohnalkova AC, Hu D, Metz TO, Fredrickson JK, Lindemann SR.** 2014. Phototrophic biofilm assembly in microbial-mat-derived unicyanobacterial consortia: model systems for the study of autotroph-heterotroph interactions. Front Microbiol **5:**109.

98. **Sakiyama T, Ueno H, Homma H, Numata O, Kuwabara T.** 2006. Purification and characterization of a hemolysin-like protein, Sll1951, a nontoxic member of the RTX protein family from the Cyanobacterium Synechocystis sp. strain PCC 6803. J Bacteriol **188:**3535-3542.

99. **Trautner C, Vermaas WF.** 2013. The sll1951 gene encodes the surface layer protein of Synechocystis sp. strain PCC 6803. J Bacteriol **195:**5370-5380.

100. **Auger S, Ramarao N, Faille C, Fouet A, Aymerich S, Gohar M.** 2009. Biofilm formation and cell surface properties among pathogenic and nonpathogenic strains of the Bacillus cereus group. Appl Environ Microbiol **75:**6616-6618.

101. **Yoshihara S, Geng X, Okamoto S, Yura K, Murata T, Go M, Ohmori M, Ikeuchi M.** 2001. Mutational analysis of genes involved in pilus structure, motility and transformation competency in the unicellular motile cyanobacterium Synechocystis sp. PCC 6803. Plant Cell Physiol **42:**63-73.

102. **Kim YH, Kim JY, Kim SY, Lee JH, Lee JS, Chung YH, Yoo JS, Park YM.** 2009. Alteration in the glycan pattern of pilin in a nonmotile mutant of Synechocystis sp. PCC 6803. Proteomics **9:**1075-1086.

103. **Hultgren SJ, Normark S, Abraham SN.** 1991. Chaperone-assisted assembly and molecular architecture of adhesive pili. Annu Rev Microbiol **45:**383-415.

104. **Bhaya D, Bianco NR, Bryant D, Grossman A.** 2000. Type IV pilus biogenesis and motility in the cyanobacterium Synechocystis sp. PCC6803. Mol Microbiol **37:**941-951.

105. **Pratt LA, Kolter R.** 1998. Genetic analysis of Escherichia coli biofilm formation: roles of flagella, motility, chemotaxis and type I pili. Mol Microbiol **30:**285-293.

106. **Burriesci M, Bhaya D.** 2008. Tracking phototactic responses and modeling motility of Synechocystis sp. strain PCC6803. J Photochem Photobiol B **91:**77-86.

107. **Hoiczyk E, Baumeister W.** 1997. Oscillin, an extracellular, Ca2+-binding glycoprotein essential for the gliding motility of cyanobacteria. Mol Microbiol **26:**699-708.

108. **Hoiczyk E, Baumeister W.** 1998. The junctional pore complex, a prokaryotic secretion organelle, is the molecular motor underlying gliding motility in cyanobacteria. Curr Biol **8:**1161-1168.

109. **De Philippis R, Vincenzini M.** 1998. Exocellular polysaccharides from cyanobacteria and their possible applications. FEMS Microbiol Rev **22:**151-175.

110. **Pereira S, Zille A, Micheletti E, Moradas-Ferreira P, De Philippis R, Tamagnini P.** 2009. Complexity of cyanobacterial exopolysaccharides: composition, structures, inducing factors and putative genes involved in their biosynthesis and assembly. FEMS Microbiol Rev **33:**917-941.

111. **Panoff JM, Priem B, Morvan H, Joset F.** 1988. Sulfated exopolysaccharides produced by 2 unicellular strains of cyanobacteria, Synechocystis PCC-6803 and PCC-6714. Arch Microbiol **150:**558-563.

112. **Whitfield C.** 2006. Biosynthesis and assembly of capsular polysaccharides in Escherichia coli. Annu Rev Biochem **75:**39-68.

113. **Camacho C, Coulouris G, Avagyan V, Ma N, Papadopoulos J, Bealer K, Madden TL.** 2009. BLAST+: architecture and applications. BMC Bioinformatics **10:**421.

114. **Temel DB, Dutta K, Alphonse S, Nourikyan J, Grangeasse C, Ghose R.** 2013. Regulatory interactions between a bacterial tyrosine kinase and its cognate phosphatase. J Biol Chem **288:**15212-15228.

115. **Pereira SB, Mota R, Vieira CP, Vieira J, Tamagnini P.** 2015. Phylum-wide analysis of genes/proteins related to the last steps of assembly and export of extracellular polymeric substances (EPS) in cyanobacteria. Sci Rep **5:**14835.

116. **Huang F, Hedman E, Funk C, Kieselbach T, Schroder WP, Norling B.** 2004. Isolation of outer membrane of Synechocystis sp. PCC 6803 and its proteomic characterization. Mol Cell Proteomics **3:**586-595.

117. **Dong C, Beis K, Nesper J, Brunkan-Lamontagne AL, Clarke BR, Whitfield C, Naismith JH.** 2006. Wza the translocon for E. coli capsular polysaccharides defines a new class of membrane protein. Nature **444:**226-229.

118. **Li YZ, Tang JL, Tang DJ, Ma QS.** 2001. Pathogenicity of EPS-deficient mutants (gumB(-), gumD(-) and gumE(-)) of Xanthomonas campestris pv. campestris. Progress in Natural Science **11:**871-875.

119. **Smith CS, Hinz A, Bodenmiller D, Larson DE, Brun YV.** 2003. Identification of genes required for synthesis of the adhesive holdfast in Caulobacter crescentus. J Bacteriol **185:**1432-1442.

120. **Rigano LA, Siciliano F, Enrique R, Sendin L, Filippone P, Torres PS, Questa J, Dow JM, Castagnaro AP, Vojnov AA, Marano MR.** 2007. Biofilm formation, epiphytic fitness, and canker development in Xanthomonas axonopodis pv. citri. Mol Plant Microbe Interact **20:**1222-1230.

121. **Jittawuttipoka T, Planchon M, Spalla O, Benzerara K, Guyot F, Cassier-Chauvat C, Chauvat F.** 2013. Multidisciplinary evidences that Synechocystis PCC6803 exopolysaccharides operate in cell sedimentation and protection against salt and metal stresses. PLoS One **8:**e55564.

122. **Cuthbertson L, Powers J, Whitfield C.** 2005. The C-terminal domain of the nucleotide-binding domain protein Wzt determines substrate specificity in the ATP-binding cassette transporter for the lipopolysaccharide O-antigens in Escherichia coli serotypes O8 and O9a. J Biol Chem **280:**30310-30319.

123. **Majdalani N, Heck M, Stout V, Gottesman S.** 2005. Role of RcsF in signaling to the Rcs phosphorelay pathway in Escherichia coli. J Bacteriol **187:**6770-6778.

124. **Altschul SF, Madden TL, Schaffer AA, Zhang J, Zhang Z, Miller W, Lipman DJ.** 1997. Gapped BLAST and PSI-BLAST: a new generation of protein database search programs. Nucleic Acids Res **25:**3389-3402.

125. **White AP, Gibson DL, Collinson SK, Banser PA, Kay WW.** 2003. Extracellular polysaccharides associated with thin aggregative fimbriae of Salmonella enterica serovar enteritidis. J Bacteriol **185:**5398-5407.

126. **Zhao C, Li Z, Li T, Zhang Y, Bryant DA, Zhao J.** 2015. High-yield production of extracellular type-I cellulose by the cyanobacterium Synechococcus sp. PCC 7002. Cell Discovery **1:**15004.

127. **Nobles DR, Romanovicz DK, Brown RM, Jr.** 2001. Cellulose in cyanobacteria. Origin of vascular plant cellulose synthase? Plant Physiol **127:**529-542.

128. **Enomoto G, Nomura R, Shimada T, Ni Ni W, Narikawa R, Ikeuchi M.** 2014. Cyanobacteriochrome SesA Is a Diguanylate Cyclase That Induces Cell Aggregation in Thermosynechococcus. Journal of Biological Chemistry **289:**24801-24809.

129. **Wong HC, Fear AL, Calhoon RD, Eichinger GH, Mayer R, Amikam D, Benziman M, Gelfand DH, Meade JH, Emerick AW, et al.** 1990. Genetic organization of the cellulose synthase operon in Acetobacter xylinum. Proc Natl Acad Sci U S A **87:**8130-8134.

130. **Jenal U.** 2004. Cyclic di-guanosine-monophosphate comes of age: a novel secondary messenger involved in modulating cell surface structures in bacteria? Curr Opin Microbiol **7:**185-191.

131. **Agostoni M, Koestler BJ, Waters CM, Williams BL, Montgomery BL.** 2013. Occurrence of cyclic di-GMP-modulating output domains in cyanobacteria: an illuminating perspective. MBio **4**.

132. **Agostoni M, Waters CM, Montgomery BL.** 2016. Regulation of biofilm formation and cellular buoyancy through modulating intracellular cyclic di-GMP levels in engineered cyanobacteria. Biotechnol Bioeng **113:**311-319.

133. **Scott M, McCollum C, Vasil'ev S, Crozier C, Espie GS, Krol M, Huner NP, Bruce D.** 2006. Mechanism of the down regulation of photosynthesis by blue light in the Cyanobacterium synechocystis sp. PCC 6803. Biochemistry **45:**8952-8958.

134. **Kariisa AT, Grube A, Tamayo R.** 2015. Two nucleotide second messengers regulate the production of the Vibrio cholerae colonization factor GbpA. BMC Microbiol **15:**166.

135. **Rippka R DJ, Waterbury JB, Herdman M, Stanier RY** 1979. Generic assignments, strain histories and properties of pure cultures cyanobacteria. J Gen Microbiol **111**.

136. **Zevin AS, Nam T, Rittmann B, Krajmalnik-Brown R.** 2015. Effects of phosphate limitation on soluble microbial products and microbial community structure in semi-continuous Synechocystis-based photobioreactors. Biotechnol Bioeng **112:**1761-1769.

137. **James G.** 2010. Universal Bacterial Identification by PCR and DNA Sequencing of 16S rRNA Gene, p. 209-214. *In* Schuller M, Sloots TP, James GS, Halliday CL, Carter IWJ (ed.), PCR for Clinical Microbiology. Springer Netherlands.

138. **Sambrook J, E. F. Fritsch, and T. Maniatis. .** 1989. Molecular cloning: a laboratory manual, 2nd edition. . Cold Spring Harbor Laboratory, Cold Spring Harbor, New York.

139. **Lagarde D, Beuf L, Vermaas W.** 2000. Increased Production of Zeaxanthin and Other Pigments by Application of Genetic Engineering Techniques to Synechocystis sp. Strain PCC 6803. Appl Environ Microbiol **66:**64-72.

140. **Mitschke J, Georg J, Scholz I, Sharma CM, Dienst D, Bantscheff J, Voss B, Steglich C, Wilde A, Vogel J, Hess WR.** 2011. An experimentally anchored map of transcriptional start sites in the model cyanobacterium Synechocystis sp. PCC6803. Proc Natl Acad Sci U S A **108:**2124-2129.

141. **Ludwig A, Heimbucher T, Gregor W, Czerny T, Schmetterer G.** 2008. Transformation and gene replacement in the facultatively chemoheterotrophic, unicellular cyanobacterium Synechocystis sp. PCC6714 by electroporation. Appl Microbiol Biotechnol **78:**729-735.

142. **Kufryk GI, Sachet M, Schmetterer G, Vermaas WF.** 2002. Transformation of the cyanobacterium Synechocystis sp. PCC 6803 as a tool for genetic mapping: optimization of efficiency. FEMS Microbiol Lett **206:**215-219.

143. **Cao Y, Johnson HM, Bazemore-Walker CR.** 2012. Improved enrichment and proteomic identification of outer membrane proteins from a Gram-negative bacterium: focus on Caulobacter crescentus. Proteomics **12:**251-262.

144. **Wang Q, Nomura CT.** 2010. Monitoring differences in gene expression levels and polyhydroxyalkanoate (PHA) production in Pseudomonas putida KT2440 grown on different carbon sources. J Biosci Bioeng **110:**653-659.

145. **Klausen M, Gjermansen M, Kreft JU, Tolker-Nielsen T.** 2006. Dynamics of development and dispersal in sessile microbial communities: examples from Pseudomonas aeruginosa and Pseudomonas putida model biofilms. FEMS Microbiol Lett **261:**1-11.

146. **Oliveira C, Rubio J.** 2012. A short overview of the formation of aerated flocs and their applications in solid/liquid separation by flotation. Minerals Engineering **39:**124-132.

147. **Liu XW, Yu HQ, Ni BJ, Sheng GP.** 2009. Characterization, modeling and application of aerobic granular sludge for wastewater treatment. Adv Biochem Eng Biotechnol **113:**275-303.

148. **Allakhverdiev SI, Nishiyama Y, Takahashi S, Miyairi S, Suzuki I, Murata N.** 2005. Systematic analysis of the relation of electron transport and ATP synthesis to the photodamage and repair of photosystem II in Synechocystis. Plant Physiol **137:**263-273.

149. **Bottomley PJ, Stewart WD.** 1976. ATP pools and transients in the blue-green alga, Anabaena cylindrica. Arch Microbiol **108:**249-258.

150. **Kim HW, Vannela R, Zhou C, Harto C, Rittmann BE.** 2010. Photoautotrophic nutrient utilization and limitation during semi-continuous growth of Synechocystis sp. PCC6803. Biotechnology and Bioengineering **106:**553-563.

151. **Paithoonrangsarid K, Shoumskaya MA, Kanesaki Y, Satoh S, Tabata S, Los DA, Zinchenko VV, Hayashi H, Tanticharoen M, Suzuki I, Murata N.** 2004. Five histidine kinases perceive osmotic stress and regulate distinct sets of genes in Synechocystis. J Biol Chem **279:**53078-53086.

152. **Shoumskaya MA, Paithoonrangsarid K, Kanesaki Y, Los DA, Zinchenko VV, Tanticharoen M, Suzuki I, Murata N.** 2005. Identical Hik-Rre systems are involved in perception and transduction of salt signals and hyperosmotic signals but regulate the expression of individual genes to different extents in synechocystis. J Biol Chem **280:**21531-21538.

153. **Juntarajumnong W, Eaton-Rye JJ, Incharoensakdi A.** 2007. Two-component signal transduction in Synechocystis sp. PCC 6803 under phosphate limitation: role of acetyl phosphate. J Biochem Mol Biol **40:**708-714.

154. **Suzuki S, Ferjani A, Suzuki I, Murata N.** 2004. The SphS-SphR two component system is the exclusive sensor for the induction of gene expression in response to phosphate limitation in synechocystis. J Biol Chem **279:**13234-13240.

155. **Carson JL, Brown RM.** 1978. Studies of Hawaiian freshwater and soil algae II. Algal colonjization and succession on a dated volcanic substrate. Journal of Phycology **14:**171-178.

156. **Boutte CC, Crosson S.** 2013. Bacterial lifestyle shapes stringent response activation. Trends Microbiol **21:**174-180.

157. **Magnusson LU, Farewell A, Nystrom T.** 2005. ppGpp: a global regulator in Escherichia coli. Trends Microbiol **13:**236-242.

158. **Gaca AO, Colomer-Winter C, Lemos JA.** 2015. Many means to a common end: the intricacies of (p)ppGpp metabolism and its control of bacterial homeostasis. J Bacteriol **197:**1146-1156.

159. **Potrykus K, Cashel M.** 2008. (p)ppGpp: still magical? Annu Rev Microbiol **62:**35-51.

160. **Natori Y, Tagami K, Murakami K, Yoshida S, Tanigawa O, Moh Y, Masuda K, Wada T, Suzuki S, Nanamiya H, Tozawa Y, Kawamura F.** 2009. Transcription activity of individual rrn operons in Bacillus subtilis mutants deficient in (p)ppGpp synthetase genes, relA, yjbM, and ywaC. J Bacteriol **191:**4555-4561.

161. **Miao X, Liu H, Ning D.** 2011. [Characterization of the Rela/SpoT homologue slr1325 (syn-rsh) of the cyanobacterium Synechocystis sp. PCC6803]. Wei Sheng Wu Xue Bao **51:**898-905.

162. **Atkinson GC, Tenson T, Hauryliuk V.** 2011. The RelA/SpoT homolog (RSH) superfamily: distribution and functional evolution of ppGpp synthetases and hydrolases across the tree of life. PLoS One **6:**e23479.

163. **English BP, Hauryliuk V, Sanamrad A, Tankov S, Dekker NH, Elf J.** 2011. Single-molecule investigations of the stringent response machinery in living bacterial cells. Proc Natl Acad Sci U S A **108:**E365-373.

164. **Hauryliuk V, Atkinson GC, Murakami KS, Tenson T, Gerdes K.** 2015. Recent functional insights into the role of (p)ppGpp in bacterial physiology. Nat Rev Microbiol **13:**298-309.

165. **Nomura Y, Izumi A, Fukunaga Y, Kusumi K, Iba K, Watanabe S, Nakahira Y, Weber AP, Nozawa A, Tozawa Y.** 2014. Diversity in guanosine 3',5'-bisdiphosphate (ppGpp) sensitivity among guanylate kinases of bacteria and plants. J Biol Chem **289:**15631-15641.

166. **Kvint K, Hosbond C, Farewell A, Nybroe O, Nystrom T.** 2000. Emergency derepression: stringency allows RNA polymerase to override negative control by an active repressor. Mol Microbiol **35:**435-443.

167. **Godfrey HP, Bugrysheva JV, Cabello FC.** 2002. The role of the stringent response in the pathogenesis of bacterial infections. Trends Microbiol **10:**349-351.

168. **Germain E, Roghanian M, Gerdes K, Maisonneuve E.** 2015. Stochastic induction of persister cells by HipA through (p)ppGpp-mediated activation of mRNA endonucleases. Proc Natl Acad Sci U S A **112:**5171-5176.

169. **Magnusson LU, Nystrom T, Farewell A.** 2003. Underproduction of sigma 70 mimics a stringent response. A proteome approach. J Biol Chem **278:**968-973.

170. **Moreira RN, Domingues S, Viegas SC, Amblar M, Arraiano CM.** 2012. Synergies between RNA degradation and trans-translation in Streptococcus pneumoniae: cross regulation and co-transcription of RNase R and SmpB. BMC Microbiol **12:**268.

171. **Bridger WA, Paranchych W.** 1978. relA Gene control of bacterial glycogen synthesis. Can J Biochem **56:**403-406.

172. **Potrykus K, Wegrzyn G, Hernandez VJ.** 2004. Direct stimulation of the lambdapaQ promoter by the transcription effector guanosine-3',5'-(bis)pyrophosphate in a defined in vitro system. J Biol Chem **279:**19860-19866.

173. **Kanjee U, Ogata K, Houry WA.** 2012. Direct binding targets of the stringent response alarmone (p)ppGpp. Mol Microbiol **85:**1029-1043.

174. **Nystrom T.** 2004. Stationary-phase physiology. Annu Rev Microbiol **58:**161-181.

175. **Kanjee U, Ogata K, Houry WA.** 2012. Direct binding targets of the stringent response alarmone (p)ppGpp. Mol Microbiol **85:**1029-1043.

176. **Boutte CC, Crosson S.** 2011. The complex logic of stringent response regulation in Caulobacter crescentus: starvation signalling in an oligotrophic environment. Mol Microbiol **80:**695-714.

177. **Acosta R, Lueking DR.** 1987. Stringency in the absence of ppGpp accumulation in Rhodobacter sphaeroides. J Bacteriol **169:**908-912.

178. **Hood RD, Higgins SA, Flamholz A, Nichols RJ, Savage DF.** 2016. The stringent response regulates adaptation to darkness in the cyanobacterium Synechococcus elongatus. Proc Natl Acad Sci U S A **113:**E4867-4876.

179. **Braeken K, Moris M, Daniels R, Vanderleyden J, Michiels J.** 2006. New horizons for (p)ppGpp in bacterial and plant physiology. Trends Microbiol **14:**45-54.

180. **Balzer GJ, McLean RJ.** 2002. The stringent response genes relA and spoT are important for Escherichia coil biofilms under slow-growth conditions. Can J Microbiol **48:**675-680.

181. **Nakanishi N, Abe H, Ogura Y, Hayashi T, Tashiro K, Kuhara S, Sugimoto N, Tobe T.** 2006. ppGpp with DksA controls gene expression in the locus of enterocyte effacement (LEE) pathogenicity island of enterohaemorrhagic Escherichia coli through activation of two virulence regulatory genes. Mol Microbiol **61:**194-205.

182. **Taylor CM, Beresford M, Epton HA, Sigee DC, Shama G, Andrew PW, Roberts IS.** 2002. Listeria monocytogenes relA and hpt mutants are impaired in surface-attached growth and virulence. J Bacteriol **184:**621-628.

183. **Boutte CC, Henry JT, Crosson S.** 2012. ppGpp and polyphosphate modulate cell cycle progression in Caulobacter crescentus. J Bacteriol **194:**28-35.

184. **Crawford EW, Jr., Shimkets LJ.** 2000. The stringent response in Myxococcus xanthus is regulated by SocE and the CsgA C-signaling protein. Genes Dev **14:**483-492.

185. **Ning D, Qian Y, Miao X, Wen C.** 2011. Role of the all1549 (ana-rsh) gene, a relA/spoT homolog, of the Cyanobacterium Anabaena sp. PCC7120. Curr Microbiol **62:**1767-1773.

186. **Cohen SE, Golden SS.** 2015. Circadian Rhythms in Cyanobacteria. Microbiol Mol Biol Rev **79:**373-385.

187. **Shultzaberger RK, Boyd JS, Diamond S, Greenspan RJ, Golden SS.** 2015. Giving Time Purpose: The Synechococcus elongatus Clock in a Broader Network Context. Annu Rev Genet **49:**485-505.

188. **Browse J, Roughan PG, Slack CR.** 1981. Light control of fatty acid synthesis and diurnal fluctuations of fatty acid composition in leaves. Biochem J **196:**347-354.

189. **Kleinig H, Liedvogel B.** 1979. On the energy requirements of fatty acid synthesis in spinach chloroplasts in the light and in the dark. FEBS Lett **101:**339-342.

190. **Singer RA, Doolittle WF.** 1975. Control of gene expression in blue-green algae. Nature **253:**650-651.

191. **Aken BL, Ayling S, Barrell D, Clarke L, Curwen V, Fairley S, Fernandez Banet J, Billis K, García Girón C, Hourlier T, Howe K, Kähäri A, Kokocinski F, Martin FJ, Murphy DN, Nag R, Ruffier M, Schuster M, Tang YA, Vogel J-H, White S, Zadissa A, Flicek P, Searle SMJ.** 2016. The Ensembl gene annotation system. Database **2016**.

192. **Kanesaki Y, Shiwa Y, Tajima N, Suzuki M, Watanabe S, Sato N, Ikeuchi M, Yoshikawa H.** 2012. Identification of substrain-specific mutations by massively parallel whole-genome resequencing of Synechocystis sp. PCC 6803. DNA Res **19:**67-79.

193. **DeLuca DS, Levin JZ, Sivachenko A, Fennell T, Nazaire M-D, Williams C, Reich M, Winckler W, Getz G.** 2012. RNA-SeQC: RNA-seq metrics for quality control and process optimization. Bioinformatics **28:**1530-1532.

194. **Trapnell C, Pachter L, Salzberg SL.** 2009. TopHat: discovering splice junctions with RNA-Seq. Bioinformatics **25:**1105-1111.

195. **Trapnell C, Hendrickson DG, Sauvageau M, Goff L, Rinn JL, Pachter L.** 2013. Differential analysis of gene regulation at transcript resolution with RNA-seq. Nat Biotech **31:**46-53.

196. **Robinson MD, McCarthy DJ, Smyth GK.** 2010. edgeR: a Bioconductor package for differential expression analysis of digital gene expression data. Bioinformatics **26:**139-140.

197. **Huang da W, Sherman BT, Lempicki RA.** 2009. Systematic and integrative analysis of large gene lists using DAVID bioinformatics resources. Nat Protoc **4:**44-57.

198. **Huang da W, Sherman BT, Lempicki RA.** 2009. Bioinformatics enrichment tools: paths toward the comprehensive functional analysis of large gene lists. Nucleic Acids Res **37:**1-13.

199. **Ashburner M, Ball CA, Blake JA, Botstein D, Butler H, Cherry JM, Davis AP, Dolinski K, Dwight SS, Eppig JT, Harris MA, Hill DP, Issel-Tarver L, Kasarskis A, Lewis S, Matese JC, Richardson JE, Ringwald M, Rubin GM, Sherlock G.** 2000. Gene ontology: tool for the unification of biology. The Gene Ontology Consortium. Nat Genet **25:**25-29.

200. **Wada A, Mikkola R, Kurland CG, Ishihama A.** 2000. Growth phase-coupled changes of the ribosome profile in natural isolates and laboratory strains of Escherichia coli. J Bacteriol **182:**2893-2899.

201. **Tagami K, Nanamiya H, Kazo Y, Maehashi M, Suzuki S, Namba E, Hoshiya M, Hanai R, Tozawa Y, Morimoto T, Ogasawara N, Kageyama Y, Ara K, Ozaki K, Yoshida M, Kuroiwa H, Kuroiwa T, Ohashi Y, Kawamura F.** 2012. Expression of a small (p)ppGpp synthetase, YwaC, in the (p)ppGpp(0) mutant of Bacillus subtilis triggers YvyD-dependent dimerization of ribosome. Microbiologyopen **1:**115-134.

202. **Kvint K, Nachin L, Diez A, Nystrom T.** 2003. The bacterial universal stress protein: function and regulation. Curr Opin Microbiol **6:**140-145.

203. **Diez A, Gustavsson N, Nystrom T.** 2000. The universal stress protein A of Escherichia coli is required for resistance to DNA damaging agents and is regulated by a RecA/FtsK-dependent regulatory pathway. Mol Microbiol **36:**1494-1503.

204. **Kadowaki T, Nishiyama Y, Hisabori T, Hihara Y.** 2015. Identification of OmpR-family response regulators interacting with thioredoxin in the Cyanobacterium Synechocystis sp. PCC 6803. PLoS One **10:**e0119107.

205. **Tamoi M, Miyazaki T, Fukamizo T, Shigeoka S.** 2005. The Calvin cycle in cyanobacteria is regulated by CP12 via the NAD(H)/NADP(H) ratio under light/dark conditions. Plant J **42:**504-513.

206. **Garcia-Dominguez M, Reyes JC, Florencio FJ.** 1999. Glutamine synthetase inactivation by protein-protein interaction. Proc Natl Acad Sci U S A **96:**7161-7166.

207. **Muro-Pastor MI, Reyes JC, Florencio FJ.** 2001. Cyanobacteria perceive nitrogen status by sensing intracellular 2-oxoglutarate levels. J Biol Chem **276:**38320-38328.

208. **Himeno H, Kurita D, Muto A.** 2014. tmRNA-mediated trans-translation as the major ribosome rescue system in a bacterial cell. Front Genet **5:**66.

209. **Milon P, Tischenko E, Tomsic J, Caserta E, Folkers G, La Teana A, Rodnina MV, Pon CL, Boelens R, Gualerzi CO.** 2006. The nucleotide-binding site of

bacterial translation initiation factor 2 (IF2) as a metabolic sensor. Proc Natl Acad Sci U S A **103:**13962-13967.

210. **Corrigan RM, Bellows LE, Wood A, Grundling A.** 2016. ppGpp negatively impacts ribosome assembly affecting growth and antimicrobial tolerance in Gram-positive bacteria. Proc Natl Acad Sci U S A **113:**E1710-1719.

211. **McGinn PJ, Price GD, Maleszka R, Badger MR.** 2003. Inorganic carbon limitation and light control the expression of transcripts related to the CO2-concentrating mechanism in the cyanobacterium Synechocystis sp. strain PCC6803. Plant Physiol **132:**218-229.

212. **Takano S, Tomita J, Sonoike K, Iwasaki H.** 2015. The initiation of nocturnal dormancy in Synechococcus as an active process. BMC Biol **13:**36.

213. **Saha R, Liu D, Hoynes-O'Connor A, Liberton M, Yu J, Bhattacharyya-Pakrasi M, Balassy A, Zhang F, Moon TS, Maranas CD, Pakrasi HB.** 2016. Diurnal Regulation of Cellular Processes in the Cyanobacterium Synechocystis sp. Strain PCC 6803: Insights from Transcriptomic, Fluxomic, and Physiological Analyses. MBio **7:**e00464-00416.

214. **Herranen M, Aro EM, Tyystjarvi T.** 2001. Two distinct mechanisms regulate the transcription of photosystem II genes in Synechocystis sp. PCC 6803. Physiol Plant **112:**531-539.

215. **Mohamed A, Eriksson J, Osiewacz HD, Jansson C.** 1993. Differential expression of the psbA genes in the cyanobacterium Synechocystis 6803. Mol Gen Genet **238:**161-168.

216. **Vernotte C, Picaud M, Kirilovsky D, Olive J, Ajlani G, Astier C.** 1992. Changes in the photosynthetic apparatus in the cyanobacterium Synechocystis sp. PCC 6714 following light-to-dark and dark-to-light transitions. Photosynth Res **32:**45-57.

217. **Smart LB, McIntosh L.** 1991. Expression of photosynthesis genes in the cyanobacterium Synechocystis sp. PCC 6803: psaA-psaB and psbA transcripts accumulate in dark-grown cells. Plant Mol Biol **17:**959-971.

218. **Gaca AO, Kajfasz JK, Miller JH, Liu K, Wang JD, Abranches J, Lemos JA.** 2013. Basal levels of (p)ppGpp in Enterococcus faecalis: the magic beyond the stringent response. MBio **4:**e00646-00613.

219. **Tan X.** 2012. Physiological and ecological characteristics in the life cycle of bloom-forming cyanobacteria. Journal of Food Agriculture & Environment **10:**929-934.

220. **Deng W, Monks L, Neuer S.** 2015. Effects of clay minerals on the aggregation and subsequent settling of marine Synechococcus. Limnology and Oceanography **60:**805-816.

221. **da Silva TL, Gouveia L, Reis A.** 2014. Integrated microbial processes for biofuels and high value-added products: the way to improve the cost effectiveness of biofuel production. Appl Microbiol Biotechnol **98:**1043-1053.

222. **Misra N, Panda PK, Parida BK.** 2013. Agrigenomics for microalgal biofuel production: an overview of various bioinformatics resources and recent studies to link OMICS to bioenergy and bioeconomy. Omics **17:**537-549.

223. **Pires JC, Alvim-Ferraz MC, Martins FG, Simoes M.** 2013. Wastewater treatment to enhance the economic viability of microalgae culture. Environ Sci Pollut Res Int **20:**5096-5105.

224. **Elena Kazamia DCA, Alison G. Smith.** Synthetic ecology – A way forward for sustainable algal biofuel production? Journal of Biotechnology **162:**163–169.

225. **Levenbach S.** 2009. Grazing intensity influences the strength of an associational refuge on temperate reefs. Oecologia **159:**181-190.

226. **Shurin JB, Abbott RL, Deal MS, Kwan GT, Litchman E, McBride RC, Mandal S, Smith VH.** 2013. Industrial-strength ecology: trade-offs and opportunities in algal biofuel production. Ecol Lett **16:**1393-1404.

227. **Venturelli OS, Egbert RG, Arkin AP.** 2016. Towards Engineering Biological Systems in a Broader Context. J Mol Biol **428:**928-944.

228. **Stenuit B, Agathos SN.** 2015. Deciphering microbial community robustness through synthetic ecology and molecular systems synecology. Curr Opin Biotechnol **33:**305-317.

229. **Song H, Ding MZ, Jia XQ, Ma Q, Yuan YJ.** 2014. Synthetic microbial consortia: from systematic analysis to construction and applications. Chem Soc Rev **43:**6954-6981.

230. **Xiong W, Abraham PE, Li Z, Pan C, Hettich RL.** 2015. Microbial metaproteomics for characterizing the range of metabolic functions and activities of human gut microbiota. Proteomics **15:**3424-3438.

231. **Gangl D, Zedler JA, Rajakumar PD, Martinez EM, Riseley A, Wlodarczyk A, Purton S, Sakuragi Y, Howe CJ, Jensen PE, Robinson C.** 2015. Biotechnological exploitation of microalgae. J Exp Bot **66:**6975-6990.

232. **Cheney SaT, David W. .** 2011. Comprehensive economic model of industrial-scale production of fatty-acid derived J8 jet fuel from genetically modified *Synechocystis*. Diversified Energy, Gilbert, Arizona.

233. **Rittmann B, Vermaas W., Nielsen, D.** c2016, posting date. "ARPA-E Cyanobacteria Designed for Solar-Powered Highly Efficient Production of Biofuels". Elsevier. [Online.]

234. **Langille MGI, Zaneveld J, Caporaso JG, McDonald D, Knights D, Reyes JA, Clemente JC, Burkepile DE, Vega Thurber RL, Knight R, Beiko RG, Huttenhower C.** 2013. Predictive functional profiling of microbial communities using 16S rRNA marker gene sequences. Nat Biotech **31:**814-821.

235. **Barry M.** 2014. Overcoming the Impacts of Extreme Weather and Dissolved Organic Matter on the Treatability of Water using Ozone Dissertation. Arizona State University.

236. **Zhang Z, Schwartz S, Wagner L, Miller W.** 2000. A greedy algorithm for aligning DNA sequences. J Comput Biol **7:**203-214.

237. **Gilbert J, Jansson, Janet K and Knight, R.** The Earth Microbiome project: successes and aspirations. BMC Biol. **12**.

238. **Youssef N, Sheik CS, Krumholz LR, Najar FZ, Roe BA, Elshahed MS.** 2009. Comparison of species richness estimates obtained using nearly complete fragments and simulated pyrosequencing-generated fragments in 16S rRNA gene-based environmental surveys. Appl Environ Microbiol **75:**5227-5236.

239. **Edgar RC.** 2010. Search and clustering orders of magnitude faster than BLAST. Bioinformatics **26:**2460-2461.

240. **Wang Q.. Garrity G.M. TJ, Cole J.R.** 2007. Naïve Bayesian Classifier for Rapid Assignment of rRNA Sequences into the New Bacterial Taxonomy Appl Environ Microbiol **73:**5261–5267.

241. **Daniel McDonald MNP, Julia Goodrich, Eric P Nawrocki, Todd Z DeSantis, Alexander Probst, Gary L Andersen, Rob Knight, Philip Hugenholtz.** 2012. An improved Greengenes taxonomy with explicit ranks for ecological and evolutionary analyses of bacteria and archaea. ISME J **6:**610–618.

242. **Caporaso JG, Bittinger K, Bushman FD, DeSantis TZ, Andersen GL, Knight R.** 2010. PyNAST: a flexible tool for aligning sequences to a template alignment. Bioinformatics **26:**266-267.

243. **Price MN, Dehal PS, Arkin AP.** 2009. FastTree: computing large minimum evolution trees with profiles instead of a distance matrix. Mol Biol Evol **26:**1641-1650.

244. **Haas BJ, Gevers D, Earl AM, Feldgarden M, Ward DV, Giannoukos G, Ciulla D, Tabbaa D, Highlander SK, Sodergren E, Methe B, DeSantis TZ, Petrosino JF, Knight R, Birren BW.** 2011. Chimeric 16S rRNA sequence formation and detection in Sanger and 454-pyrosequenced PCR amplicons. Genome Res **21:**494-504.

245. **Heidorn T, Camsund D, Huang H-H, Lindberg P, Oliveira P, Stensjö K, Lindblad P.** 2011. Chapter Twenty-Four - Synthetic Biology in Cyanobacteria: Engineering and Analyzing Novel Functions, p. 539-579. *In* Chris V (ed.), Methods in Enzymology, vol. Volume 497. Academic Press.

246. 2010. Minitab Statistical Software, 17 ed. Minitab, Inc., State College, PA.

247. **Montgomery DC.** 2006. Design and Analysis of Experiments. John Wiley & Sons.

248. 1989-2007. JMP® Pro, 12 ed. SAS Institute Inc., Cary, NC.

249. **Szklarczyk D, Franceschini A, Wyder S, Forslund K, Heller D, Huerta-Cepas J, Simonovic M, Roth A, Santos A, Tsafou KP, Kuhn M, Bork P, Jensen LJ, von Mering C.** 2015. STRING v10: protein-protein interaction networks, integrated over the tree of life. Nucleic Acids Res **43:**D447-452.

250. **Kanehisa M, Sato Y, Kawashima M, Furumichi M, Tanabe M.** 2016. KEGG as a reference resource for gene and protein annotation. Nucleic Acids Res **44:**D457-462.

251. **Eiler A, Bertilsson S.** 2007. Flavobacteria blooms in four eutrophic lakes: linking population dynamics of freshwater bacterioplankton to resource availability. Appl Environ Microbiol **73:**3511-3518.

252. **Hunte C, Screpanti E, Venturi M, Rimon A, Padan E, Michel H.** 2005. Structure of a Na+/H+ antiporter and insights into mechanism of action and regulation by pH. Nature **435:**1197-1202.

253. **Rius N, Sole M, Francia A, Loren JG.** 1995. Buffering capacity and H+ membrane conductance of gram-negative bacteria. FEMS Microbiol Lett **130:**103-110.

254. **Dumbrell AJ, Nelson M, Helgason T, Dytham C, Fitter AH.** 2010. Relative roles of niche and neutral processes in structuring a soil microbial community. ISME J **4:**337-345.

255. **Yang H, Schmitt-Wagner D, Stingl U, Brune A.** 2005. Niche heterogeneity determines bacterial community structure in the termite gut (Reticulitermes santonensis). Environ Microbiol **7:**916-932.

256. **Inaba M, Sakamoto A, Murata N.** 2001. Functional expression in Escherichia coli of low-affinity and high-affinity Na(+)(Li(+))/H(+) antiporters of Synechocystis. J Bacteriol **183:**1376-1384.

257. **Burke C, Steinberg P, Rusch D, Kjelleberg S, Thomas T.** 2011. Bacterial community assembly based on functional genes rather than species. Proc Natl Acad Sci U S A **108:**14288-14293.

258. **Morris JJ, Lenski RE, Zinser ER.** 2012. The Black Queen Hypothesis: evolution of dependencies through adaptive gene loss. MBio **3**.

259. **Foster KR, Bell T.** 2012. Competition, not cooperation, dominates interactions among culturable microbial species. Curr Biol **22:**1845-1850.

260. **Macarthur RH, Wilson EO.** 1967. The Theory of Island Biogeography, REV - Revised ed. Princeton University Press.

261. **Freilich S, Kreimer A, Meilijson I, Gophna U, Sharan R, Ruppin E.** 2010. The large-scale organization of the bacterial network of ecological co-occurrence interactions. Nucleic Acids Res **38:**3857-3868.

262. **Hubbell S.** 2001. The Unified Neutral Theory of Biodiversity and Biogeography. Princeton University Press.

263. **MacArthur RH.** 1958. Population ecology of some warblers of northeastern coniferous forests. Ecology **39:**599–619.

264. **Woodcock S, van der Gast CJ, Bell T, Lunn M, Curtis TP, Head IM, Sloan WT.** 2007. Neutral assembly of bacterial communities. FEMS Microbiol Ecol **62:**171-180.

265. **Sale PM.** Coexistence of coral reef fishes — a lottery for living space. Environmental Biology of Fishes **3:** 85-102.

266. **Munday PL.** 2004. Competitive coexistence of coral-dwelling fishes: The lottery hypothesis revisited. Ecology **85:**6.

267. **Villa F, Pitts B, Lauchnor E, Cappitelli F, Stewart PS.** 2015. Development of a Laboratory Model of a Phototroph-Heterotroph Mixed-Species Biofilm at the Stone/Air Interface. Front Microbiol **6:**1251.

268. **Rittmann BE, Krajmalnik-Brown R, Halden RU.** 2008. Pre-genomic, genomic and post-genomic study of microbial communities involved in bioenergy. Nat Rev Microbiol **6:**604-612.

269. **Crawford A, Wilson D.** 2015. Essential metals at the host-pathogen interface: nutritional immunity and micronutrient assimilation by human fungal pathogens. FEMS Yeast Res **15**.

270. **Kelliher JL, Kehl-Fie TE.** 2016. Competition for Manganese at the Host-Pathogen Interface. Prog Mol Biol Transl Sci **142:**1-25.

271. **Soares MP, Weiss G.** 2015. The Iron age of host-microbe interactions. EMBO Rep **16:**1482-1500.

272. **Shaw AJ, Lam FH, Hamilton M, Consiglio A, MacEwen K, Brevnova EE, Greenhagen E, LaTouf WG, South CR, van Dijken H, Stephanopoulos G.** 2016. Metabolic engineering of microbial competitive advantage for industrial fermentation processes. Science **353:**583-586.

APPENDIX A

TABLES OF GENE EXPRESSION DATA FOR CHAPTER 3

Table A.1: Differentially expressed genes grouped by categories of gene function.

Entry	Gene	logFC [a]	PValue	Homology	Function
			Category 1: Hypotheticals		
1	slr0272	5.0142	0.0002	conserved hypothetical	unknown
2	ssr2843	4.9496	0.0147	conserved hypothetical	Tryptophan-rich conserved hypothetical
3	slr0443	4.6126	0.0004	conserved hypothetical	unknown
4	sll0944	4.2472	0.0052	conserved hypothetical	conserved domain of unknown function
5	sll0376	3.7784	0.0023	conserved hypothetical	unknown
6	sll0442	3.5440	0.0051	conserved hypothetical	unknown
7	sll1338	2.6673	0.0201	conserved hypothetical	unknown
8	sll0676	2.5492	0.0377	conserved hypothetical	GxWxG domain conserved hypothetical
9	slr0587	2.4653	0.0306	conserved hypothetical	possible hydrolase conserved domain
10	sll0481	2.4377	0.0451	conserved hypothetical	unknown

Table A.1: Differentially expressed genes grouped by categories of gene function.

Entry	Gene	logFC [a]	PValue	Homology	Function
			Category 1: Hypotheticals		
11	ssr1528	5.0142	0.0543	conserved hypothetical	conserved hypothetical
12	slr0668	4.9496	0.0467	conserved hypothetical	conserved hypothetical
13	slr0971	4.6126	0.0465	conserved hypothetical	conserved hypothetical
14	sll0181	4.2472	0.0360	conserved hypothetical	conserved hypothetical
15	sll1698	3.7784	0.0321	conserved hypothetical	conserved hypothetical
16	sll1240	3.5440	0.0302	conserved hypothetical	conserved hypothetical
17	sll1606	2.6673	0.0190	conserved hypothetical	conserved hypothetical
18	slr1907	2.5492	0.0179	conserved hypothetical	conserved hypothetical
19	slr0921	2.4653	0.0162	conserved hypothetical	conserved hypothetical
20	ssr2009	2.4377	0.0340	conserved hypothetical	conserved hypothetical

Table A.1: Differentially expressed genes grouped by categories of gene function.

Entry	Gene	logFC [a]	PValue	Homology	Function
			Category 1: Hypotheticals		
21	slr0325	-3.6984	0.0031	conserved hypothetical	MEKHLA domain.
22	sll0364	-4.0065	0.0090	conserved hypothetical	conserved domain of unknown function
23	ssl3829	-4.5098	0.0032	conserved hypothetical	conserved domain of unknown function
24	sll1236	-4.9288	0.0001	conserved hypothetical	unknown
25	sll1853	-4.9809	0.0004	conserved hypothetical	conserved domain of unknown function
26	ssl3446	-5.4443	0.0004	conserved hypothetical	conserved domain of unknown function
27	ssr2551	-6.7090	0.0004	conserved hypothetical	conserved domain of unknown function
			Category 2: Transposases (transposon motility)		
28	ssr2227	5.7731	0.0000	ssr2227	putative transposase
29	sll1791	3.6889	0.0158	ISY802a	putative transposase [ISY802a: 852462 - 853369]

Table A.1: Differentially expressed genes grouped by categories of gene function.

Entry	Gene	logFC [a]	PValue	Homology	Function
			Category 2: Transposases (transposon motility)		
30	ssr2227	5.7731	0.0000	ssr2227	putative transposase [ISY523o(partial copy): 2225804 - 2226597]
31	sll1791	3.6889	0.0158	ISY802a	putative transposase [ISY120f(partial copy): 664387 - 664775]
32	sll1861	-2.4027	0.0413	ISY523o	putative transposase [ISY352a(partial copy): 572672 - 572905]
33	sll0986	-3.7133	0.0025	ISY120f	putative transposase [ISY120b: 1385747 - 1386548]
34	ssr3452	-3.7356	0.0028	ISY352a	putative transposase [ISY523c: 1513158 - 1514023]
			Category 3: Nutrient Transport / Uptake		
35	cysT	3.2375	0.0160	cysT	sulfate transport system permease protein
36	mntA	2.9193	0.0138	mntA	manganese transport system ATP-binding protein MntA
37	ccmL	2.7228	0.0221	ccmL	carbon dioxide concentrating mechanism protein Ccm
38	mgtC	2.6197	0.0244	mgtC	Mg2+ transport ATPase

Table A.1: Differentially expressed genes grouped by categories of gene function.

Entry	Gene	logFC [a]	PValue	Homology	Function
			Category 3: Nutrient Transport / Uptake		
39	slr1492	2.6099	0.0307	fecB	iron(III) dicitrate transport system substrate-binding protein
40	sll0409	2.4756	0.0354	menC	similar to O-succinylbenzoate-CoA synthase
41	slr1261	2.3976	0.0356		Rhodanese-related sulfurtransferase [Inorganic ion transport and metabolism]
42	glcP	2.3647	0.0393	glcP, gtr, tgr	glucose transport protein
43	amt1	2.2570	0.0458	amt1, amt	ammonium/methylammonium permease.
44	natD	-2.2678	0.0469	natD	Integral membrane protein of the ABC-type Nat permease for uptake of neutral amino acids NatD
45	slr1978	-2.8267	0.0155		Cobalt transport protein
46	sll1734	-2.9221	0.0117	cupA, chpY, sll1734	protein involved in low CO2-inducible, high affinity CO2 uptake
47	cysA	-3.5954	0.0028	cysA	sulfate transport system ATP-binding protein
48	sll0732	-2.7804	0.0213		Carbonic anydrase converts CO2 to bicarbonate.

Table A.1: Differentially expressed genes grouped by categories of gene function.

Entry	Gene	logFC [a]	PValue	Homology	Function
Category 4: Salt / osmotic / pH / redox stress response; nutrient limitation tolerance and/or adaptation					
49	sll0594	3.9714	0.0018		signal transduction: regulatory subunit of cAMP-dependent protein kinase.
50	slr0623	2.4172	0.0347	trxA	thioredoxin regulates redox status during transition to or from acive phoosynhesis.
51	cysH	-2.3242	0.0409	cysH	phosphoadenosine phosphosulfate reductase
52	ssr1558	-2.3643	0.0424		UPF0016 superfamily conserved hypothetical. Putative Ca2+/H+ antiporter.
53	hisB	-2.6099	0.0307	hisB	two-component response regulator OmpR subfamily
54	slr2010	-2.9301	0.0145	mrpE	Na+/H+ sodium exporter in alkalophilic Bacillus
55	slr0530	-4.1689	0.0033	ggtC	glucosylglycerol transport system permease protein
56	sll0685	-6.1098	0.0013		Thiol-disulfide isomerase or thioredoxin [Posttranslational modification, s]
57	sll1318	-7.5408	0.0001		Putative Ca2+/H+ antiporter, TMEM165/GDT1 family
58	smtB	-5.5004	0.0003	ziaR	Represses zinc sequestration.

Table A.1: Differentially expressed genes grouped by categories of gene function.

Entry	Gene	logFC [a]	PValue	Homology	Function
			Category 5: Biomolecule export		
59	slr1046	2.4887	0.0313	pilA3	putative TatA protein
60	pilA4	-2.3662	0.0425	gspG	Group 4 pilin-like protein, or general secretion pathway protein G
61	slr1819	-3.5321	0.0031	rfrM	Uncharacterized protein YjbI
62	slr0516	-4.7106	0.0168	rfrD	Secreted effector protein PipB2
			Category 6: Glycosyltransferase and methyltransferase and N-acetyltransferase		
63	sll1173	2.3455	0.0543		methyltransferase, FkbM family
64	slr1537	2.1863	0.0527		Glycosyltransferase family A.
65	sll1664	-2.2384	0.0479		Glycosyltransferase, GT2 family.
66	slr1039	-2.5300	0.0310		S-adenosylmethionine-dependent methyltransferases.
67	crtE	-2.5575	0.0254	crtE	solanesyl diphosphate synthase

Table A.1: Differentially expressed genes grouped by categories of gene function.

Entry	Gene	logFC [a]	PValue	Homology	Function
Category 6: Glycosyltransferase and methyltransferase and N-acetyltransferase					
68	icsA	-2.6996	0.0272	icsA	probable glycosyltransferase
69	slr0491	-5.1802	0.0007		Uncharacterized conserved protein YtfP, gamma-glutamylcyclotransferase
70	sll0786	-7.4170	0.0001		putative N-acetyltransferase, MSMEG_0567 N-terminal domain family (GNAT family)
Category 7: ABC Transporters					
71	ycf16	-2.3710	0.0364	sufC	ABC transporter ATP-binding protein
72	slr0610	-2.4308	0.0379	evrC	ABC-type uncharacterized transport system, permease component
73	sll1623	-3.0594	0.0117	ndhM	ABC transporter ATP-binding protein
Category 8: Sigma factors and signal transduction and transcription regulators					
74	sll1169	3.5048	0.0120		signal transduction: cAMP-binding domain of CRP
75	sll0241	2.7168	0.0200		Periplasmic ligand-binding sensor domain [Signal transduction mechanisms).

Table A.1: Differentially expressed genes grouped by categories of gene function.

Entry	Gene	logFC [a]	PValue	Homology	Function
Category 9: Energy / transport (ATP, NAD(P)H, cytochromes, ferrodoxin, chlororespiration					
76	chlL	3.4196	0.0039	chlL	light-independent protochlorophyllide reductase iron protein subunit ChlL
77	gdhA	3.1509	0.0080	gdhA	glutamate dehydrogenase (NADP+)
78	chlN	3.1434	0.0073	chlN	light-independent protochlorophyllide reductase subunit ChlN
79	sll0572	3.1169	0.0083		
80	purK	3.0109	0.0100	purK	phosphoribosylaminoimidazole carboxylase ATPase subunit
81	petF	2.7699	0.0163	petF	ferredoxin, petF-like protein
82	sll1308	2.6806	0.0346		short-chain dehydrogenase/reductase with NADP binding site
83	petL	2.5553	0.0271	petL	cytochrome b6f.
84	sll1504	-2.2519	0.0475		HAS domain
85	glcF	-2.3702	0.0381	glcF	glycolate oxidase subunit, (Fe-S)protein

Table A.1: Differentially expressed genes grouped by categories of gene function.

Entry	Gene	logFC [a]	PValue	Homology	Function
Category 9: Energy / transport (ATP, NAD(P)H, cytochromes, ferrodoxin, chlororespiration					
86	mrpC	-2.5675	0.0252	mrpC	hypothetical protein
87	sll0088	-2.6089	0.0229	sufR	hypothetical protein. iron-sulfur cluster biosynthesis transcriptional regulator SufR
88	petM	-2.7065	0.0456	petM	cytochrome b6-f complex subunit PetM
89	slr0091	-2.9776	0.0108		NAD(P) binding site
90	nadD	-3.1327	0.0089	nadD	hypothetical protein
91	sll0509	-4.3323	0.0006		ATP adenylyltransferase [Nucleotide transport and metabolism]
92	ssl3451	-5.7963	0.0024	sipA	chlororespiratory reduction
Category 10: Transcription and translation machinery					
93	trnY	6.6955	0.0004		amino-acyl tRNA biosynthesis for tyrosine
94	rpl29	3.1827	0.0075	rpmC	50S ribosomal protein L29

Table A.1: Differentially expressed genes grouped by categories of gene function.

Entry	Gene	logFC [a]	PValue	Homology	Function
Category 10: Transcription and translation machinery					
95	slr0033	3.9511	0.0013	slr0033	glutamyl-tRNA(Gln) amidotransferase subunit C
96	ssl2781	3.6345	0.0058		
97	purN	2.9396	0.0123	purN	phosphoribosylglycinamide formyltransferase
98	pyrH	2.8953	0.0130	pyrH	uridine monophosphate kinase
99	purL	2.7011	0.0210	purL	phosphoribosyl formylglycinamidine synthase
100	sll0546	2.6015	0.0240		putative rRNA binding site [nucleotide binding]; translation initiation factor
101	lrtA	2.5755	0.0308	hpf	light repressed protein A homolog
102	thrC	-2.2346	0.0485	thrC	threonine synthase
103	trpF	-2.2871	0.0504	trpF	N-(5-phosphoribosyl)anthranilate isomerase. Anthraniline is an amino acid.
104	nifS	-2.3512	0.0381	sufS	cysteine desulfurase

Table A.1: Differentially expressed genes grouped by categories of gene function.

Entry	Gene	logFC [a]	PValue	Homology	Function
Category 10: Transcription and translation machinery					
105	tyrS	-5.5486	0.0039	tyrS	similar to tyrosyl tRNA synthetase
106	trnL	-6.4674	0.0006		amino-acyl tRNA synthesis, leucine
107	exsB	-2.7403	0.0284	exsB	homolog of an alternative nucleoside tRNA that promostes translation continuity.
Category 11: Phage stress response, toxin-antitoxin defense, other stress response					
108	slr0725	5.4645	0.0004		toxin from toxin-antitoxin system
109	slr0244	4.3097	0.0007	UspA putative	USP-like, Usp: Universal stress protein family.
110	comB	3.4894	0.0041		2-phosphosulfolactate phosphatase.
111	slr1912	2.1914	0.0520		anti-sigmaF factor. SigmaF is group 3 stress response.
112	smpB	-2.2706	0.0453	smpB	SsrA-binding protein. Trans-translation for stalled ribosome recovery mechanism.
113	sll0162	-2.3695	0.0387		phage shock protein A (IM30), suppresses sigma54-dependent transcription

Table A.1: Differentially expressed genes grouped by categories of gene function.

Entry	Gene	logFC [a]	PValue	Homology	Function
Category 10: Transcription and translation machinery					
114	ssr0336	-2.5542	0.0261		Predicted nuclease of the RNAse H fold, HicB family [Defense mechanisms]
115	sll0687	-2.8049	0.0227	sigI.	Group 3 sigma factor related to stress response
116	slr2100	-2.8078	0.0162	rre20	two-component response regulator of UV-B sress response
117	hsp17	-3.2950	0.0052	hspA	heat shock protein known to be highly expressed in the dark.
118	ssr2067	-3.3355	0.0058		Predicted RNAse H [Defense mechanisms]
119	sll1400	-3.7070	0.0032		Predicted nuclease, contains PIN domain, potential toxin-antitoxin system component
120	vapB	-3.9668	0.0051	vapB	virulence-associated protein
121	vapC	-7.1379	0.0001	vapC.	High expression levels under heat stress and in the absence of light
122	cbiC	-8.0565	0.0000	cobH	cobalt-dependent transcriptional regulator. Shown to confer tolerance to ethanol.

Table A.1: Differentially expressed genes grouped by categories of gene function.

Entry	Gene	logFC [a]	PValue	Homology	Function
			Category 12: Phototrophy		
123	psaD	3.0203	0.0094	psaD	photosystem I subunit II
124	apcB	2.9054	0.0121	apcB	allophycocyanin beta subunit
125	slr0146	2.8666	0.0132		
126	psaL	2.4379	0.0319	psaL	photosystem I subunit XI
127	apcE	2.3336	0.0392	apcE	phycobilisome core-membrane linker polypeptide
128	apcA	2.3205	0.0403		allophycocyanin.
129	slr1870	-2.6937	0.0219		Uncharacterized conserved protein, LabA/DUF88 family
			Category 13: Cell wall modification; appendage biogenesis		
130	sll0501	-2.2736	0.0443		Bactoprenol Glucosyl transferase. Cell wall biogenesis.
131	slr0769	-2.5971	0.0235		Lipoprotein-anchoring transpeptidase ErfK [Cell wall/membrane/envelope biogenesis]

Table A.1: Differentially expressed genes grouped by categories of gene function.

Entry	Gene	logFC [a]	PValue	Homology	Function
Category 13: Cell wall modification; appendage biogenesis					
132	sll1834	-2.6540	0.0244		flagellar basal body-associated protein FliL
133	ssl0331	-2.8704	0.0164		Haemolytic domain. membrane protein insertion efficiency factor YidD
134	sll0886	-3.8177	0.0017		Uncharacterized membrane protein YozV
135	slr0061	-3.8938	0.0020		protein-protein interaction motif tetratricopeptide repeat
Category 14: central carbon metabolism					
136	sucC	2.8476	0.0139	sucC	succinyl-CoA synthetase beta chain
137	sll0445	2.4920	0.0286	ppsA, pps	phosphoenolpyruvate synthase
138	slr0553	-2.2098	0.0523		Dephospho-CoA kinase [Coenzyme transport and metabolism]
139	pgk	-4.0513	0.0009	pgk	the first ATP-generating step of the glycolytic pathway

Table A.1: Differentially expressed genes grouped by categories of gene function.

Entry	Gene	logFC [a]	PValue	Homology	Function
Category 15: Secondary metabolism: vitamin B, terpenes, others.					
140	moaE	3.4136	0.0249	moaE	molybdopterin (MPT) converting factor, subunit 2
141	pdxH	2.6007	0.0263	pdxH	pyridoxamine 5-phosphate oxidase
142	pyrF	2.5354	0.0298	pyrF	orotidine 5 monophosphate decarboxylase, nucleoside intermediate
143	slr0596	2.4296	0.0343		creatinine amidohydrolase involved in riboflavin and F420 biosynthesis
144	entC	-2.2936	0.0460	menF	salicylate biosynthesis isochorismate synthase
145	degT	-2.5339	0.0279	degT	pleiotropic regulatory protein homolog
146	sll0787	-2.9869	0.0110		AIR synthase-related protein, sll0787.
147	sll0403	-4.8204	0.0005		Catalytic NodB homology domain of the carbohydrate esterase 4 superfamily.
148	cbiM	-6.6336	0.0000	cbiM	cobalamin biosynthesis protein M
149	slr0953	-2.5231	0.0294	spsB	sucrose-phosphate phosphatase

Table A.1: Differentially expressed genes grouped by categories of gene function.

Entry	Gene	logFC [a]	PValue	Homology	Function
Category 15: Secondary metabolism: vitamin B, terpenes, others.					
150	ipk	-2.7161	0.0200	ipk	isopentenyl monophosphate kinase, biosynthesis of terpenes and terpenoids.
Category 16: DNA replication, recombination, repair					
151	ssl2789	5.3312	0.0001		similar to resolvase
152	sll0544	-2.5270	0.0278		
153	phr	-2.7315	0.0200	phrA	DNA photolyase. Light-dependent DNA repair
154	ruvB	-7.5349	0.0001	ruvB	Holliday junction DNA helicase RuvB
Category 17: Cell division / cell cycle control					
155	slr1478	2.4736	0.0367	SpoIIM	Uncharacterized membrane protein [Cell cycle control, cell division, chromosome partitioning]

Table A.1: Differentially expressed genes grouped by categories of gene function.

Entry	Gene	logFC [a]	PValue	Homology	Function
			Category 18: Proteases, hydrolases, nucleases		
156	slr0287	2.6075	0.0257		Predicted RNA-binding protein YlqC
157	slr0709	2.3286	0.0472		reactive intermediate/imine deaminase. Endoribonuclease.
158	slr0241	2.2467	0.0484		Zn-dependent protease with chaperone function
159	sll0914	-2.4124	0.0354		GDSL-like Lipase/Acylhydrolase
160	slr1636	-2.6501	0.0391		Predicted metal-dependent hydrolase
161	sll0639	-2.8266	0.0146		nanoRNase/pAp phosphatase, hydrolyzes c-di-AMP and oligoRNAs.
162	slr1827	-2.9925	0.0128		hydrolase, alpha/beta fold family protein
163	xthA	-4.8263	0.0016	xthA	exodeoxyribonuclease III
164	nth	-6.5196	0.0005	nth	endonuclease III
165	mutT	-7.2019	0.0001	mutT	mutator MutT protein

a LogFC is the $\log_{10}$ fold change of the fragments per kilobase of exon per million fragments mapped (FPKM).

Table A.2: All *Synechocystis* genes predicted to be up-regulated during stringent response.

Entry	Gene	logFC [a]	PValue	Homology	Function
1		6.6955	0.0004	trnY	amino-acyl tRNA biosynthesis for tyrosine
2	slr0244	4.3097	0.0007	UspA putative	USP-like, Usp: Universal stress protein.
3	slr1492	2.6099	0.0307	fecB	iron(III) dicitrate transport system substrate-binding protein
4	lrtA	2.5755	0.0308	hpf	light repressed protein A homolog; ribosome hibernation promotion factor
5	sll0445	2.4920	0.0286	ppsA, pps	phosphoenolpyruvate synthase
6	slr0623	2.4172	0.0347	trxA	protein disulfide oxidoreductase activity
7	slr0009	1.5936	0.1495	rbcL	ribulose bisphosphate carboxylase large subunit
8	slr1106	1.1892	0.2780	phb	prohibitin
9	sll1898	1.1383	0.2970	ggtA	salt tolerance
10	ctaB	1.0907	0.3177	sll1899	cytochrome c oxidase folding protein

Table A.2: All *Synechocystis* genes predicted to be up-regulated during stringent response.

Entry	Gene	logFC [a]	PValue	Homology	Function
11	gidB	0.3061	0.7796		glucose inhibited division protein B
12	slr1428	0.0891	0.9342		
13	katG	0.0465	0.9659		catalase peroxidase
14	clpB	-0.1261	0.9071		ClpB protein
15	sll0247	-0.1422	0.8953	isiA	iron-stress chlorophyll-binding protein
16	slr1452	-0.1845	0.8646	spbA	sulfate transport system substrate-binding protein
16	slr1139	-0.2244	0.8657	trx	thioredoxin
18	slr1516	-0.6238	0.5733	sodB	superoxide dismutase
19	slr0955	-0.7311	0.5019		
20	slr1390	-0.7589	0.4840	ftsH	cell division protein FtsH

Table A.2: All *Synechocystis* genes predicted to be up-regulated during stringent response.

Entry	Gene	logFC [a]	PValue	Homology	Function
21	slr0955	-0.9185	0.3997		probable tRNA/rRNA methyltransferase
22	slr1739	-0.9711	0.3725	psbW	photosystem II 13 kDa protein homolog
23	ssl1633	-1.5338	0.1664	hliC	high light-inducible polypeptide HliC
24	sll1911	-1.8061	0.1040		elongation factor EF-G
25	slr1184	-1.9940	0.0746	atpG	ATP synthase subunit b
26	slr1639	-2.0594	0.0662	smpB	
27	pilA4	-2.1053	0.0769		
28	petM	-2.2706	0.0453		
29	ssl1911	-2.5905	0.1040	gifA	glutamine synthetase inactivating factor IF7
30	sll1514	-3.2950	0.0052	hspA	16.6 kDa small heat shock protein, molecular chaperone

Table A.3: All *Synechocystis* genes predicted to be down-regulated during stringent response.

Entry	Gene	logFC [a]	PValue	Homology	Function
Category 2: Genes predicted to be down-regulated during stringent response					
1	ssl3436	3.1827	0.0075	rpl29	50S ribosomal protein L29
2	slr1986	2.9054	0.0121	apcB	allophycocyanin beta subunit
3	slr0146	2.8666	0.0132		phycobillisome
4	sll1198	2.4669	0.0312	trmD	tRNA (guanine-N1)-methyltransferase
5	sll1452	1.3017	0.2370	nrtC	nitrate/nitrite transport system ATP-binding protein
6	sll0070	0.6038	0.5776	purU	phosphoribosylglycinamide formyltransferase
7	slr1348	0.1380	0.8986	cysE	serine acetyltransferase
8	slr1512	0.1042	0.9239	sbtA	sodium-dependent bicarbonate transporter
9	sll1112	0.0518	0.9618	aroQ	3-dehydroquinate dehydratase
10		-0.0609	0.9563	ribG	putative riboflavin-specific deaminase

Table A.3: All *Synechocystis* genes predicted to be down-regulated during stringent response.

Entry	Gene	logFC [a]	PValue	Homology	Function
11	slr1842	-0.0975	0.9282	cysK	cysteine synthase
12	slr1512	-0.1028	0.9241	slr1512	sodium-dependent bicarbonate transporter
13	slr1653	-0.4094	0.7059	ama	N-acyl-L-amino acid amidohydrolase
14		-0.8506	0.4439	trmB	tRNA methyltransferase
15	sll1509	-1.3493	0.2223	ycf20	hypothetical protein YCF20
16	slr0041	-1.5888	0.1514	cmpB	bicarbonate transport system permease protein
17	slr1197	-2.0134	0.0759	slr1197	SMF protein
18	slr2007	-2.0398	0.0710	ndhD5	NADH dehydrogenase subunit 4

a LogFC is the $\log_{10}$ fold change of the fragments per kilobase of exon per million fragments mapped (FPKM).

APPENDIX B

SUPPLEMENTARY FIGURES

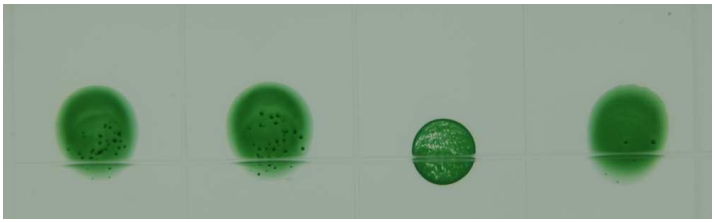

Figure B.1. Genes for S-layer, Wza are not required for phototactic motility.
The *pilC* mutant is a negative control, known to be impaired for pili-dependent twitching motility of phototaxis.

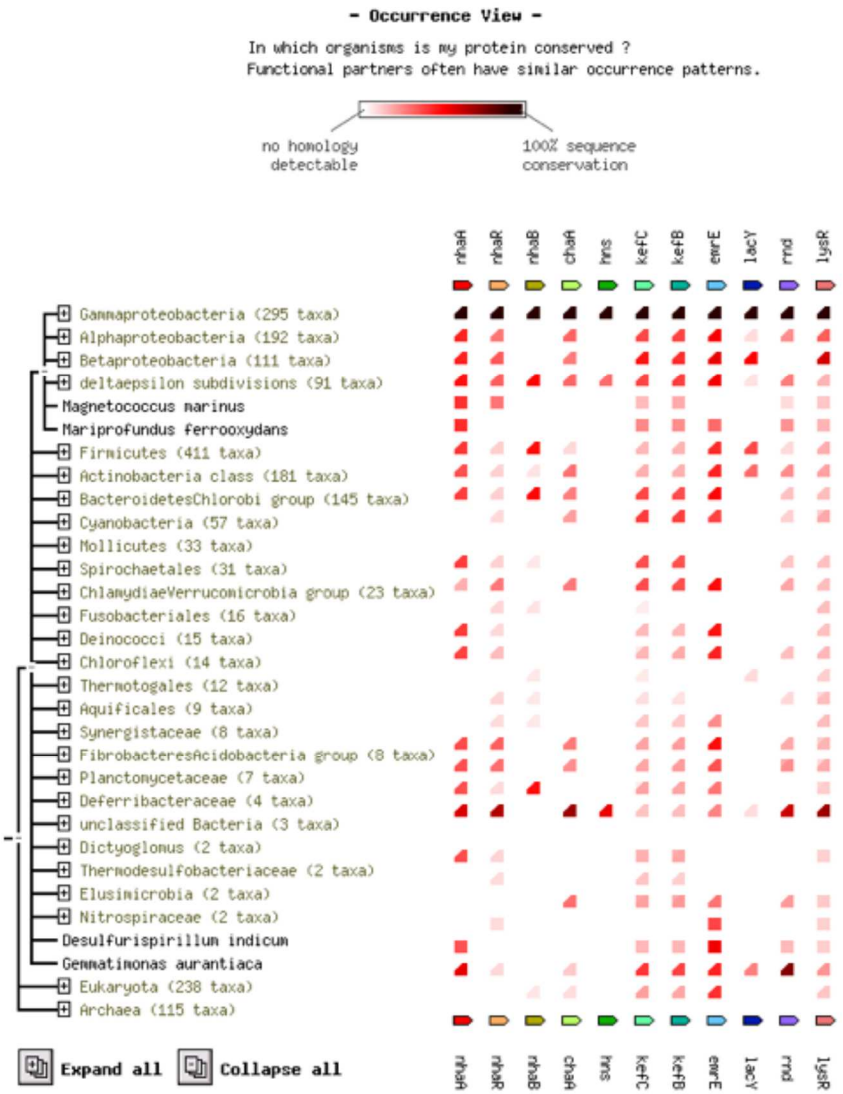

Figure B.2. STRING Occurrence View output for NhaA.
Output for NhaA is described by heat map indicating % homology. Cut squares signify that NhaA occurs in some but not all taxa within a clade along the left vertical axis. Uncut squares indicate NhaA is conserved across all the taxa in the clade. Functional partners to NhaA are listed to the right along the x-axis.

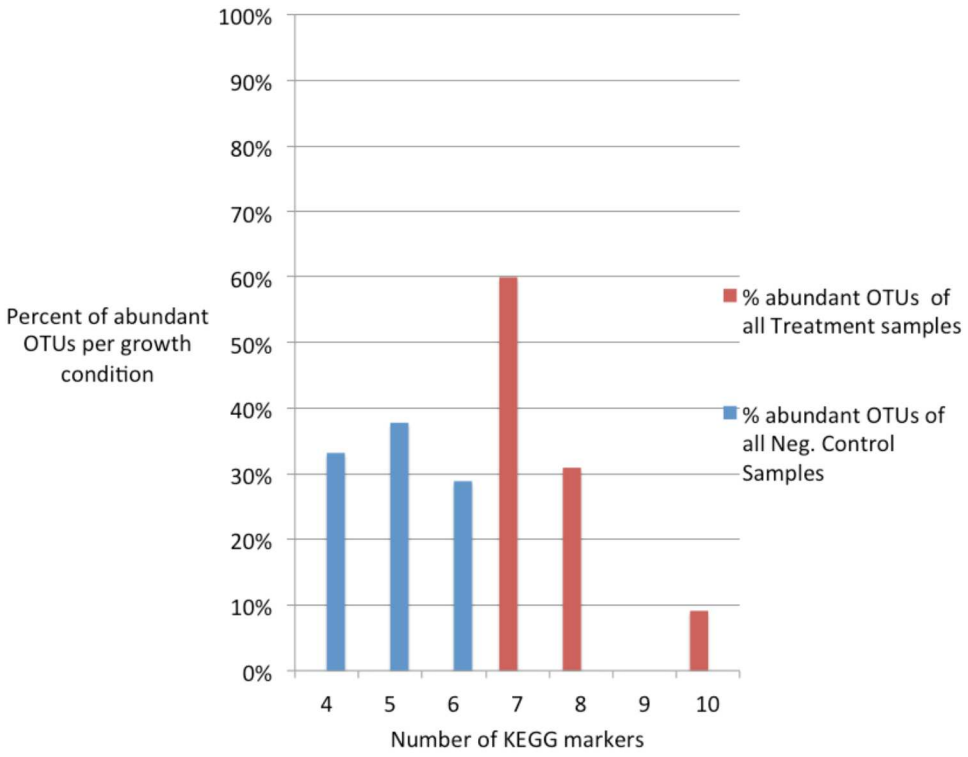

Figure B.3. Weighted average number of KEGG markers per growth condition.
Contribution of total number of markers was weighted by relative abundance of its phylotype in all samples. These weighed numbers were then binned into either the treatment or control condition to calculate the average number of markers per condition, weighted by relative abundance of marker-bearing phylotypes in that condition.